INFORMATION TO USERS

This manuscript has been reproduced from the microfilm master. UMI films the text directly from the original or copy submitted. Thus, some thesis and dissertation copies are in typewriter face, while others may be from any type of computer printer.

The quality of this reproduction is dependent upon the quality of the copy submitted. Broken or indistinct print, colored or poor quality illustrations and photographs, print bleedthrough, substandard margins, and improper alignment can adversely affect reproduction.

In the unlikely event that the author did not send UMI a complete manuscript and there are missing pages, these will be noted. Also, if unauthorized copyright material had to be removed, a note will indicate the deletion.

Oversize materials (e.g., maps, drawings, charts) are reproduced by sectioning the original, beginning at the upper left-hand corner and continuing from left to right in equal sections with small overlaps. Each original is also photographed in one exposure and is included in reduced form at the back of the book.

Photographs included in the original manuscript have been reproduced xerographically in this copy. Higher quality 6" x 9" black and white photographic prints are available for any photographs or illustrations appearing in this copy for an additional charge. Contact UMI directly to order.

UMI

A Bell & Howell Information Company
300 North Zeeb Road, Ann Arbor MI 48106-1346 USA
313/761-4700 800/521-0600

UNIVERSITÉ D'OTTAWA
UNIVERSITY OF OTTAWA

NEAR-FIELD COMPUTATION USING THE FINITE ELEMENT METHOD

by

Hassan O. Ali B.Sc, M.A.Sc

a thesis submitted to the
School of Graduate Studies and Research
in partial fulfillment of the requirements
for the degree of
Doctor of Philosophy

Ottawa-Carleton Institute for Electrical Engineering

Department of Electrical Engineering
Faculty of Engineering
University of Ottawa
January 1997

Abstract

This thesis introduces techniques of analysis of electromagnetic wave propagation problems that can be used in the computation of near field using the Finite Element Method. The techniques are usable in situations involving three-dimensional structures as well as those exhibiting axial symmetry. For three-dimensional structures vector finite element formulation is employed for the computation of both magnetic and electric field vectors. For the axisymmetric configurations nodal finite element method has been implemented in modelling coaxially driven structures. The methods are used to model problem configurations involving structures of interest in the field of EMI/EMC and antennas, such as a dielectric ring resonator antenna, coaxial junctions and a cylindrical monopole antenna. The modelling is done in frequency domain and the results of the modelled structures are provided. A neural network approach to the solution of electromagnetic field problems is also introduced. The results compare well with the published experimental as well as theoretical results obtained on the same structures.

Acknowledgements

I would like to express my sincere gratitude and appreciation to my supervisors Dr. George Costache and Dr. Emil Petriu for the support, guidance and encouragement that they were ever ready to give me during the whole period that took me to complete this work. My special thanks are due to my colleagues, department teaching, support and technical staff, and to all my friends and relatives who helped me in different ways that contributed to the success of this work. I owe a debt of gratitude to my dear wife, Sabra, and our daughter, Umrat, whose combined moral support and understanding gave me the peace of mind that I badly needed to accomplish this work. I would have never been able to undertake this work, were it not for the generous financial support of the Canadian Commonwealth Scholarship and Fellowship Commitee and the Telecommunication Research Institute of Ontario (TRIO), to which I wish to extend my sincere thanks.

List of Symbols

$\vec{A}$ magnetic vector potential

a radius of the inner conductor of a coaxial line

$\vec{B}$ magnetic flux density, in webers/meter^2

b inner radius of the external conductor of a coaxial line

CAD computer-aided design

CCW counter clockwise

$\vec{D}$ electric flux density, in coulombs/meter^2

$\vec{E}$ electric field intensity, in volts/meter

$\vec{E}^{inc}$ incident electric field

$\vec{E}^{sc}$ scattered electric field

E_t tangential component of electric field

e error vector in NN, also $e = 2.718282$

EM electromagnetic

EMC electromagnetic compatibility

EMI electromagnetic interference

f frequency

FEM finite element method

$\vec{H}$ magnetic field intensity, in amperes/meter

$\vec{H}^{inc}$ incident magnetic field

$\vec{H}^{sc}$ scattered magnetic field

H_t tangential component of magnetic field

I electric current

$\vec{J}$ electric current density, in amperes/meter^2

$\vec{J}_s$ surface electric current density

k wave number or propagation constant

$\vec{l}$ length vector

L_i linear, three-dimensional nodal FEM interpolatory function at node i

L_i simplex coordinate corresponding to node i

ℓ_i length of a tetrahedral element edge

LHS left-hand side

$\vec{M}$ magnetic dipole polarization per unit volume

n number of element nodes

$\vec{n}$, $\hat{n}$ unit vector normal

$N_j^{(k)}$ nodal FEM interpolatory function at the jth node for element k

NN neural network

r magnitude of a position vector $\vec{r}$

r,ϕ,z cylindrical coordinates

$\hat{r}$ unit vector normal to a spherical surface

RHS right-hand side

S_{11} input reflection coefficient

S^e elemental surface

TEM transverse electromagnetic

V voltage, volt, volume

V^e elemental volume

VFEM vector finite element method

W_i three-dimensional vector (edge-based) FEM basis function at edge i

x,y,z Cartesian (rectangular) coordinates

$\hat{x}$,$\hat{y}$,$\hat{z}$ unit vectors in rectangular coordinate system

Y admittance

Z impedance

δ_{ij} delta function - $\delta_{ij} = 1$ for $i = j$, $\delta_{ij} = 0$ otherwise

ϵ electric permittivity

ϵ_r relative permittivity

ϵ_0 electric permittivity of free space = $10^{-9}/36\pi$ farad/meter

Φ electric scalar potential

η intrinsic impedance of a medium

λ wavelength

μ magnetic permeability

μ_0 magnetic permeability of free space $= 4\pi \times 10^{-7}$ henry/meter

μ_r relative permeability

ρ electric charge density, in coulombs/meter^3

σ electrical conductivity

ω radian frequency, $\omega = 2\pi f$ for node i

χ_e, (χ_m) electric, (magnetic) susceptibilty

∇ the nabla operator

Contents

List of Figures

Chapter 1

Introduction

1.1 Motivation

The finite element method (FEM) has been widely used, for a very long time in computational electromagnetics. Several papers and books have been written detailing the theory and application of the FEM in electrostatics, magnetostatics, and electromagnetic wave propagation problems. FEM is found handy for its ease in dealing with strongly inhomogeneous problems and those configurations comprising structures of irregular shapes.

Despite the FEM's popularity in electromagnetics, it is only closed boundary-value problems that have been dealt with extensively. Problems that involve scattering and radiation of electromagnetic fields have not been covered much owing to the difficulty in accomodating the open boundaries which are often encountered while modelling those types of problems. Moreover, while radiation problems have been attempted in a few cases, the modelling of the excitation source in most cases has not been accurate - approximate, non-practical feed models have been used.

The traditional FEM that uses nodal basis functions in many cases is known to suffer from the problem of implementing correctly material interface boundary conditions. As will be discussed in detail in Chapter 2, the most common way of assigning a single value of the uknown field at all the nodes placed directly at the interface of two different materials, only satisfies exactly the continuity of the tangential component of the computed field but violates the continuity condition for the normal component

of the field. One is forced to use fine discretization [1] near the interface to alleviate the problem.

If the problem geometry consists of sharp conducting and/or dielectric edges and tips, the traditional node-based FEM suffers from the problem of singularity [2]-[5] of the transverse field. Since some of the components of the field are infinite at the edges and tips, it becomes impossible to implement boundary conditions associated with those field componets. Without proper implementation of the boundary conditions the solution cannot be unique. There are various techniques suggested to alleviate this problem as discussed in greater details in Chapter 2, but the fact remains that sharp edges and tips are not handled well with the traditional FEM.

Added to the above limitations and shortfalls, there has always been the problem of spurious [6], non-physical solutions resulting from the implementation of nodal FEM. Spurious solutions are discussed in greater details in Chapter 2, but in short, they are explained to be a result of the failure of the nodal FEM formulation to satisy the divergence condition: $\nabla \cdot (\mu \vec{H}) = 0$ for the magnetic field and $\nabla \cdot (\epsilon \vec{E}) = 0$ for the electric field, in a source free region.

Several approaches have been used to curb the problem of spurious solutions, from the use of special interpolatory functions, to the use of penalty functions, both in the nodal FEM formulation. Those approaches increase the complexity of the problems and in most cases have been found not to serve the purpose.

The purpose of this work is to develop FEM modelling tools that do not suffer from the above-mentioned shortfalls and yet covering a broad range of problems of practical interest. A technique is developed for modelling radiation problems with very correct models of the feeds in the way they are practically realized in many cases. The work introduces a simple and accurate method of analysis of a class of microwave structures that are coaxially-fed with emphasis put on driven antenna structures.

The problem of the implementation of boundary and material interface conditions as well as that of spurious solutions is tackled by the use of the vector finite element method (VFEM). A detailed three-dimensional vector finite element analysis of scattering as well as radiation problems is covered in this work.

The prime motive is to devise a tool that would accurately model situations of interest in the field of Electromagnetic Interference and Compatibility (EMI/EMC)

as well as in antennas. In this age where faster and faster high speed systems are invented and widely used, the problem of EMI has never been more important and especially right at the component level. The clock rates used and the high power demand have outgrown and rendered useless the conventional ways of using circuit models that were only useful in low frequencies. Now more and more designers rely on full wave analysis and modelling of the systems and components involved. And that is what makes this work very important to the task in question.

The second main motive, although somewhat related to the first, needs a separate mention. There has been a great concern these days of the hazards associated with electromagnetic waves especially in the near field. Measurements have shown potential hazards associated with poor designs of hand-held mobile phones. It is also known that in the proximity of high-powered broadcasting antennas, there exist "hot spots" of very high field values especially on the nearby building structures. To analyze all those cases one needs to obtain the near field solution which is not only difficult but also requires a lot of computer resources. This work is intended to offer an alternative to the computation of near field in an optimum usage of the computer resources.

1.2 Thesis Organization

The thesis has five main chapters covering all the aspects of this work including the underlying theory upon which it is based.

Chapter 1 of the thesis, briefly explains the motivation behind this work, the organization of the thesis and the contributions made.

The finite element method as applied in electromagnetics is introduced in Chapter 2. First a brief introduction of the basic concepts and equations in electromagnetics is provided. Emphasis has been put on the theories governing electromagnetic wave propagation and Maxwell's equations. A special section is included to cover various boundary conditions frequently encountered in electromagnetics. Various aspects of the implementation of the FEM in electromanetics are discussed in this chapter. The problems arising from the implementation of the FEM in electromagnetics are discussed in depth along with the ways to avoid them.

Chapter 3 of this thesis introduces frequency domain analysis of coaxially driven axisymmetric microwave structures. Discussion of the implementation of the nodal FEM to closed and open problems involving coaxial feeds is provided. Results are provided from the implementation of the method to a dielectric resonator antenna. A rigorous explanation is given for the accurate modelling of the coaxial feed and the implementation of the radiation boundary conditions. The beginning of the chapter reviews several works that attempt to solve the problem in question using various techniques. This chapter includes the discussion on the implementation of neural network techniques in typical electromagnetic field problems. As an example, the implementation of neural networks in the design of a dielectric ring resonator antenna is introduced and discussed.

Vector finite elements are introduced in Chapter 4 of this work, first the theory and then the three-dimensional implementation in the solution of scattering and radiation problems. Both the electric and magnetic field formulations are provided. Computational results are provided for both scattering and radiation problems solved using the vector finite element method.

Chapter 5 of this work is the Conclusions in which a summary of the work done is provided and recommendations for future work are given.

Appendix A describes the diagonally preconditioned biconjugate gradient method used to solve sparse complex system of equations resulting from the three-dimensional vector finite element formulation.

1.3 Contributions and Accomplishments

As mentioned earlier in this chapter, the main motive of this work was to realize an electromagnetic field modelling tool that could be easily integrated with the available computer-aided design (CAD) tools that are presently incapable of solving very high frequency problems. That task was successfully accomplished by providing a three-dimensional electromagnetic field modelling tool that can solve both scattering and radiation problems, as well as a specialized tool for geometries exhibiting axial symmetry and driven by coaxial lines. The modelling tool is already being employed in the novel technique for field computation using neural networks. The modelling

tool provides the training data sets.

In the course of realizing the field modelling tools, the following contributions were made:

- A novel technique to model accurately the coaxial feed in the finite element frequency domain solution, is introduced. The feed model takes into account the higher order modes that may be present due to discontinuities.

- With the new feed model and the application of absorbing boundary conditions, a new technique is introduced for frequency domain modelling of coaxially driven radiating microwave devices. New dielectric resonator antennas of novel shapes and superior broadband characteristics are modelled with this technique and introduced for the first time in this work.

- Electromagnetic field solution that implements neural network techniques along with the finite element method is introduced and shown to work very well.

- As far as I know this work is among a few in the literature that implements vector (edge) finite element method (VFEM) not only to scattering problems but also to *driven* antenna problems. Closed-form expressions for the resulting integrals for almost all the cases of interest are provided for the first time in this work. Those will be of great benefit to future researchers in that area.

Chapter 2

The Finite Element Method in Electromagnetics

For the sake of completeness, a brief review of the implementation of the finite element method in the field of electromagnetics will be provided in this chapter. The first to be discussed will be the most important concepts of electromagnetics. This is to provide the reader with the background upon which this work is based on. The emphasis will be put on the theories, equations and boundary conditions encountered in electromagnetic analysis of the problems tackled in this work. In general, solution of most problems of electromagnetics, involves the solution of the famous Maxwell's equations. The Maxwell's equations and the way they are used to formulate boundary-value problems ready to be solved using the finite element method [6], will be the main subject of this chapter.

2.1 Maxwell's Equations

Electromagnetic phenomena are governed at the macroscopic level by a set of fundamental equations called, Maxwell's equations, named after James Clerk Maxwell who published them in 1873. The equations relate various electric and magnetic quantities. In their point or differential form, the general time-varying Maxwell's equations are written as follows:

$$\nabla \times \vec{E} = \frac{-\partial \vec{B}}{\partial t} \tag{2.1}$$

$$\nabla \times \vec{H} = \frac{-\partial \vec{D}}{\partial t} + \vec{J} \tag{2.2}$$

$$\nabla \cdot \vec{D} = \rho \tag{2.3}$$

$$\nabla \cdot \vec{B} = 0 \tag{2.4}$$

All the electric and magnetic vector quantities are functions of space and time and are defined as follows:

$\vec{E}$ is the electric field intensity, in $volts/meter$

$\vec{H}$ is the magnetic field intensity, in $amperes/meter$

$\vec{D}$ is the electric flux density, in $coulombs/meter^2$

$\vec{B}$ is the magnetic flux density, in $webers/meter^2$

$\vec{J}$ is the electric current density, in $amperes/meter^2$

ρ is the electric charge density, in $coulombs/meter^3$.

The *equation of continuity* is another fundamental equation and can be written as:

$$\nabla \cdot \vec{J} = -\frac{\partial \rho}{\partial t} \tag{2.5}$$

The continuity equation specifies the conservation of charge.

Of the five equations above only three are independent. The remaining two can actually be derived from the independent equations and are thus called *auxilliary equations*. The independent equations are taken either to be 2.1, 2.2 and 2.3 or 2.1, 2.2 and 2.5.

Equation 2.2 is actually derived from the Ampere's law. The Ampere's law relates the line integral of the magnetic field vector $\vec{H}$ around a closed path to the enclosed current I, and it is given as

$$\oint \vec{H} \cdot d\vec{l} = I \tag{2.6}$$

Replacing the current I by the surface integral of the conduction-current density $\vec{J}$ over an area bounded by the path of integration of $\vec{H}$, and also adding a displacement-current density $\frac{\partial \vec{D}}{\partial t}$ (Maxwell's addition) to make it more general, the Ampere's law

now becomes

$$\oint \vec{H} \cdot d\vec{l} = \int_S \left(\vec{J} + \frac{\partial \vec{D}}{\partial t} \right) \cdot d\vec{S} \tag{2.7}$$

The above is the integral or *mesh* form of the Maxwell's equation derived from the Ampere's law. The differential or *point* form given in equation 2.2 is obtained by applying Stoke's theorem to 2.7.

Equation 2.1 is obtained in a similar way starting with the Faraday's law relating emf induced in a circuit to the time rate of change of the total magnetic flux linking the circuit. Equations 2.3 is derived from Gauss' law relating surface integral of the electric flux density to the enclosed charge. When Gauss' is applied to magnetic field equation 2.4 is easily derived. Each of the Maxwell's equation thus have integral as well as differential forms.

When the field quantities are time-invariant, we do have a case of a static field. In that case equations 2.1, 2.2 and 2.5 can be written as

$$\nabla \times \vec{E} = 0 \tag{2.8}$$

$$\nabla \times \vec{H} = \vec{J} \tag{2.9}$$

$$\nabla \cdot \vec{J} = 0 \tag{2.10}$$

whereas equations 2.3 and 2.4 remain the same. It can be observed from the above equations that in a static case there is no interaction of electric and magnetic fields and we can separately have an *electrostatic* case described by 2.3 and 2.8 or a *magnetostatic* case described by equations 2.4 and 2.9, with 2.10 being a natural consequence of 2.10 since vectorially divergence of a curl is always zero.

When the fields expressed in the Maxwell's equations are harmonically (sinusoidally) oscillating functions with a single frequency, we have a case of a *time-harmonic field*. By using the phasor representation, the time derivative $\partial/\partial t$ may be replaced by the factor $j\omega$ since $\partial e^{j\omega t}/\partial t = j\omega e^{j\omega t}$. Hence the Maxwell's equations in a time-harmonic form or for a steady-state sinusoidal time dependence can be written as:

$$\nabla \times \vec{E} = -j\omega \vec{B} \tag{2.11}$$

$$\nabla \times \vec{H} = j\omega\vec{D} + \vec{J} \tag{2.12}$$

$$\nabla \cdot \vec{D} = \rho \tag{2.13}$$

$$\nabla \cdot \vec{B} = 0 \tag{2.14}$$

where the time convention $e^{j\omega t}$ is used and suppressed.

2.2 Constitutive relations

The three independent Maxwell's equation decribed in the previous section have more unknowns than the number of equations. Hence the equations are *indefinite*. To make them *definite* the *constitutive relations* between the field quantities are specified. The *constitutive relations* are the relationships of $\vec{H}$ to $\vec{B}$ and of $\vec{D}$ to $\vec{E}$.

For a case of an electric field $\vec{E}$ applied to a material body, the resulting electric flux density can generally be written as:

$$\vec{D} = \epsilon_0\vec{E} + \vec{P} \tag{2.15}$$

where $\vec{P}$ is the dipole moment per unit volume of the created electric dipoles and $\epsilon_0 = 10^{-9}/36\pi$ farad/meter is the permittivity of vacuum. For linear media, the dipole moment per unit volume can be written as

$$\vec{P} = \epsilon_0\chi_e\vec{E} \tag{2.16}$$

where χ_e is a complex constant of proportionality called the electric susceptibility. The equation for $\vec{D}$ then becomes

$$\vec{D} = \epsilon_0\vec{E} + \vec{P} = \epsilon_0(1 + \chi_e)\vec{E} \tag{2.17}$$

$$= \epsilon\vec{E} = \epsilon_r\epsilon_0\vec{E} = (\epsilon' - j\epsilon'')\vec{E} \tag{2.18}$$

where $\epsilon = \epsilon_0(1 + \chi_e)$ is called the permittivity, and $\epsilon_r = \epsilon/\epsilon_0$, the dielectric constant or relative permittivity of the medium.

The constitutive relation for a magnetic case is defined as

$$\mu_0\vec{H} = \vec{B} - \mu_0\vec{M} \tag{2.19}$$

where $\vec{M}$ is the magnetic dipole polarization per unit volume and $\mu_0 = 4\pi \times 10^{-7}$ henry/meter, is the permeability of vacuum. For most material, $\vec{M}$ is linearly related to $\vec{H}$ by the equation

$$\vec{M} = \chi_m \vec{H} \tag{2.20}$$

where χ_m is called the magnetic susceptibility. Using the above equation, the constitutive relation now becomes

$$\vec{B} = \mu_0(\vec{M} + \vec{H}) = \mu_0(1 + \chi_m)\vec{H} = \mu\vec{H} \tag{2.21}$$

where $\mu = \mu_0(1 + \chi_m)$ is called the permeability of the medium which is complex in the presence of damping forces just like permittivity in the electric case. Permittivity and permeability for anisotropic materials are tensors rather than single numbers in the case of linear isotropic materials.

Another constitutive relation relates the conduction current density $\vec{J}$ to electric field $\vec{E}$ as

$$\vec{J} = \sigma\vec{E} \tag{2.22}$$

where σ is the electric conductivity of the medium.

2.3 Scalar and Vector Potentials

In a static electric case, it is seen from equation 2.8 that static electric field has a zero curl. In vector algebra, then, the static electric field can be expressed as a gradient of a scalar potential function Φ since curl of a gradient of a scalar function is identically zero. The electric field can thus be written as

$$\vec{E} = -\nabla\Phi \tag{2.23}$$

Substituting 2.23 into 2.3 and substituting $\vec{D} = \epsilon\vec{E}$ give

$$-\nabla \cdot \vec{E} = \nabla^2\Phi = -\frac{\rho}{\epsilon} \tag{2.24}$$

Equation 2.24 is the famous Poisson's equation. When $\rho = 0$, Poisson's equation reduces to Laplace's equation given as

$$\nabla^2 \Phi = 0 \tag{2.25}$$

Solution of electrostatic fields is most of the times facilitated by solving the Poisson's or Laplace's equation for the potential function Φ that satisfies the boundary conditions of the problem.

In magnetostatic problems the idea of potential is also applied. Since according to equation 2.4, the divergence of $\vec{B}$ is always zero, it can then be derived from the curl of a vector potential $\vec{A}$ since the divergence of the curl of a vector is identically zero. That is

$$\vec{B} = \nabla \times \vec{A} \tag{2.26}$$

Making use of the constitutive relation $\vec{B} = \mu \vec{H}$ and substituting 2.26 into 2.9 gives

$$\nabla \times \mu \vec{H} = \nabla \times \vec{B} = \nabla \times \nabla \times \vec{A} = \mu \vec{J} \tag{2.27}$$

which by the use of the vector identity $\nabla \times \nabla \times \vec{A} = \nabla \nabla \cdot \vec{A} - \nabla^2 \vec{A}$, and using the *gauge condition* $\nabla \cdot \vec{A} = 0$, becomes

$$\nabla^2 \vec{A} = -\mu \vec{J} \tag{2.28}$$

The above equation is a vector Poisson's equation which can be decoupled into scalar Poisson's equation for the vector components only in a rectangular coordinate system.

2.4 Wave Equations

Using the costitutive relations discussed before, either electric field, $\vec{E}$ or magnetic field, $\vec{H}$ can be eliminated from the Maxwell's curl equations 2.1 and 2.2 to give rise to a second order partial differential equation of only one unknown. For example, when the current density, $\vec{J}$, is assumed to be zero, the elimination of $\vec{H}$ from the Maxwell's curl equations yields

$$\nabla \times \nabla \times \vec{E} = -\mu\epsilon \frac{\partial^2 \vec{E}}{\partial t^2} \tag{2.29}$$

Upon expanding $\nabla \times \nabla \times \vec{E}$ it becomes

$$\nabla\nabla \cdot \vec{E} - \nabla^2 \vec{E} = -\mu\epsilon \frac{\partial^2 \vec{E}}{\partial t^2} \tag{2.30}$$

With the assumption that $\rho = 0$ and ϵ is constant; $\nabla \cdot \vec{E} = 0$, and hence the above equation becomes

$$\nabla^2 \vec{E} - \mu\epsilon \frac{\partial^2 \vec{E}}{\partial t^2} = 0 \tag{2.31}$$

which is a three-dimensional wave equation. The velocity of propagation v is equal to $1/\sqrt{\mu\epsilon}$.

For a case of a field that changes harmonically with time, the wave equation becomes

$$\nabla^2 \vec{E} + k^2 \vec{E} = 0 \tag{2.32}$$

where $k^2 = \omega^2 \mu\epsilon$, and k is the wave number. The above equation is also referred to as the Helmhotz equation. The wave eqution in terms of the magnetic field, $\vec{H}$. is of the same form.

In a medium with finite conductivity, the conduction current density $\vec{J} = \sigma \vec{E}$ exists and the corresponding wave equation in terms of the $\vec{E}$ field can be shown to be

$$\nabla^2 \vec{E} - \mu_0 \sigma \frac{\partial \vec{E}}{\partial t} - \mu_0 \epsilon_0 \frac{\partial^2 \vec{E}}{\partial t^2} = 0 \tag{2.33}$$

where it is assumed that the permittivity and permeability of the conducting medium are eaqual to those of a free space. The above equation is also satisfied by the magnetic field $\vec{H}$.

For the time-harmonic case, the Helmhotz equation in this case can be written as

$$\nabla^2 \vec{E} + \omega^2 \mu_0 \epsilon_0 \left(1 - j\frac{\sigma}{\omega\epsilon_0}\right) \vec{E} = 0 \tag{2.34}$$

For good conductors such as metals, the conduction current $\sigma\vec{E}$ is very much larger than the displacement current $\omega\epsilon_0\vec{E}$ and the latter can thus be safely neglected to give rise to the following simplified diffusion equation

$$\nabla^2\vec{E} - \mu_0\sigma\frac{\partial\vec{E}}{\partial t} = 0 \tag{2.35}$$

for the time-domain case and

$$\nabla^2\vec{E} - j\omega\mu_0\sigma\vec{E} = 0 \tag{2.36}$$

for the time-harmonic case.

2.5 Boundary conditions

A solution to an electromagnetic problem, just as is the case with any problem that involves solution of differential equations, is unique only if the solution takes into consideration the boundary conditions associated with the problem. The boundary conditions describe the behaviour of the field around the boundary of the problem.

In numerical solution of differential equations such as using the finite element method, boundaries are necessary to limit the size of the problem to make it solvable in limited computer resources. Where a natural boundary does not exist, such as in the solution of antenna problems, artificial (absorbing or radition) boundaries are used to simulate propagation of waves to infinity. This section will discuss various boundary conditions often encountered in solving electromagnetic problems.

2.5.1 Boundary at the interface of two dielectric media

Consider two media with parameters ϵ_1, μ_1 and ϵ_2, μ_2 as shown in Figure 2.1(a). In the absence of surface charge on the boundary placed in the middle of the coin-shaped volume as depicted in Figure 2.1(b), the integral of the displacement flux, $\vec{D}$, in the limit as h tends to zero, is

$$\lim_{h\to 0}\oint_S \vec{D}\cdot d\vec{S} = D_{2n}\Delta S - D_{1n}\Delta S = 0 \tag{2.37}$$

or

$$D_{2n} = D_{1n} = \vec{n}\cdot\vec{D}_2 = \vec{n}\cdot\vec{D}_1 \tag{2.38}$$

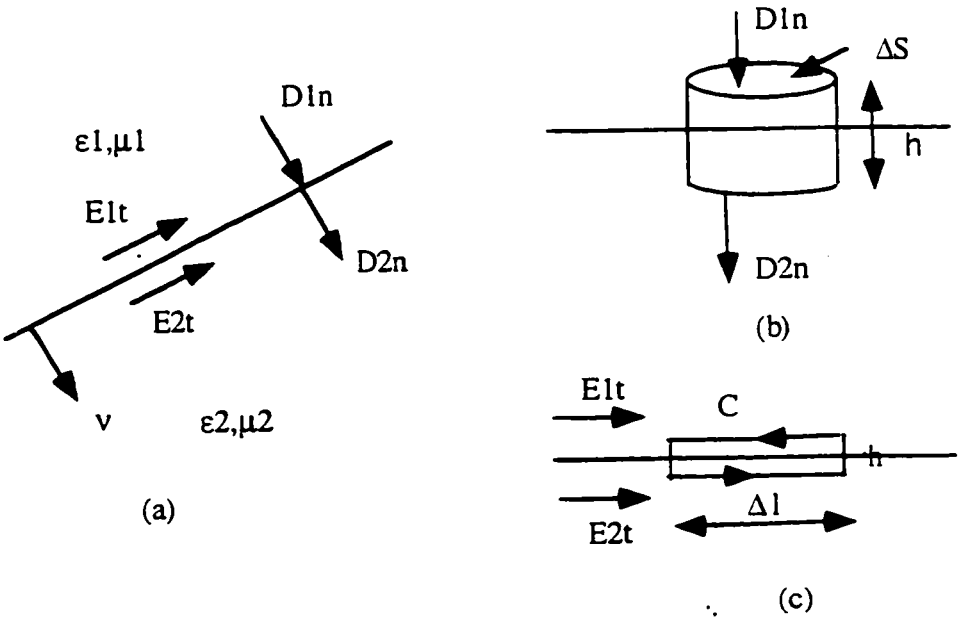

Figure 2.1: Boundary at the interface of two media

where n denotes the normal component. What the above equation states is that the electric flux linnes are continuous in the direction normal to the boundary. Similar results hold for magnetic flux lines. That is,

$$B_{2n} = B_{1n} = \vec{n} \cdot \vec{B}_2 = \vec{n} \cdot \vec{B}_1 \tag{2.39}$$

The boundary conditions for the tangential components of the electric field and magnetic field are obtained by considering the integral of the electric and magnetic field respectively over a contour C enclosing the boundary as depicted in Figure 2.1(c). When the width h of the contour is made to approach zero, the magnetic flux flowing through the contour must vanish,

$$\lim_{h \to 0} \oint_C \vec{E} \cdot d\vec{l} = \lim_{h \to 0} -j\omega \int_S \vec{B} \cdot d\vec{S} = E_{2t}\Delta l - E_{1t}\Delta l = 0 \tag{2.40}$$

or

$$E_{2t} = E_{1t} \tag{2.41}$$

Likewise, as $h \rightarrow 0$, the total displacement current vanishes.

$$\lim_{h\to 0} \oint_C \vec{H} \cdot d\vec{l} = \lim_{h\to 0} -j\omega \int_S \vec{D} \cdot d\vec{S} = H_{2t}\Delta l - H_{1t}\Delta l = 0 \tag{2.42}$$

or

$$H_{2t} = H_{1t} \tag{2.43}$$

where t denotes the components tangential to the boundary surface. The above relations state that the tangential electric and magnetic field components are continuous across the boundary. Mathematically, the boundary conditions above can be better expressed as,

$$\hat{n} \times (\vec{E}_2 - \vec{E}_1) = 0 \tag{2.44}$$

$$\hat{n} \cdot (\vec{D}_2 - \vec{D}_1) = 0 \tag{2.45}$$

$$\hat{n} \times (\vec{H}_2 - \vec{H}_1) = 0 \tag{2.46}$$

$$\hat{n} \cdot (\vec{B}_2 - \vec{B}_1) = 0 \tag{2.47}$$

where $\hat{n}$ is the unit vector normal to the surface pointing from medium 1 into medium 2.

In the above relations, the assumption was that neither surface currents nor surface charges exist at the interface. In the presence of surface current density $\vec{J}_s$ and surface charge density ρ_s, the boundary conditions can now be written as:

$$\hat{n} \cdot (\vec{D}_2 - \vec{D}_1) = \rho_s \tag{2.48}$$

$$\hat{n} \times (\vec{H}_2 - \vec{H}_1) = \vec{J}_s \tag{2.49}$$

2.5.2 Boundary at a perfectly conducting surface

A perfect conductor is know to be not capable of sustaining any field inside. hence on the surface of a perfect conductor, the field must vanish. That is

$$\hat{n} \times \vec{E} = 0 \tag{2.50}$$

$$\hat{n} \cdot \vec{B} = 0 \tag{2.51}$$

where $\vec{E}$ and $\vec{B}$ are fields exterior to the conductor and $\hat{n}$ points away from the conductor. This boundary can always support a surface current ($\vec{J}_s = \hat{n} \times \vec{H}$) and a surface charge ($\rho_s = \hat{n} \cdot \vec{D}$)

2.5.3 Radiation conditions

For unbounded problems where the outer boundary is at infinity, a problem domain is truncated using an artificial radiation boundary. The boundary conditions at the radiation boundary are such as to simulate the propagation of waves to infinity. For that reason, such an artificial boundary is also referred to as an "absorbing" boundary since it "absorbs" the electromagnetic field waves incident on it.

The most simple radiation boundary is the one that satisfies the Sommerfeld radiation condition [6], which for general three-dimensional fields can be written as

$$\lim_{r\to\infty} r\left[\nabla \times \begin{pmatrix} \vec{E} \\ \vec{H} \end{pmatrix} + jk_0\hat{r} \times \begin{pmatrix} \vec{E} \\ \vec{H} \end{pmatrix}\right] = 0 \tag{2.52}$$

where $r = \sqrt{x^2 + y^2 + z^2}$. This radiation condition can only be applied with the assumption that the sources and the objects are all enclosed within the boundary which itself should be in the far field.

To understand the derivation of the Sommerfeld radiation condition let us first discuss a two-dimensional case. If a scatterer or radiator is within a finite distance from the origin, the scattered/radiated field, ϕ^{sc}, in the far zone has the asymptotic form [6]

$$\phi^{sc} = A(\varphi)\frac{e^{-jk\rho}}{\sqrt{\rho}} \tag{2.53}$$

where $\rho = \sqrt{x^2 + y^2}$ and $A(\varphi)$ is a function independent of ρ. The partial derivative of 4.33 with respect to ρ yields

$$\frac{\partial\phi^{sc}}{\partial\rho} = \left(-jk - \frac{1}{2\rho}\right)A(\varphi)\frac{e^{-jk\rho}}{\sqrt{\rho}} = \left(-jk - \frac{1}{2\rho}\right)\phi^{sc} \tag{2.54}$$

Equation 4.34 is the first-order absorbing boundary condition for a two-dimensional case.

In a general form, it can be shown [7] that the more accurate asymptotic expansion of the Helmhotz equation for the scattered/radiated field satisfying the Sommerfeld radiation condition is given by

$$\phi(\rho,\varphi) = H_0^{(2)}(k\rho)\sum_{n=0}^{\infty}\frac{f_n(\varphi)}{\rho^n} + H_1^{(2)}(k\rho)\sum_{n=0}^{\infty}\frac{g_n(\varphi)}{\rho^n} \tag{2.55}$$

where $H_0^{(2)}$ and $H_1^{(2)}$ are the zeroth- and first-order hankel functions of the second kind, respectively. Using the asymptotic form for $H_0^{(2)}$ and $H_1^{(2)}$, equation 2.55 can be written as

$$\phi^{sc} = \frac{e^{-jk\rho}}{\sqrt{\rho}}\sum_{n=0}^{\infty}\frac{a_n(\varphi)}{\rho^n} \tag{2.56}$$

which is the Wilcox expansion of the wave equation [8]. Taking partial derivative of 2.56 with respect to ρ yields

$$\frac{\partial\phi^{sc}}{\partial\rho} = \left(-jk - \frac{1}{2\rho}\right)\phi^{sc} - \frac{e^{-jk\rho}}{\sqrt{\rho}}\sum_{n=1}^{\infty}\frac{na_n(\varphi)}{\rho^{n+1}} \tag{2.57}$$

If the terms of order $O(\rho^{-5/2})$ or higher are neglected, the first order condition 4.34 results.

Accuracy and computational efficiency demand that the radiation boundary should be placed much closer to the object to reduce the size of the problem domain while at the same time limiting the reflection of the outgoing field back into the problem domain. Higher-order radiation conditions, although more complex to implement, become useful in that case.

For a three-dimensional case, it can be shown [9] that on a spherical surface enclosing a radiating source, the electromagnetic fields satisfy the higher order radiation condition,

$$\mathcal{B}_m\begin{pmatrix}\vec{E}\\ \vec{H}\end{pmatrix} = O(r^{-2m-1}) \qquad m = 1,2,3,\cdots \tag{2.58}$$

where $O(r^{-2m-1})$ denotes terms of order $-2m-1$ and the operator $\mathcal{B}_m$ is given by

$$\mathcal{B}_1(\vec{E}) = \hat{r}\times\nabla\times\vec{E} - jk\vec{E}_t + (s-1)\nabla_t E_r \tag{2.59}$$

$$\mathcal{B}_2(\vec{E}) = \hat{r} \times \nabla \times \vec{E} - jk\vec{E}_t - \frac{r}{2(1+jkr)} \times \{\nabla \times [\hat{r}(\nabla \times \vec{E})_r] + (s-1)\nabla_t(\nabla \cdot \vec{E}_t) + jk(2-s)\nabla_t E_r\} \quad (2.60)$$

for $m = 1, 2$. Neglecting $O(r^{-2m-1})$, we obtain the approximate absorbing boundary conditions, $\mathcal{B}_m(\vec{E}) = 0$. The first- and second-order absorbing boundary conditions can readily be obtained by equating to zero the expressions given in equations refrdc and refrdc1, respectively.

s is an arbitrary number which when set to 1, equation 2.59 reduces to the Sommerfeld radiation condition. The optimum choice for s is shown to be $s = \frac{1}{2}$ [6], but that leads to nonsymmetric system of equations when applied to the finite element formulation as the first-order derivative ($\nabla_t E_r^{sc}$) is retained. Symmetric systems of equations are desirable as they allow only upper or lower triangular matrices to be stored in memory reducing considerably the computer memory requirement. For that purpose a choice of $s = 1$, is a compromise for 2.59 and $s = 2$ is suitable for 2.60 [6].

The parameter s is generally set to simplify computational complexity while not sacrificing the ability of the radiation boundary to simulate an infinite domain. The subscript r denotes the radial component while subscript t denotes the transverse component with respect to $\hat{r}$, the outer vector normal to the boundary.

2.6 The Basics of the Finite Element Method

The finite element method, FEM, has been widely used in engineering and science in the approximate solution of boundary-value problems that cannot be solved analytically. There are several references about finite element and its application the most popular of which is the book written by Zienkiewicz and Taylor [10]. In this chapter we will try to give a brief introduction to the finite element method with emphasis to the way the method was used in this work.

There are two classical methods of solving boundary-value problems, namely, Rayleigh-Ritz variational method and Galerkin's method. Those two classical methods form the basis of the finite element method as implemented today.

The Rayleigh-Ritz method is a variational approach to a solution of a differential equation

$$L\phi = f \quad (2.61)$$

in a problem domain Ω, subject to boundary conditions on the boundary, Γ. L above is a differential operator, f is the excitation function and ϕ is the unknown variable. In electromagnetics, equations that take the form of equation 2.61, are so many. For example, Poisson equation, Laplace equation, Helmhotz equation etc. The boundary conditions of the problem range from simple Dirichlet (forced) and Neumann boundary conditions, to complicated impedance and radiation boundary conditions of different orders.

Solution of equation 2.61 by Rayleigh-Ritz method relies on the computation of the functional associated with the problem. The solution is given by the values of the unknown variables that minimize the functional. If the operator L is self-adjoint, that is,

$$\langle L\phi, \psi \rangle = \langle \phi, L\psi \rangle \tag{2.62}$$

and positive definite, that is,

$$\langle L\phi, \phi \rangle \begin{cases} > 0 & \phi \neq 0 \\ = 0 & \phi = 0 \end{cases} \tag{2.63}$$

then the solution to 2.61 can be obtained by minimizing the functional [11]

$$F(\tilde{\phi}) = \frac{1}{2}\langle L\tilde{\phi}, \tilde{\phi} \rangle - \frac{1}{2}\langle \tilde{\phi}, f \rangle - \frac{1}{2}\langle f, \tilde{\phi} \rangle \tag{2.64}$$

with respect to $\tilde{\phi}$, where $\tilde{\phi}$ denotes the trial function. The angle brackets $\langle\rangle$ denote inner product which is defined as

$$\langle \phi, \psi \rangle = \int_\Omega \phi \psi^* \, d\Omega \tag{2.65}$$

The trial function is given as

$$\tilde{\phi} = \sum_{j=1}^{N} c_j v_j = \{c\}^T \{v\} = \{v\}^T \{c\} \tag{2.66}$$

where v_j are the expansion functions and c_j are constant undetermined coefficients.

When the trial function is substituted in 2.64 the partial derivatives with respect to c_i should vanish at minimum $F(\tilde{\phi})$, that is

$$\frac{\partial F}{\partial c_i} = \frac{1}{2}\sum_{j=1}^{N} c_j \int_\Omega (v_i L v_j + v_j L v_i) \, d\Omega - \int_\Omega v_i f \, d\Omega \tag{2.67}$$

$$= 0 \quad i = 1, 2, 3, \cdots, N \tag{2.68}$$

The resulting system of algebraic equations is of the form

$$[S]\{c\} = \{b\} \tag{2.69}$$

which when solved the values of c_i would reflect the approximate solution of the differential equation.

Now, let us discuss the underlying theory behind the Galerkin's method.

Suppose $\tilde{\phi}$ is an approximate solution to equation 2.61, the residual, r is defined as,

$$r = L\tilde{\phi} - f \neq 0 \tag{2.70}$$

The best approximation for $\tilde{\phi}$ is the one that minimizes the residual. By the Galerkin's method, same as other weighted residual methods, the following condition is enforced:

$$R_i = \int_\Omega w_i r \, d\Omega = 0 \tag{2.71}$$

where R_i is the weighted residual and w_i is the weighting function.

The Galerkin's method differs from other weighted residual methods by choosing the weighting functions w_i same as the expansion functions v_i. Thus, the residual then becomes,

$$R_i = \int_\Omega (v_i L\{v\}^T\{c\} - v_i f) \, d\Omega = 0 \quad i = 1, 2, 3, \cdots, N \tag{2.72}$$

which leads to a system of algebraic equations as in the Ritz method.

Both Ritz and Galerkin methods requires one to find a suitable trial function defined over the entire domain of the problem. For some complex two- and three-dimensional problems, that is a formidable task. To alleviate that problem, the problem domain is discretized into smaller subdomains (elements), and trial solutions are found for those elements. That simplifies the process considerably.

For example, in a one-dimensional case, the line joining the first point (node) with the last point can be divided into subsections. Assuming the line to be stretching along the x-axis, the trial solution, assumed linear, can be written as

$$\tilde{\phi} = \phi_i \frac{x_{i+1} - x}{x_{i+1} - x_i} + \phi_{i+1} \frac{x - x_i}{x_{i+1} - x_i} \tag{2.73}$$

for $x_i \leq x \leq x_{i+1}$ and $i = 1, 2, 3, \cdots, N$. Where N is the number of nodes on the line.

When boundary conditions are applied, the unknowns can be computed using the Ritz or Galerkin's method.

The technique mentioned above is known as the **finite element method**, FEM. The FEM solution procedure that uses the Ritz method is known as the **variational finite element method** while the one that employs the Galerkin's method is known as the **Galerkin finite element method**. Furthermore, the traditional FEM attaches the degrees of freedom on the nodes making up the elements hence it is also known as the **nodal finite element method**. The FEM solution that attaches the degrees of freedom to the edges of the elements is known as the **edge finite element method** or **vector finite element method**.

The FEM trial solution can be linear or of higher order. The higher the order the better the accuracy of the solution. While for one-dimensional problems the elements are line segments, for two-dimensional problems, triangular or rectangular elements are often used. However, triangular elements are better in modelling irregular geometries. For three-dimensional problems tetrahedra, triangular prisms or rectangular bricks are used to discretize the geometry. The general rule of thumb is, the finer the elements the higher the accuracy.

The trial function for an element is defined as

$$\tilde{\phi}^e = \sum_{j=1}^{n} N_j^e \phi_j^e \tag{2.74}$$

where n is the number of nodes in the element, ϕ_j^e is the value of ϕ at node j of the element, and N_j^e is the FEM interpolation function which is also known as the basis or expansion function. N_j^e is such that it is nonzero only within element e. For a triangular element, the linear nodal interpolation function can be written as,

$$N_j^e(x,y) = \frac{1}{2\Delta^e}(a_j^e + b_j^e x + c_j^e y) \quad j = 1,2,3 \tag{2.75}$$

where

$$\begin{aligned}
a_1^e &= x_2^e y_3^e - y_2^e x_3^e; \quad b_1^e = y_2^e - y_3^e; \quad c_1^e = x_3^e - x_2^e \\
a_2^e &= x_3^e y_1^e - y_3^e x_1^e; \quad b_2^e = y_3^e - y_1^e; \quad c_2^e = x_1^e - x_3^e \\
a_3^e &= x_1^e y_2^e - y_1^e x_2^e; \quad b_3^e = y_1^e - y_2^e; \quad c_3^e = x_2^e - x_1^e
\end{aligned}$$

and the area of the eth element is given as,

$$\Delta^e = \frac{1}{2}\begin{vmatrix} 1 & x_1^e & y_1^e \\ 1 & x_2^e & y_2^e \\ 1 & x_3^e & y_3^e \end{vmatrix} = \frac{1}{2}(b_1^e c_2^e - b_2^e c_1^e)$$

x_j^e and y_j^e denote the coordinates of the jth node of the eth element.

The interpolation functions have the property that,

$$N_i^e(x_j^e, y_j^e) = \delta_{ij} = \begin{cases} 1 & i = j \\ 0 & i \neq j \end{cases} \tag{2.76}$$

and hence at node i, ϕ^e assumes the nodal value ϕ_i^e.

For a three-dimensional tetrahedral element, the linear nodal interpolation function is written as,

$$N_i^e(x, y, z) = \frac{1}{6V^e}(a_i^e + b_i^e x + c_i^e y + d_i^e z) \tag{2.77}$$

where the coeffients a_i^e, b_i^e, c_i^e and d_i^e can be generally expressed as:

$$\begin{aligned} a_i^e &= (-i)^{i+1}\left[x_{i+1}(y_{i+2}z_{i+3}) - z_{i+2}y_{i+3}) + x_{i+2}(y_{i+3}z_{i+1}) - z_{i+3}y_{i+1}\right) \\ &\quad + x_{i+3}(y_{i+1}z_{i+2}) - z_{i+1}y_{i+2})] \qquad (2.78) \\ b_i^e &= (-i)^{i}(y_{i+1}z_{i+2} - z_{i+1}y_{i+2} + y_{i+2}z_{i+3} - z_{i+2}y_{i+3} \\ &\quad + y_{i+3}z_{i+1} - z_{i+3}y_{i+1}) \qquad (2.79) \\ c_i^e &= (-i)^{i+1}(x_{i+1}z_{i+2} - z_{i+1}x_{i+2} + x_{i+2}z_{i+3} - z_{i+2}x_{i+3} \\ &\quad + x_{i+3}z_{i+1} - z_{i+3}x_{i+1}) \qquad (2.80) \\ d_i^e &= (-i)^{i}(x_{i+1}y_{i+2} - y_{i+1}x_{i+2} + x_{i+2}y_{i+3} - y_{i+2}x_{i+3} \\ &\quad + x_{i+3}y_{i+1} - y_{i+3}x_{i+1}) \qquad (2.81) \end{aligned}$$

where i proceeds modulo 4 and represents tetrahedron node numbers. The volume of the element is given as,

$$V^e = \frac{1}{6}\begin{vmatrix} 1 & 1 & 1 & 1 \\ x_1^e & x_2^e & x_3^e & x_4^e \\ y_1^e & y_2^e & y_3^e & y_4^e \\ z_1^e & z_2^e & z_3^e & z_4^e \end{vmatrix}$$

Same as the two-dimensional case, the interpolation function have the property that.

$$N_i^e(x_j^e, y_j^e, z_j^e) = \delta_{ij} = \begin{cases} 1 & i = j \\ 0 & i \neq j \end{cases} \tag{2.82}$$

In this work, the Galerkin finite element method is used through out.

2.7 Problems of applying the finite element method in electromagnetics

Although the traditional node-based finite element method is known to work well in modelling many problems of interest in electromagnetics, it is known to suffer from some limitations and shortfalls. We will discuss in this section the most serious problems encountered.

2.7.1 Implementation of interface boundary conditions

As mentioned in the previous sections, the FEM solution is only unique when appropriate boundary and material interface conditions are included into the formulation. At the interface between two different media, the following continuity conditions need to be enforced explicitly:

$$\hat{n} \times \vec{E}^+ = \hat{n} \times \vec{E}^- \tag{2.83}$$

$$\hat{n} \times \vec{H}^+ = \hat{n} \times \vec{H}^- \tag{2.84}$$

The above conditions can also be written as

$$\frac{1}{\mu_r^+}\hat{n} \times (\nabla \times \vec{E}^+) = \frac{1}{\mu_r^-}\hat{n} \times (\nabla \times \vec{E}^-) \tag{2.85}$$

$$\frac{1}{\epsilon_r^+}\hat{n} \times (\nabla \times \vec{H}^+) = \frac{1}{\epsilon_r^-}\hat{n} \times (\nabla \times \vec{H}^-) \tag{2.86}$$

When the continuity conditions 2.83 and 2.84 are imposed the natural conditions 2.85 and 2.86 are automatically satisfied. The imposition of the continuity conditions at the interface is normally done by assigning single value of the unknown

field at each node placed right on the interface. By doing so, the continuity of the tangential components of the field is appropriately enforced but unfortunately so is the continuity of the normal components of the field. That is in conflict with the actual conditions for the normal field component on the interface given as

$$\hat{n} \cdot (\epsilon_r^+ E^+) = \hat{n} \cdot (\epsilon_r^- E^-) \quad (2.87)$$

$$\hat{n} \cdot (\mu_r^+ H^+) = \hat{n} \cdot (\mu_r^- H^-) \quad (2.88)$$

But looking closely, we see that conditions 2.87 and 2.88 have the same form as the natural conditions 2.85 and 2.86. Since the latter get satisfied automatically it is reasonable to assume that the former also get satisfied to some degree. The best way to ensure that, is to use fine discretization at the interface. That technique was suggested and tested by Ferrari and Naidu [1] and it was found that with fine discretization, the normal component of the field changes rapidly across the interface just as demanded by 2.87 and 2.88. The only drawback of this technique is that with fine discretization, the number of unknowns increases considerably thereby increasing the computer storage requirement as well as the time required to obtain the solution.

Another approach which is a little more difficult to implement is to introduce two nodes, side by side, at the interface, and impose explicitly all the continuity conditions for the tangential as well as the normal field components on either side of the boundary.

2.7.2 Field singularities on sharp edges and tips

Practical problems of interest in electromagnetics in most cases consist of sharp conducting and/or material edges and tips. It has been shown [2]-[5] that some of the field components assume infinite values at sharp edges and tips. In that situation it becomes impossible to specify the boundary conditions at the tip and that causes a problem in field modelling using the node-based FEM.

To have a better understanding of the problem of field singularities on edges and tips, take an example of a conducting wedge of angle α. The behaviour of the field around the edge can be described same as for the case of a static field where the

electric field can be expressed as $\vec{E} = -\nabla o$. where o denotes the electric scalar potential satisfying the Poisson equation

$$\frac{1}{\rho}\frac{\partial}{\partial \rho}\left(\rho\frac{\partial o}{\partial \rho}\right) + \frac{1}{\rho^2}\frac{\partial^2 o}{\partial \varphi^2} = 0 \tag{2.89}$$

whose solution is given by

$$o = A\rho^{\nu}\sin\nu(\varphi + \varphi_0) \tag{2.90}$$

where A, ν, and φ_0 are the constants to be determined, ρ is the radial distance from the tip of the wedge, and φ is the azimuthal angle measured from one side of the wedge. The electric field can then be expressed as

$$\vec{E} = -A\nu\rho^{\nu-1}[\hat{\rho}\sin\nu(\varphi + \varphi_0) + \hat{\varphi}\cos\nu(\varphi + \varphi_0)] \tag{2.91}$$

Using the fact that the tangential electric field iz zero on the conducting surface. the costants are determined as

$$\begin{aligned} \varphi_0 &= -\alpha \\ \nu &= \frac{\pi}{2\pi - \alpha} \end{aligned} \tag{2.92}$$

and the corresponding magnetic field is then given as

$$H_z = j\omega\epsilon A\rho^{\nu}\cos\nu(\varphi - \alpha) \tag{2.93}$$

The analysis is similar if we start with the magnetic field expressed as $\vec{H} = -\nabla\psi$. ψ being the magnetic potential satisying 2.89.

From equation 2.91, it is clear that when the wedge angle is less than π, ν is less than 1, and therefore the transverse components of $\vec{E}$ and $\vec{H}$ are singular at the edge although the field components tangential to the edge remain finite.

The singularity problem is also seen to occur with dielectric edges [3]. In that case the degree of singularity is dependent on the permittivity for the electric field and on the permeability for the magnetic field. In other words, electric field is never singular on a magnetic edge, nor is the magnetic field on an dielectric edge.

As it has been already evident, one of the solution around the singularity problem discussed above is to use electric field formulation where there are magnetic edges and magnetic field formulation in a situation involving dielectric edges. The other

solution used is to round off the edges and tips so that sharp edges are eliminated. This approximates the edges and it is expected that the error introduced by slight round off will be negligible. The other approach is to use special interpolation functions based on the known behaviour of the field around the edges and tips. But that complicates the formulation.

2.7.3 Problem with spurious solutions

As pointed out earlier, one of the major problems encountered with the traditional node-based FEM is the emergence of spurious non-physical solutions. The cause of the spurious solutions is the failure of the node-based FEM solutions to staisfy the divergence condition: $\nabla \cdot (\mu \vec{H}) = 0$ for the magnetic field and $\nabla \cdot (\epsilon \vec{E}) = -\nabla \cdot \vec{J}/j\omega$ for the electric field, which reduces to $\nabla \cdot (\epsilon \vec{E}) = 0$ in the source free region.

In the derivation of the vector Helmhotz equation for the time-harmonic field, the divergence conditions are implicitly satisfied but the problem arises in the choice of the interpolatory functions used with node-based FEM. For the divergence condition to be satisfied, the interpolatory functions need to be doubly defferentiable. That is, the interpolatory functions and their derivatives have to be continuous. But that is not the case.

In the FEM solution only the interpolatory functions are required to be continuous but their derivatives are not required to be continuous. The solution so obtained therefore only satisfies the governing differential equations in a weak sense and it is therefore just a weak solution. For that reason, the solution may well fail to satisfy the divergence condition and in that case the solution is termed as *spurious* or non-physical solution.

Several approaches have been tried to avoid spurious solutions, such as the use of interpolatory functions that have continuos derivatives, and the use of a penalty term that exclusively enforces the divergence condition. The above methods complicates the solution and they are not suitable in most cases.

One of the simplest techniques to avoid the problem of spurious solutions is to first compute the electric field and then compute the magnetic field using the Maxwell's equations and vice versa. In this way, even though the first computed field may be corrupted with spurious solutions, the field computed using the Maxwell's equations will

be guaranteed to satisfy the divergence condition. The most appropriate technique to avoid the problem of spurious solutions is to use a different kind of basis functions, called vector (or edge) basis functions. The discussion of the implementation of the vector basis functions is discussed in Chapter 4.

Chapter 3

Frequency Domain Analysis of Coaxially Driven Axisymmetric Microwave Structures

The literature is full of frequency domain analyses of microwave structures for both closed and open problems. However, analyses of microwave structures that are driven through coaxial cables has never been complete and accurate enough to faithfully model them in the way they are practically realized.

Frequency domain analysis of the coaxial feed itself as well as coaxial discontinuities has been attempted by many researchers [12]-[15]. Their analysis, however, would only apply to cases where the input and output ports of the driven structures are adapted for coaxial line connection. In other words, it would not apply to general coaxial antenna structures radiating in an open region with only one coaxial input port.

Analyses like in [16] dealing with radiating structures in frequency domain are many. The major shortcoming of those studies is the use of approximated feeds such as delta gap voltage or field functions or TEM frill generators, rather than the actual coaxial feed as is practically realized.

This chapter is devoted to the implementation of the nodal finite element method

(FEM), in the frequency domain analysis of axisymmetric coaxial microwave structures of various output configurations. The analysis sets out to overcome the above-mentioned shortcomings by introducing a way of dealing with open boundaries and accurately modelling the coaxial feed.

Although here the nodal FEM is used, the choice of the method of formulation using the azimuthal component of the magnetic field does not suffer from the problem of not treating well the material interface boundary conditions described in the previous chapter. The computed magnetic field component is always tangential to the material interfaces and due to axial symmetry and the method of excitation the magnetic field component normal to the field is always zero and we need not bother about it. Moreover, the choice of using magnetic field (as explained in the previous chapter) has the advantage of avoiding singularities on sharp dielectric edges and tips and it is also easy to implement boundary conditions especially on the conducting edges using the tangential electric field.

Coaxial microwave devices represent a very large class of structures of immense use in microwave engineering. Hence, this analysis may be found useful in many practical situations. Examples of the application of this analysis to practical problems are also provided in this chapter.

3.1 The Method

The method employed is as provided in our paper [17]. Consider an axisymmetric problem configuration in the sense that the geometry exhibits cylindrical symmetry in the azimuthal (ϕ) direction and the excitation is coaxial. The field in such a configuration may only vary in the radial (r) and axial (z) directions but must be independent of ϕ, i.e $\frac{\partial}{\partial \phi} = 0$.

The field around such a geometry is governed by the Maxwell's equations:

$$\nabla \times \vec{H} = (\sigma + j\omega\epsilon)\vec{E} \tag{3.1}$$

$$\nabla \times \vec{E} = -j\omega\mu\vec{H} \tag{3.2}$$

where the usual notation applies.

When electric field, E, is eliminated from the two Maxwell's curl equations. the

following vector equation results:

$$\nabla \times \nabla \times \vec{H} = -j\omega\mu(\sigma + j\omega\epsilon)\vec{H} \tag{3.3}$$

For this type of problem configuration we prefer to use cylindrical coordinates. With the assumptions made above, the field components H_z and H_r are all zero and thus equation 3.3 simplifies to a scalar form as:

$$-\frac{\partial}{\partial z}\left(\frac{\partial H_\phi}{\partial z}\right) - \frac{\partial}{\partial r}\left(\frac{1}{r}\frac{\partial}{\partial r}(rH_\phi)\right) = -j\omega\mu(\sigma + j\omega\epsilon)H_\phi \tag{3.4}$$

Letting $Y = (\sigma + j\omega\epsilon)^{-1}$ and $Z = j\omega\mu$, equation 3.4 can be written as,

$$Y\left[-\frac{\partial}{\partial z}\left(\frac{\partial H_\phi}{\partial z}\right) - \frac{\partial}{\partial r}\left(\frac{1}{r}\frac{\partial}{\partial r}(rH_\phi)\right)\right] + ZH_\phi = 0 \tag{3.5}$$

Now equation 3.5 is to be solved for H_ϕ in the problem domain subject to the boundary conditions of the problem. Direct solution of H_ϕ is to be made in this case.Thorough investigation of the method introduced in [16] has shown that there are more advantages gained in solving for the magnetic field, H_ϕ rather than rH_ϕ. The H_ϕ formulation simplifies a lot the working out of the associated integrals compared to the method that solves for rH_ϕ. The H_ϕ formulation used, further makes it possible to go around the singularity at $r = 0$, which was unavoidable in the rH_ϕ formulation used in [16]. The H_ϕ formulation used does not preserve the symmetry of the system matrix, a factor that is not so important if in solving the system of equations, one uses sparse matrix routines that do not care about the symmetry of the system.

Using the finite element, Galerkin formulation, equation 3.5 is discretized by first assuming a trial solution for H_ϕ for the kth element consisting of n nodes, as:

$$H_\phi^{(k)} \approx \sum_{j=1}^{n} u_j N_j^{(k)}(r,z) = U^{(k)}(r,z) \tag{3.6}$$

where u_j are unknown complex constants, N_j are real-valued FEM interpolatory functions, and U represents the approximate nodal values of the H_ϕ. The definition of N_j makes it possible for the undetermined coefficients, u_j, to reflect values of U when solved.

By the Galerkin formulation, the expansion and testing of equation 3.5 is carried out using equation 3.6 to yield.

$$\begin{aligned}\int\int_{(k)} \Bigg[& Y \frac{\partial N_i}{\partial r} \frac{\partial U^{(k)}}{\partial r} + Y \frac{\partial N_i}{\partial z} \frac{\partial U^{(k)}}{\partial z} \\ & + \frac{Y}{r} \frac{\partial N_i}{\partial r} U^{(k)} + Z N_i U^{(k)} \Bigg] \, dr dz \\ = & \oint_{(k)} \Bigg[\frac{Y}{r} \frac{\partial \left(r U^{(k)} \right)}{\partial r} \cos \alpha^{(k)} \\ & + Y \frac{\partial U^{(k)}}{\partial z} \cos \beta^{(k)} \Bigg] \, N_i \, dl \quad i = 1, 2, \ldots, n \end{aligned} \tag{3.7}$$

After some manipulations as discussed in [16], equation 3.7 reduces to,

$$\begin{aligned}\sum_{j=1}^{n} u_j \int\int_{(k)} \Bigg[& Y \frac{\partial N_i}{\partial r} \frac{\partial N_j}{\partial r} + Y \frac{\partial N_i}{\partial z} \frac{\partial N_j}{\partial z} \\ & + \frac{Y}{r} \frac{\partial N_i}{\partial r} N_j + Z N_i N_j \Bigg] \, dr dz \\ = & \oint_{(k)} E^{(k)}_{tan(CCW)} N_i \, dl \quad i = 1, 2, \ldots, n \end{aligned} \tag{3.8}$$

where $E_{tan(CCW)}$ is the tangential, counterclockwise, component of the electric field on element sides.

Equation 3.8 constitutes the FEM discretization of equation 3.5 for one element of the problem domain. When evaluated, equation 3.8 gives rise to a subsystem of n linear algebraic equations. Individual element subsystems are assembled for all the elements forming the problem domain to result into a big system of linear complex equations to be solved for undetermined coefficients u_j which reflect the values of U (the approximate values of H_ϕ) at the elemental nodes.

3.2 Boundary Conditions

For a solution to be unique, boundary conditions of the problem need to be incorporated into the formulation. To better explain the implementation of different boundary conditions, a problem configuration consisting of a cylindrical monopole antenna above a perfect ground plane, will be considered. The antenna driven by a coaxial line is as depicted in Figure 3.1.

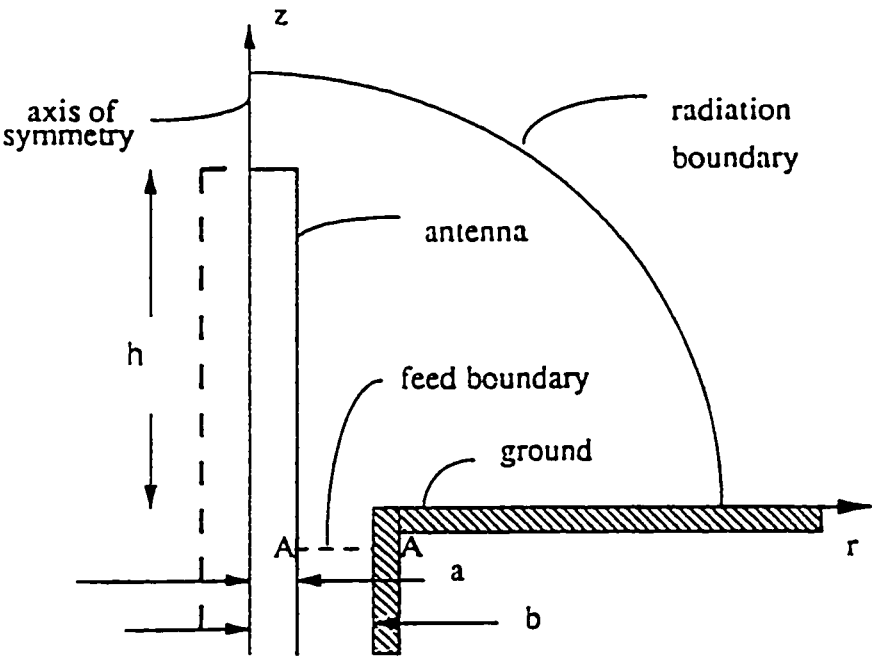

Figure 3.1: A cylindrical monopole antenna above a perfect ground plane driven by a coaxial line.

Most of the boundary conditions are easily introduced into the problem formulation by specifying the appropriate values for the tangential boundary electric field, $E_{tan(CCW)}$, in equation 3.8. Over all perfectly conducting boundaries, such as the coaxial line conductor surfaces, antenna surfaces and the perfect ground plane, the tangential electric field is zero by virtue of the continuity requirement of the tangential electric field.

Because of axial symmetry, and for computational efficiency, only half of a problem domain needs to be computed. But that is possible if an artificial boundary is placed at the axis of symmetry. If the axis of symmetry passes through a conductor the $E_{tan(CCW)} = 0$ condition will be used. However, there are cases, such as with antennas,

whereby a nonconducting boundary would be required along the axis of symmetry. In that case, it is only useful to remember that along such a boundary, H_ϕ is equally zero and needs not to be computed. In other words, one can safely eliminate the rows of the system matrix corresponding to the nodes falling on the nonconducting part of the axis of symmetry before embarking on the solution of the system of algebraic equations.

Treatment of an open boundary, when present, or any matched output termination, coaxial or otherwise, is done by assuming a plane wave propagation. In that case, assuming the termination or the outer boundary is far from the discontinuities by a measure dependent on the physical dimensions of the structures involved, the electric field at the boundary can be expressed in terms of the unknown magnetic field using,

$$\vec{H} = \frac{\hat{n} \times \vec{E}}{\eta} \tag{3.9}$$

where $\eta = \sqrt{\frac{j\omega\mu}{\sigma+j\omega\epsilon}}$ is the intrinsic impedance of the medium assumed homogeneous at the point where the boundary is located.

In terms of the tangential electric field in a counter-clockwise direction, equation 3.9 can be written as,

$$E_{tan(CCW)} = -\eta H_\phi \approx -\eta U \approx -\sqrt{\frac{j\omega\mu}{\sigma + j\omega\epsilon}} U \tag{3.10}$$

Equation 3.10 can be expanded using the trial solution given in equation 3.6 to yield,

$$E_{tan(CCW)} = -\sqrt{\frac{j\omega\mu}{\sigma + j\omega\epsilon}} \sum_{j=1}^{n} u_j N_j^{(k)}(r,z) \tag{3.11}$$

For elements with a side on the outer boundary or matched termination the appropriate substitution for the $E_{tan(CCW)}$ in equation 3.8 is obtained from equation 3.11. This particular boundary condition adds a term into the system of equation and modifies equation 3.8 to,

$$\sum_{j=1}^{n} u_j \left\{ \int\int_{(k)} \left[Y \left(\frac{\partial N_i}{\partial r}\frac{\partial N_j}{\partial r} + \frac{\partial N_i}{\partial z}\frac{\partial N_j}{\partial z} + \frac{\partial N_i}{\partial r}\frac{N_j}{r} \right) + Z N_i N_j \right] dr dz + + \eta \oint_{(k)} N_i N_j \, dl \right\} = 0 \quad i = 1, 2, \ldots, n \tag{3.12}$$

As mentioned above, the appropriate position for the outer or termination boundary depends upon the physical dimensions of the structure under consideration. For

radiating structures such as antennas and apertures, the far field conditions are fulfilled when both of the following conditions are fulfilled: $r \gg \frac{2D^2}{\lambda}$ and $r \gg \lambda$, where r is the distance to a far field point, D is the largest dimension of the radiating structure and λ is the wavelength of the exciting signal. For the most part, in addition to following the above rule of thumb, a trial and error method may be used whereby several positions of the termination boundary may be used while observing the convergence of the results. The appropriate distance is the one that gives same results as its neighbouring positions.

The most challenging boundary is the one associated with the coaxial feed. It is certainly wrong to assume a fixed delta-gap field function at the feed point to represent a coaxial feed. For one thing, if it is intended to have a boundary, (which will be called a feed boundary from here on) at a section of a coaxial line, the total field there is unknown as it is made up of the incident (known) and reflected (unknown) parts. Some researchers [19] use TEM magnetic frill generators right at the coaxial junction to simulate a coaxial feed. As it is well known that aperture (junction) field is not purely TEM, then the magnetic frill generator technique is also not accurate as it neglects the existence of evanescent higher order modes.

The technique that models best the coaxial feeding process relies on transmission line theory. The total azimuthal magnetic field propagating in the positive z-direction at a point inside a coaxial line and far from the discontinuities can be expressed as follows:

$$H_\phi = H_I e^{-jkz} - H_R e^{jkz} \tag{3.13}$$

where $H_I e^{-jkz}$ is the incident magnetic field propagating in the positive z-direction, $H_R e^{jkz}$ is the reflected magnetic field propagating in the negative z-direction and $k = \omega\sqrt{\mu\epsilon}$ is the wave number.

The partial derivative of equation 3.13 with respect to z yields,

$$\frac{\partial H_\phi}{\partial z} = -jkH_I e^{-jkz} - jkH_R e^{jkz} \tag{3.14}$$

Substituting for $H_R e^{jkz}$ in equation 3.14 using equation 3.13 yields,

$$\frac{\partial H_\phi}{\partial z} = -jk(2H_I e^{-jkz} - H_\phi) \tag{3.15}$$

which in terms of the approximate value of the magnetic field, U, can be written as.

$$\frac{\partial U}{\partial z} = -jk(2\,|H_I|\,e^{-jkz} - U) \tag{3.16}$$

The boundary conditions at the coaxial feed can be effectively and accurately implemented by substituting the derivative of U with respect to z on the right-hand side of equation 3.7 using equation 3.16. Moreover, for the assumed propagation directions, the direction cosines of an outer vector normal to the feed boundary, $\cos\alpha$ and $\cos\beta$ are respectively specified as 0 and -1.

Observe that the above implementation of the feed boundary conditions does not essentially disregard the existence of higher order modes at the coaxial junction, neither does it fix a delta-gap field. The fact that the field at any point inside a coaxial line is the sum of incident and reflected fields is duly considered in this formulation. Since the boundary field is assumed to be purely TEM, it is important to place the boundary far from discontinuities where only the TEM mode propagates. A rule of thumb [18] as to the appropriate position of the boundary field is at $r > 3(b-a)$, where a is the radius of the inner conductor of the coaxial line and b the radius of the outer conductor of the coaxial line.

The merit of this new technique of modelling the coaxial feed is confirmed in Figure 3.2. The comparison is made between this new technique, the technique that assumes a TEM coaxial arperture field and the analytical technique introduced in [20]. The test problem solved consists of an open-ended coaxial line radiating in a half-space. The dielectric constant in the coaxial line and in the half-space is taken as 2.08. The coaxial line dimensions were taken as $a = 1.4264$ mm and $b = 4.7250$ mm, and the computation using this new feed model was undertaken using the discussed FEM technique. The results show clearly that this new feed model is much more accurate compared to the TEM aperture field model.

3.3 Computational Results

The formulation discussed in the preceding section can be used successfully in analysing various axisymmetric microwave structures of interest such as cylindrical and conical monopole antennas, coaxial junctions, dielectric resonators, all driven through coaxial lines. The method can generate various outputs such as transfer characteristics and nodal magnetic field values. The near-field values calculated for antenna cases may be transformed to far-field by well known near-to-far field transfromation algorithms

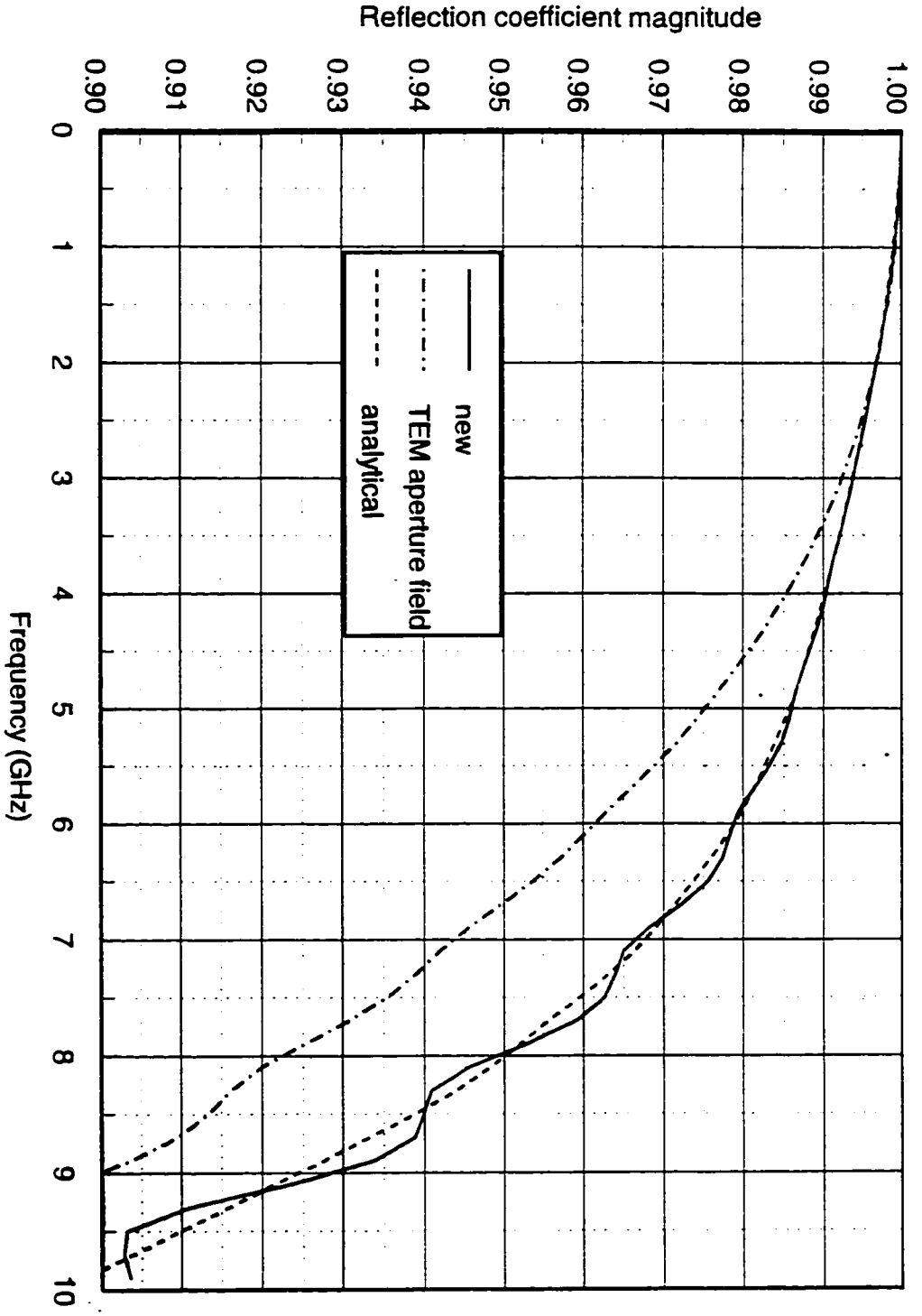

Figure 3.2: Input reflection coefficient of an open-ended coaxial line obtained with different feed models.

available in the literature.

3.3.1 A cylindrical dielectric ring resonator antenna

The method was tested for a problem consisting of a newly introduced, dielectric ring resonator antenna [21]. The finite element mesh used for that problem is as depicted in Figure 3.3, which consisted of 3111 triangular elements made up of 1682 nodes. The elements were dense around the coaxial feed and the dielectric ring where the field concentration is expected. A rule of thumb used to decide on the mesh size is $\Delta l = \lambda_{min}/20$, where Δl is the element edge length, and λ_{min} is the smallest wavelength in the considered frequency range.

Only half of the problem geometry was modelled taking advantage of the symmetry. Figure 3.4 shows the geometrical dimensions of the antenna and a plot of the input reflection coefficient, (S_{11}) results which took about 1 sec CPU time to obtain on a Sun SPARCstation 10. It can be seen that the FEM results compare very well with the experimental results reported in [21].

The dielectric ring resonator antenna modelled is seen to resonate at around 5.95GHz instead of around 6.0GHz, found in [21]. The difference is primarily due to the fact that there may be slight differences in the modelled problem dimensions compared to those used in the experiment. For example, the width of the ground plane is only assumed to be of typical value, $t = 1.67$ mm, and the diameter of the ground plane aperture is assumed to be the same as that of the center hole of the cylindrical dielectric resonator ring, i.e., $2b$. These dimensions are critical in fixing the resonant frequency of the resonator as they decide the value of the frequency-dependent capacitance of the aperture. All the other dimensions were taken same as those provided in [21]. That is, $2a = 11.95$ mm, $d = 5.4$ mm, $b/a = 0.17$, probe length, $h = 5.0$ mm and $\epsilon_r = 36.2$.

The dielectric ring resonator antenna was modelled again for different geometrical parameters and different dielectric constants of the ring. It was interesting to observe the variation of the input reflection coefficient response as a function of frequency, dielectric constant of the ring and ring dimensions. That was a good indication of how useful this modelling technique could be to designers of microwave devices. Depicted in Figure 3.5 is the plot for a geometry with dimensions, $a = 7.4286$ mm, $d = 5.1429$

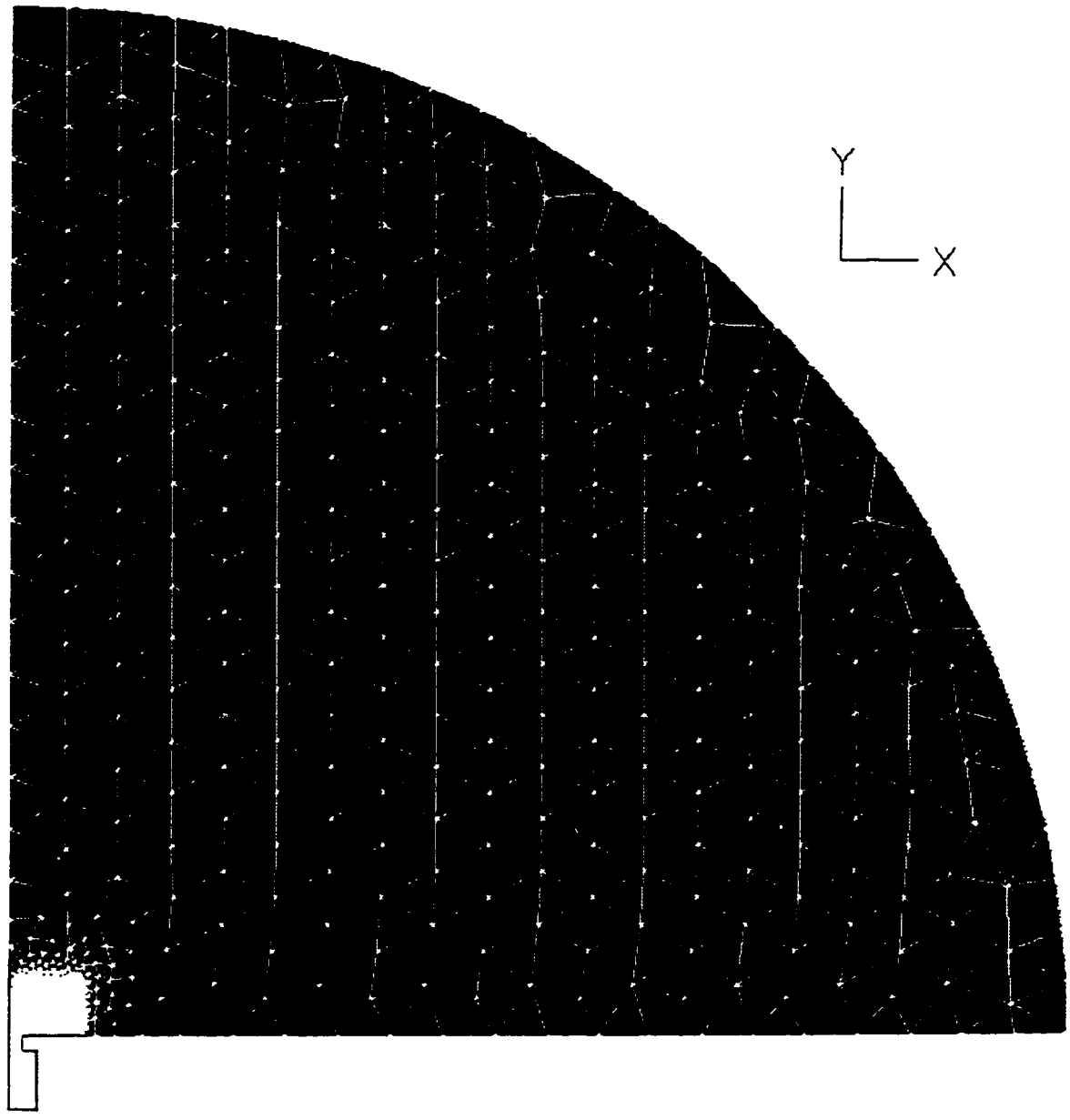

Figure 3.3: The finite element mesh for the dielectric ring resonator antenna

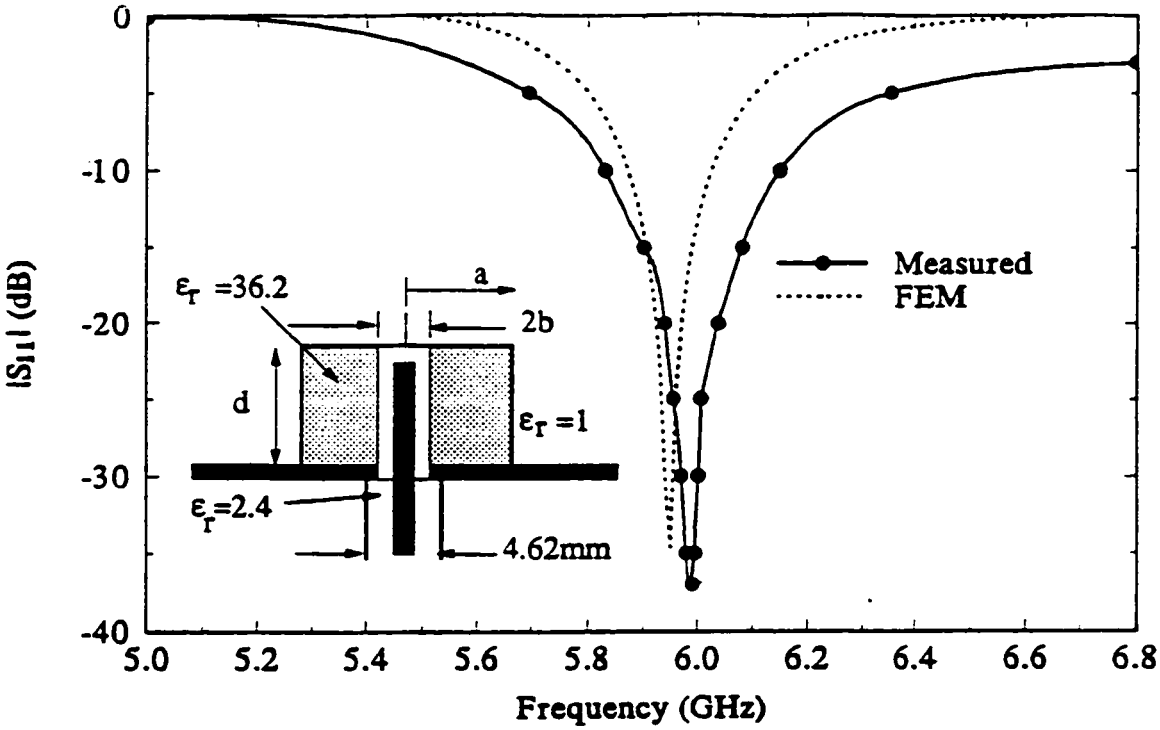

Figure 3.4: Measured and numerical results for the input return loss of a cylindrical dielectric ring resonator antenna.

mm, b = 1.01575 mm. The curves correspond to ϵ_r values of 20, 21, 22, and 23, respectively in the order of their appearance from left to right.

3.3.2 Broadband dielectric antennas

To exploit the capabilities of this method, three new dielectric antennas were modelled and were found to give new insight into the characteristic of dielectric antennas. Different feed probe models and different dielectric shapes were investigated. The investigation was very easily done with this modelling method. It would be very difficult and costly to carry out the investigations experimentally. And that is one major advantage of using numerical modelling techniques.

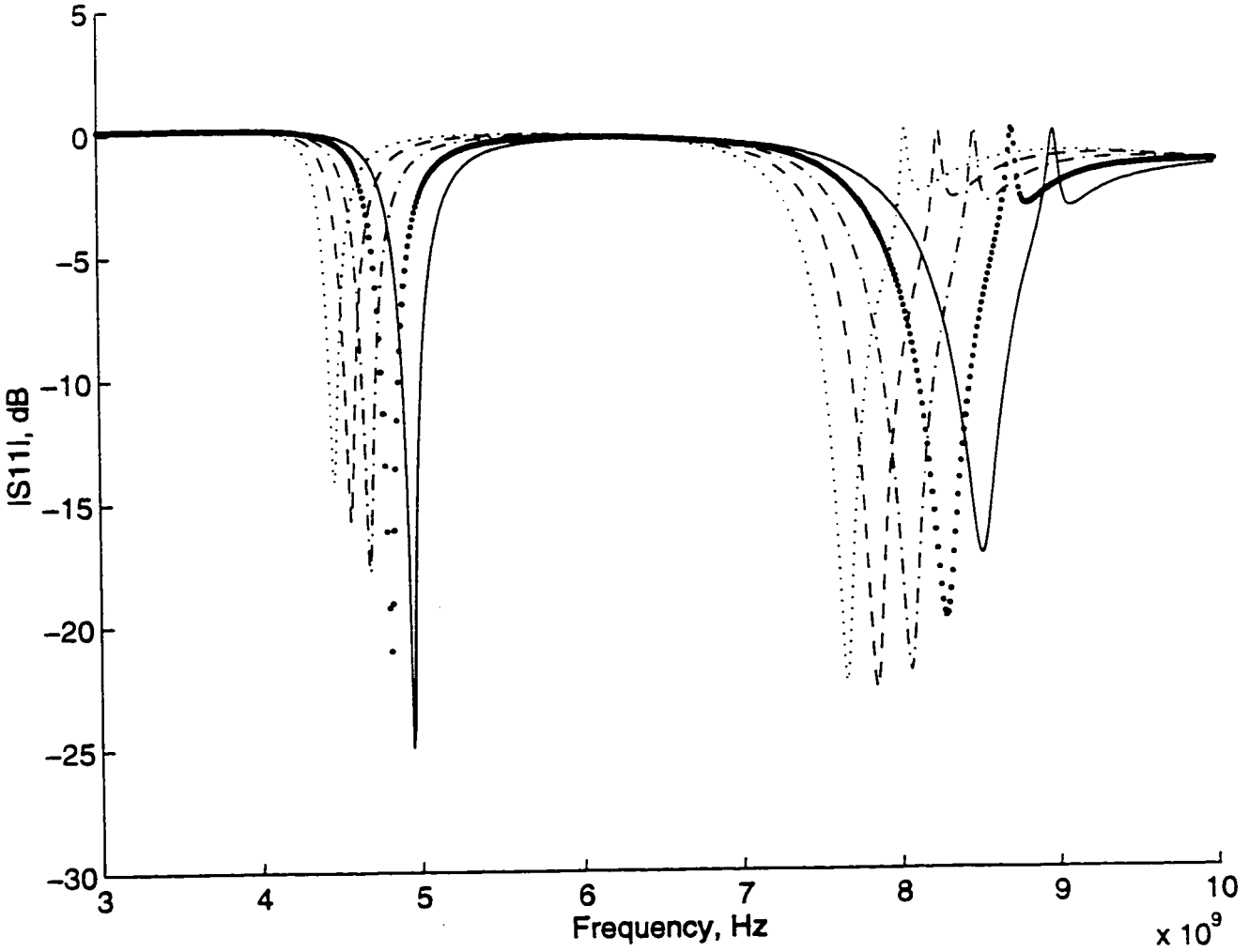

Figure 3.5: The finite element results for the input reflection coefficient of a dielectric ring resonator antenna for different values of the dielectric constant of the ring.

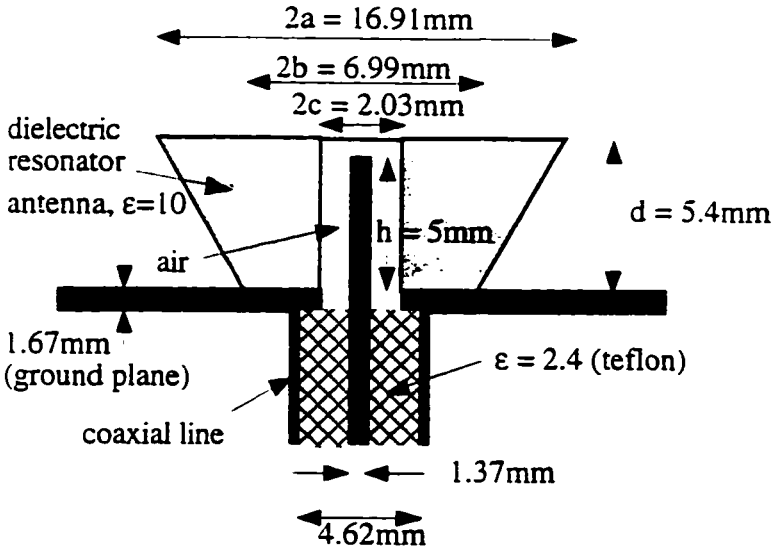

Figure 3.6: A truncated cone-shaped dielectric antenna

The first antenna geometry investigated is shown in Figure 3.6 along with its dimensions. The computation was carried out for the dielectric constant values of 10 to 15 in unit steps and for frequencies between 9 and 13 GHz. The results are shown in Figure 3.7.

An interesting thing to observe here is that the bandwidth of the antenna is very wide in most cases. The antenna presented in [21] had a 10 dB return loss bandwidth of only 10 percent while this new antenna has a 10 dB return loss bandwidth of over 22 percent at 11.6 GHz for $\epsilon_r = 11$. The plot of the magnetic field distribution in the near-field for the antenna of Figure 3.6 at 11.6 GHz and for $\epsilon_r = 11$ is shown in Figure 3.8.

The second antenna geometry investigated is shown in Figure 3.9 along with its

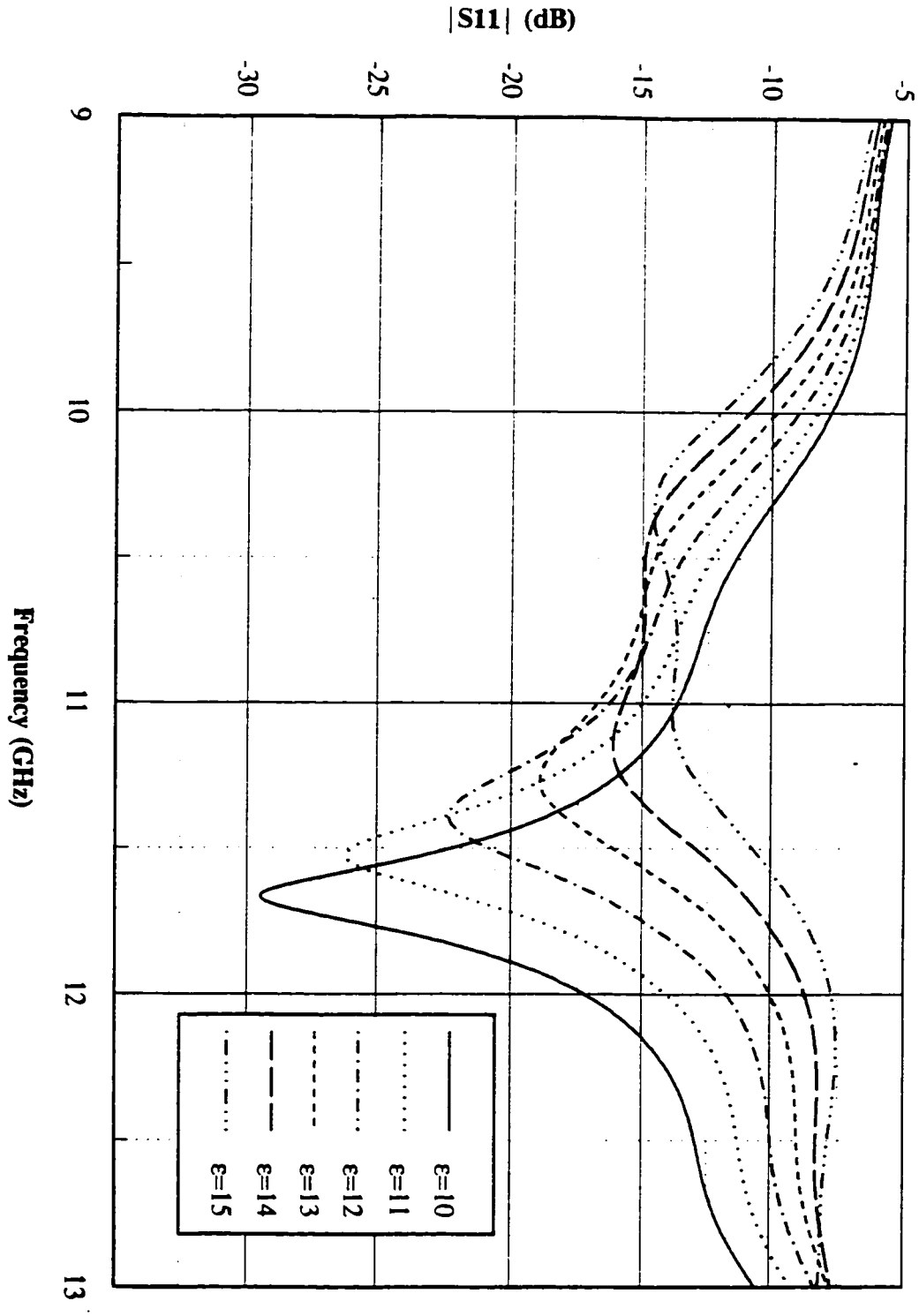

Figure 3.7: Input return loss characteristics of truncated cone-shaped dielectric antenna

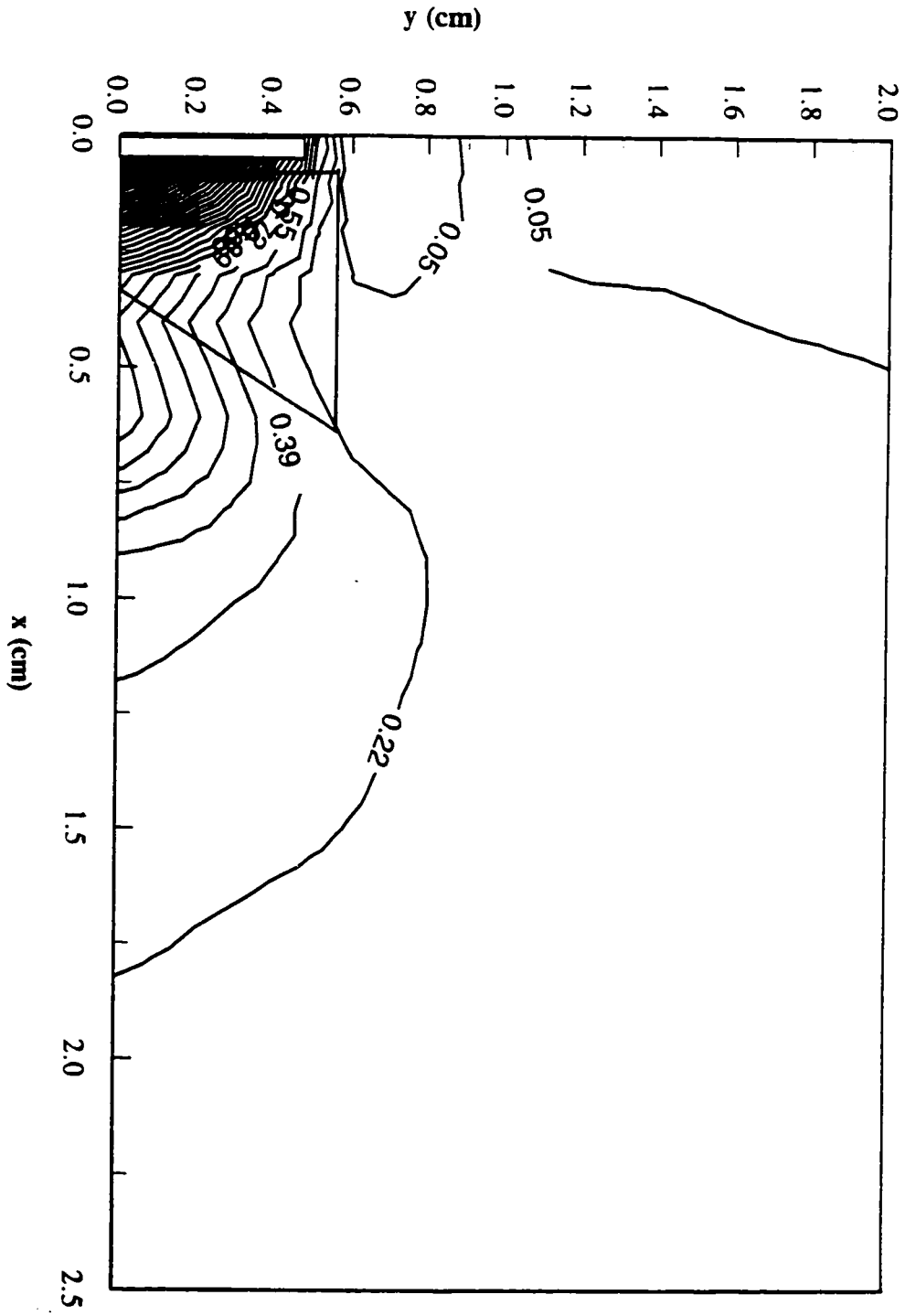

Figure 3.8: Magnetic field (A/m^2) distribution around a truncated cone-shaped dielectric antenna, $f = 11.6$ GHz, $\epsilon_r = 11$.

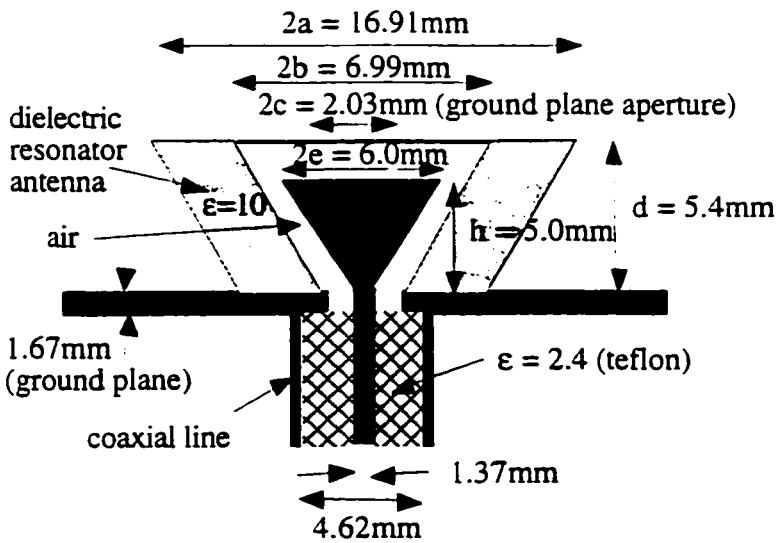

Figure 3.9: A truncated V-shaped dielectric antenna

dimensions. The antenna is excited with a conically-shaped probe. It is an attempt to exploit the broadband feature of probes of that shape. The computation was carried out for the dielectric constant values of 15 to 35 in unit steps and for frequencies between 8 and 14 GHz. The results are shown in Figure 3.10.

This antenna provides very wide bandwidth with almost flat return loss characterictics for some values of the dielectric constant. This is a very good design feature. This V-shaped antenna has a 10 dB return loss bandwidth of over 25 percent at 11.6 GHz for $\epsilon_r = 19$. The plot of the magnetic field distribution in the near-field for the antenna of Figure 3.9 at 11.6 GHz and for $\epsilon_r = 11$ is shown in Figure 3.11.

The third antenna geometry investigated is shown in Figure 3.12 along with its dimensions. The computation was carried out for the dielectric constant values of 15

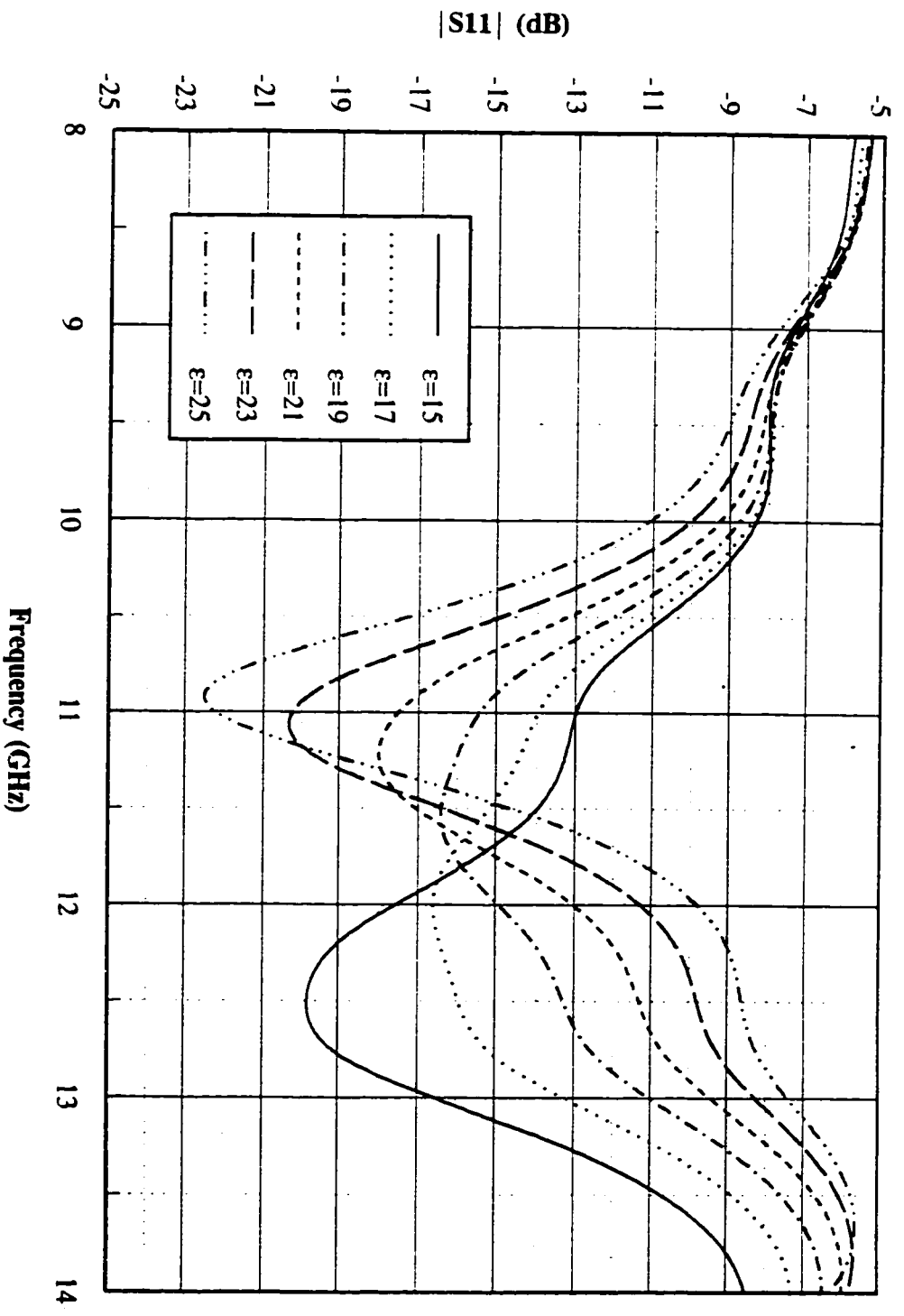

Figure 3.10: Input return loss characteristics of truncated V-shaped dielectric antenna

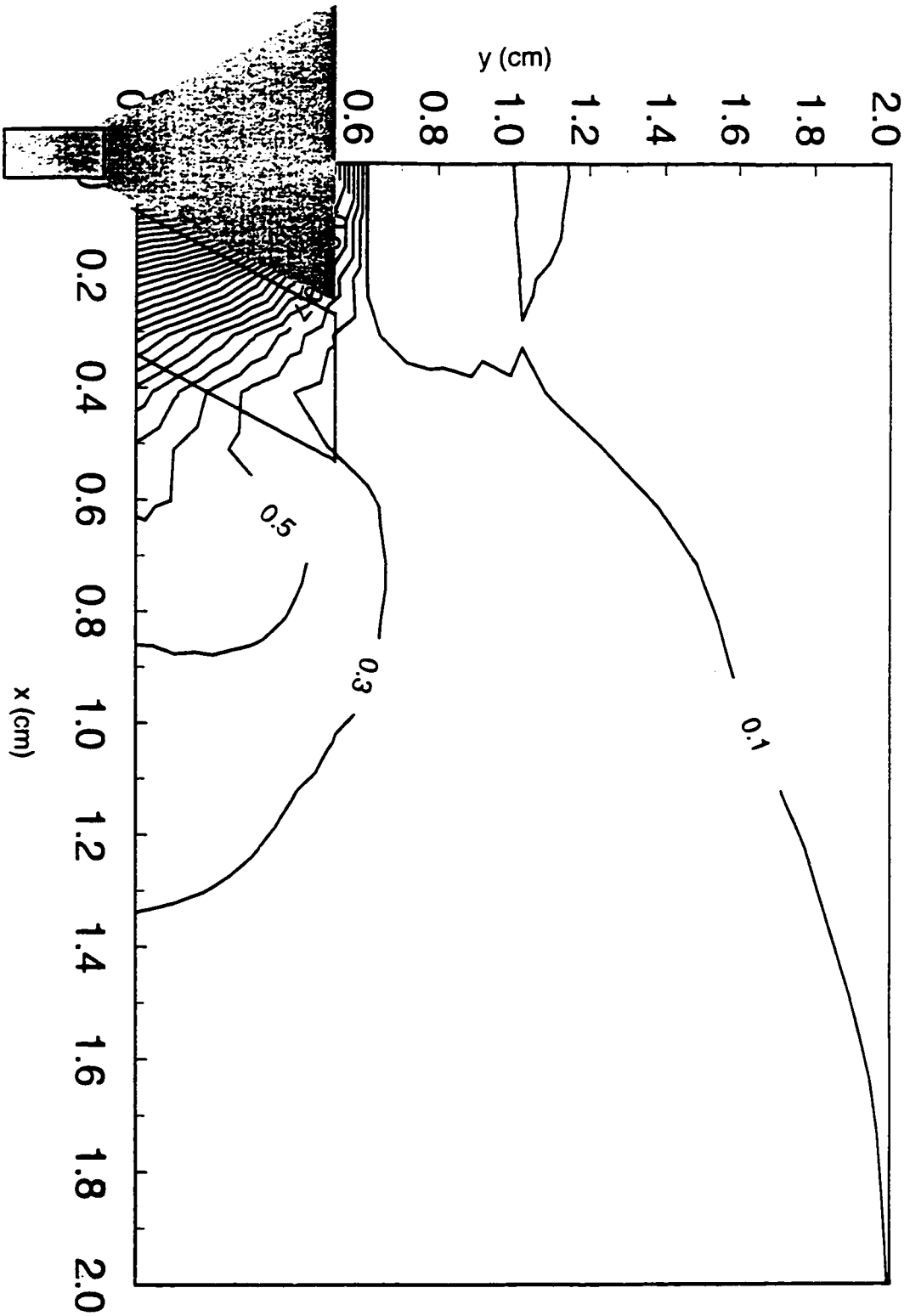

Figure 3.11: Magnetic field (A/m^2) distribution around a truncated V-shaped dielectric antenna, $f = 11.6$ GHz, $\epsilon_r = 19$.

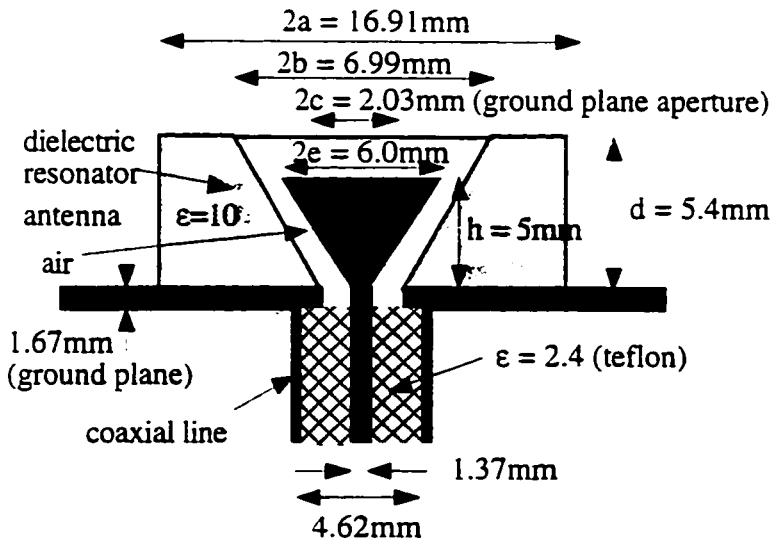

Figure 3.12: A truncated bowl-shaped dielectric antenna

to 25 in unit steps and for frequencies between 6 and 11 GHz. The results are shown in Figure 3.13.

This bowl-shaped antenna was not seen to offer considerable improvements in bandwidth and the return loss characteristics were not very good compared to the previously discussed antennas. The 10 dB return loss bandwidth was seen to be 13.5 percent at 8.1 GHz for $\epsilon_r = 16$.

3.3.3 A radial-line to coaxial-line junction

To demonstrate the ability of the formulation to model complex situations. results are given in Figure 3.14 for the phase of the reflection coefficient at the input port of a coaxial to radial line junction [22] shown in the same figure. The material inside the

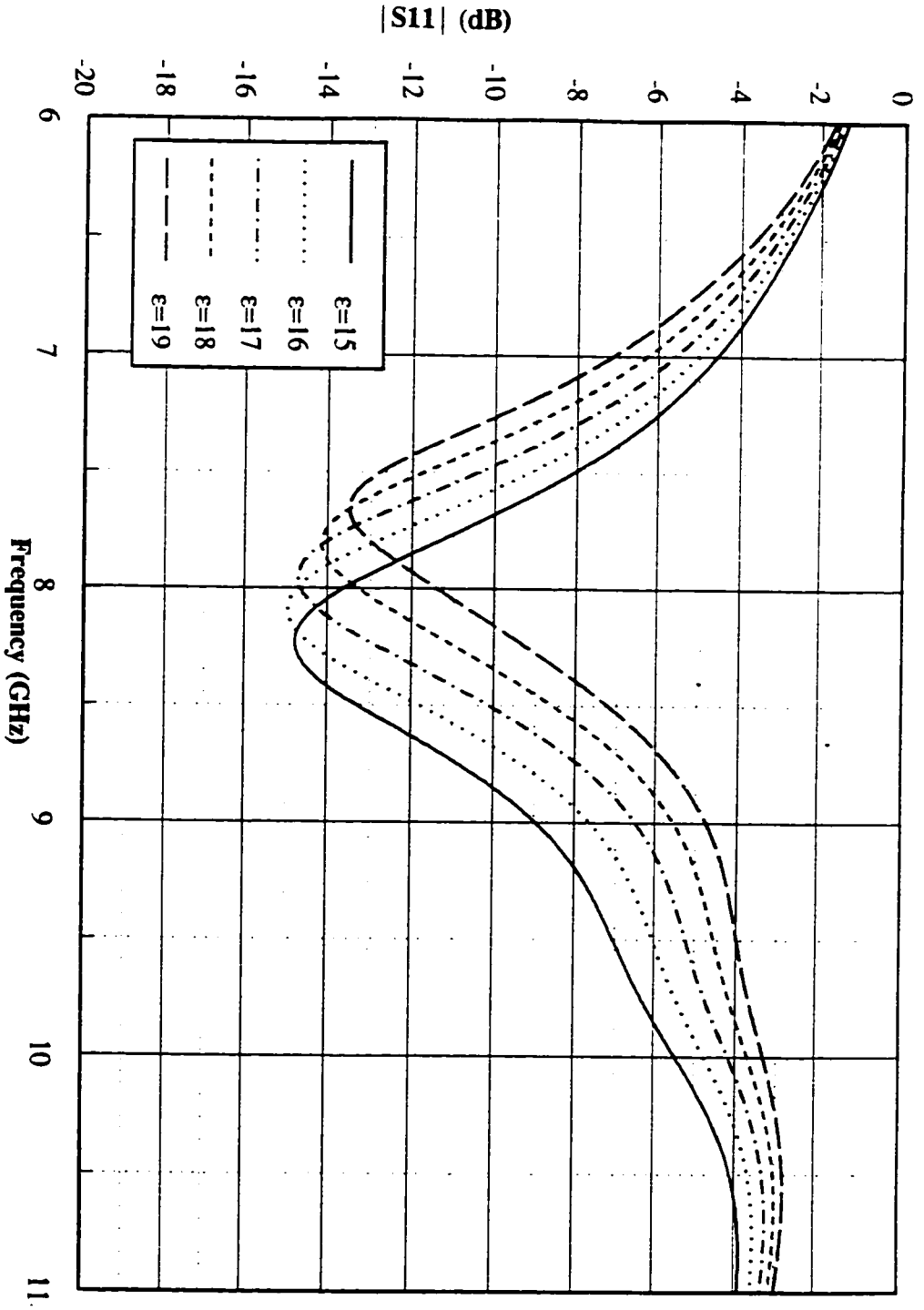

Figure 3.13: Input return loss characteristics of truncated bowl-shaped dielectric antenna

coaxial line is air. The magnitude of the reflection coefficient was found to be of value 1.0 throughout the range of frequencies considered. The dimensions of the junction are: $a = 1.55$ mm, $b = 3.48$ mm, $c = 24.25$ mm, $d = 40.77$ mm, and $h = 150.0$ mm. As seen in the figure, FEM results compare well with the measured results.

3.4 Neural Network Approach

It has been seen in the previous sections of this chapter, that the FEM can be successfully used to model various electromagnetic (EM) field problems. In typical EM field problems the solution by numerical techniques generally involves three stages. The first stage is the problem formulation which mainly involves the writing up of the system of equations to be solved. The second stage is the creation of the geometry that describes the problem and the necessary discretization of the problem domain into smaller elements. The third stage is the solution of the system of equations using any method of choice.

There are various situations where repeatitive computation of EM field is required, such as in optimization of the problem geometry for optimum outputs. As a matter of fact, such a need arises in several computer-aided design (CAD) tools used in microwave circuit design. A minor change in the problem geometry would require a different discretization of the problem domain, which is itself a time consuming exercise. In addition, the solution of the system of equations takes a lot of computer time depending on the complexity of the problem and the resulting number of equations.

Due to above shortcomings, numerical techniques such as FEM, may not be quite appropriate to be integrated with existing CAD packages such as SPICE and Libra owing to their inherent limitation of taking so much time to deliver requested outputs from them.

In this section, a new approach using neural network (NN) techniques is introduced. Using NN techniques, the outputs are readily available to be used by other CAD tools. As an example of the NN implementation, a dielectric-ring resonator antenna is modelled.

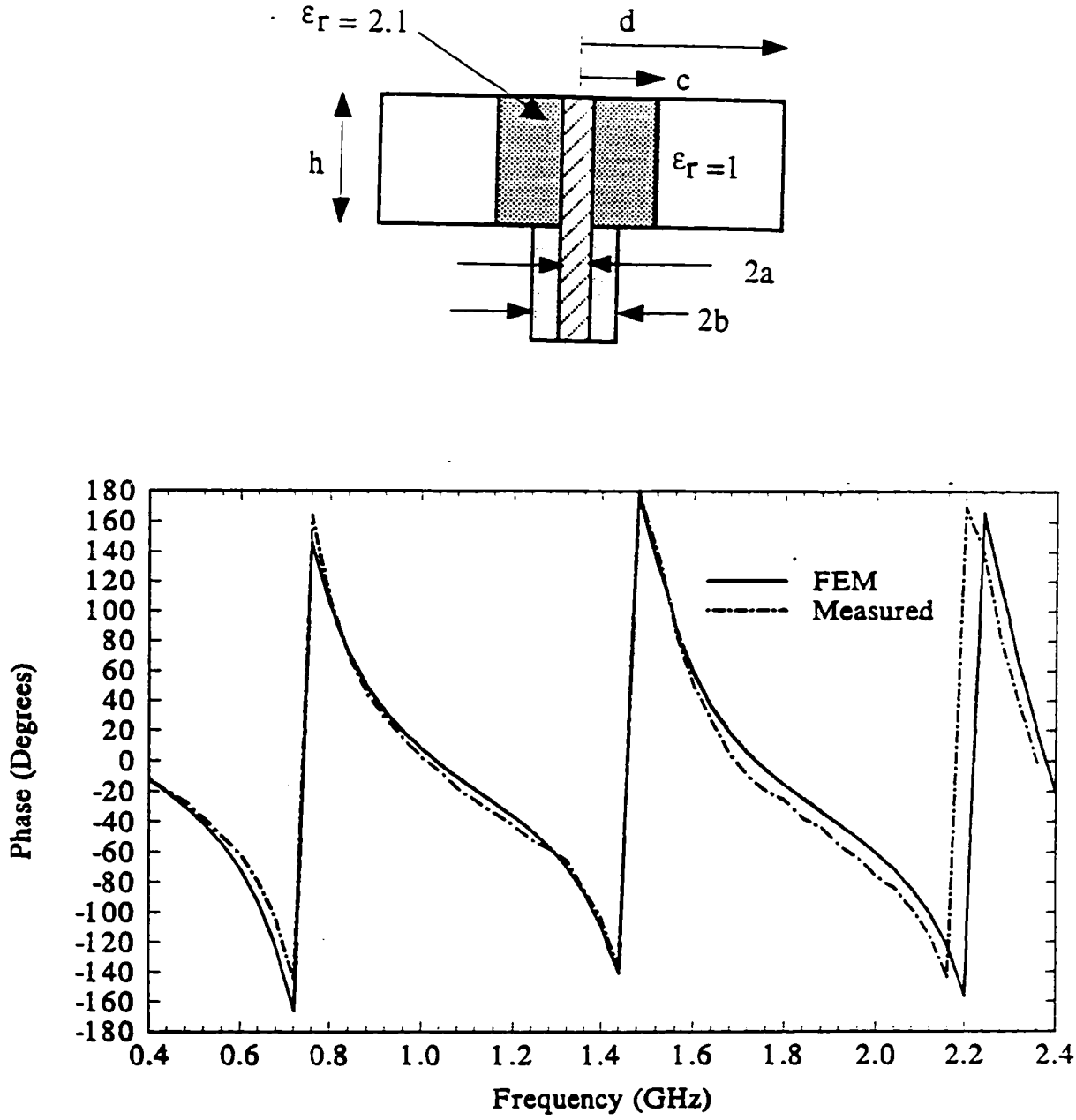

Figure 3.14: Phase of the reflection coefficient at the input port of a coaxial to radial line junction.

3.4.1 Dielectric-ring Resonator Antenna Modelled Using Neural Network Techniques

Consider the design of a dielectric-ring resonator antenna [23] shown in Figure 3.15 in which the design parameter of interest is the input reflection coefficient, S_{11}, which is a function of two variables, x_1 and x_2, representing the frequency of operation and the dielectric constant of the dielectric-ring. That is,

$$S_{11} = g(x_1, x_2) \tag{3.17}$$

where g is a continuous function of all its arguments as evidenced in Figure 3.16

Suppose that $G(x_1, x_2)$ is the approximator of the function $g(x_1, x_2)$, and it is expressed as a linear combination of other functions as follows:

$$G(x_1, x_2) = \sum_{i=1}^{M} \alpha_i \varphi(\sum_{j=1}^{2} w_{ij} x_j - \theta_i) \tag{3.18}$$

Equation 3.18 represents the output of a multilayer feedforward neural network that has 2 input nodes, (in this case frequency and dielectric constant), denoted by x_1, x_2; and a single hidden layer consisting of M neurons. Each neuron i has synaptic weights w_{i1}, w_{i2}, and threshold θ_i. The network output is a linear combination of the hidden neurons, with $\alpha_1, \ldots, \alpha_M$ as the coefficients of that combination.

According to the *universal approximation theorem* [24, 25, 26, 27], *a single hidden layer is sufficient for a multilayer perceptron to compute a uniform ε approximation to a given training set represented by the set of inputs $x_1, \ldots, x_p$ and a desired (target) output $g(x_1, \ldots, x_p)$.*

To satisfy the conditions of the theorem, the activation function φ has to be nonconstant, bounded, and monotone-increasing continuous. The common choice for it is the hyperbolic tangent function:

$$\varphi(v) = \frac{1 - exp(-2v)}{1 + exp(-2v)}$$

The derivative of $\varphi(v)$ with respect to its argument can be expressed as a function of $\varphi(v)$ as: $\varphi'(v) = 1 - \varphi^2(v)$.

Free neural network parameters are considered as the coordinates of vector $\theta \in R^L$, where L is the number of parameters. The best θ has to be found in terms of least squares, that is:

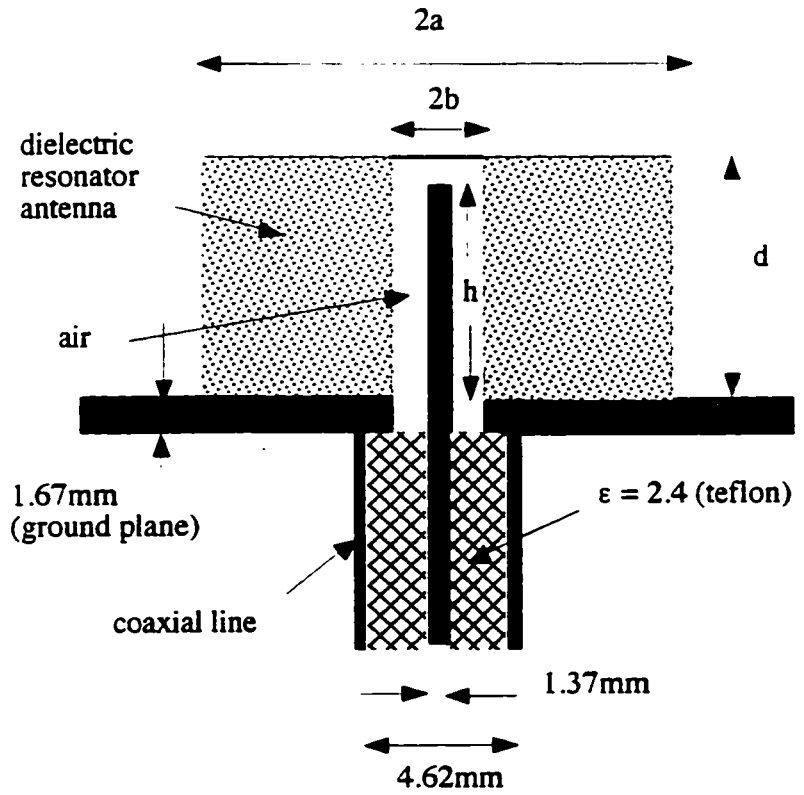

Figure 3.15: Dielectric ring resonator antenna.

$$f(x,\theta) \rightarrow \min_{\theta \in \Theta} \quad \Theta \in R^{L} \tag{3.19}$$

$$f(x,\theta) = \sum_{i=1}^{N} e_i(x,\theta)^2 = e(x,\theta)^T e(x,\theta) \tag{3.20}$$

where $e(x,\theta)$ is the error vector:

$$e(x,\theta) = t(x) - a(x,\theta)$$

$t(x)$ is the desirable NN output (target) and

$a(x, \theta)$ is the NN output as a function of the input x and the NN parameter vector θ. N in 3.20 stands for the number of input-output pairs used in the training process.

Derivation of the Basic Algorithm

Consider the general unconstrained optimization problem [28, 29]:

$$f(\theta) \rightarrow \min_{\theta \in \Theta} \quad \Theta \in R^L$$

Suppose that $f(\theta)$ is two-times differentiable on Θ, that is, can be represented in the form:

$$f(\theta + h) - f(\theta) = (\nabla f(\theta), h) + \frac{1}{2}(H(\theta)h, h) + o(h), \tag{3.21}$$

where $o(h)/\|h\|^2 \rightarrow 0$,
$\nabla f(\theta)$ is the gradient and $H(\theta)$ is the Hessian.

Necessary condition of the minimum $f(\theta^*)$ (Fermat condition) is $\nabla f(\theta^*) = 0$ and the corresponding method is called gradient method:

$$\theta^{(k+1)} = \theta^{(k)} - \lambda \nabla f(\theta^{(k)}) \tag{3.22}$$

Expressing the increment 3.21 by its linear part only and taking into account 3.22 we obtain:

$$\begin{aligned} f(\theta^{(k+1)}) - f(\theta^{(k)}) &= (\nabla f(\theta^{(k)}), \theta^{(k+1)} - \theta^{(k)}) + o(\theta^{(k+1)} - \theta^{(k)}) \\ &= -\lambda |\nabla f(\theta^{(k)})|^2 + o(\theta^{(k+1)} - \theta^{(k)}) \end{aligned}$$

To define the best $\lambda^{(k)}$ consider $f(\theta^{(k+1)})$ for the fixed value of $\theta^{(k)}$ as a function of λ only:

$$f(\lambda) = f(\theta^{(k)}) - \lambda |\nabla f(\theta^{(k)})|^2$$

then the best value for λ is:

$$\lambda = \lambda^{(k)} = \arg \min_{\lambda > 0} f(\lambda)$$

In this case the iteration process 3.22 is called *the steepest descent method* [28, 29].

If θ^* is a local minimum, Θ is a neighbourhood of θ^*, $H(\theta^*) > 0$ and $H(\theta) > 0$. $\forall\theta \in \Theta$ then the convergency speed of the gradient method is determined by the inequality:

$$\|\theta^{(n)} - \theta^*\| \leq Cq^n, \quad 0 < q < 1, \quad n = 1, 2, \ldots. \tag{3.23}$$

The Hessian $H(\theta^*)$ is positive definite symmetric matrix: $H = H^*$, $H > 0$. Therefore its eigenvalues satisfy an inequality:

$$0 < \lambda_1 \leq \ldots \lambda_n$$

The coefficient $\mu = \lambda_n/\lambda_1 \geq 1$ determines the shape of level curves of $f(\theta)$, $\forall\theta \in \Theta$ (a neighbourhood of θ^*). In the case of a 'valley' shape of level curves the method 3.22 almost does not work. Introduction of the new scalar product $(\theta, y)_A = (A\theta, y)$ with a new gradient and Hessian $A\nabla f(\theta), AH(\theta)$ respectively gives an effect like 'space expansion'. The best choice for A is:

$$A = H(\theta^*)^{-1}E,$$

and level curves have a shape of concentric circles and the iteration process becomes:

$$\theta^{(k+1)} = \theta^{(k)} - \rho^{(k)}H(\theta^{(k)})^{-1}\nabla f(\theta^{(k)}) \tag{3.24}$$

If $\rho^{(k)} = 1, \quad \forall k = 1, 2 \ldots$ then the process 3.24 is called *Newton method* [28, 29]. Its convergency speed is:

$$\|\theta^{(n)} - \theta^*\| \leq Cq^{2^n}, \quad 0 < q < 1, \quad n = 1, 2, \ldots.$$

which is much faster than 3.23.

The Levenberg-Marquardt Method and Back Propagation

Some characteristics of the least-squares minimization problem 3.19, 3.20 can be exploited to improve the iterative procedure.

Substituting the expression for the residuals $e(x, \theta)$, 3.19, 3.20 can be rewritten as:

$$f(\theta) = \|t - a(\theta)\|^2 \rightarrow \min_{\theta \in \Theta}, \quad \Theta \in R^L \tag{3.25}$$

The gradient and the Hessian in the Newton method 3.24 as obtained from 3.25, have special structures:

$$\nabla f(\theta) \equiv \frac{\partial f}{\partial \theta} = -2 \sum_{i=1}^{N} e_i \frac{\partial a(x_i, \theta)}{\partial \theta} \equiv g(\theta), \tag{3.26}$$

$$e_i = t_i - a(x_i, \theta)$$

$$H_{\alpha,\beta} = \frac{\partial^2 f}{\partial \theta_\alpha \partial \theta_\beta} = -2 \sum_{i=1}^{N} \frac{\partial^2 a_i}{\partial \theta_\alpha \partial \theta_\beta} e_i + 2 \sum_{i=1}^{N} \frac{\partial a_i}{\partial \theta_\alpha} \frac{\partial a_i}{\partial \theta_\beta}$$

As θ^i approaches θ^* the residuals e_i approaches 0. Therefore, the Hessian in the Newton method 3.24, can be approximated as follows:

$$H_{\alpha,\beta} \approx G_{\alpha,\beta} = 2 \sum_{i=1}^{N} \frac{\partial a_i}{\partial \theta_\alpha} \frac{\partial a_i}{\partial \theta_\beta}$$

where,

$$G = 2 \left(\frac{\partial a}{\partial \theta} \right)^T \left(\frac{\partial a}{\partial \theta} \right) \geq 0 \tag{3.27}$$

Such modification of the Newton method is called *the Gauss-Newton method* [28, 29, 30, 31].

To derive the iteration direction in the problem 3.25 let us expand $a(x, \theta)$ in Taylor series:

$$a(x, \theta) = a(x, \theta^{(k)}) + \left. \frac{\partial a}{\partial \theta} \right|_{\theta = \theta^{(k)}} (\theta - \theta^{(k)}) + \ldots$$

Denote the sum of the first two members of the expansion as $l(\theta)$. Then the next direction can be found as:

$$\arg \min_{\theta} \|t - l(\theta)\|^2 = \|t - a(x, \theta^{(k)}) - \frac{\partial a}{\partial \theta}(\theta - \theta^{(k)})\|^2 \tag{3.28}$$

Denote the βth component of the gradient as g_β. According to 3.26:

$$g_3 = -2\sum_{i=1}^{N} \frac{\partial a_i}{\partial \theta_3}(t - a_i) \tag{3.29}$$

Comparing 3.28 and 3.29 and using 3.27 it can be seen that the solution providing the minimum 3.28 satisfies the equation:

$$\left(\frac{\partial a}{\partial \theta}\right)^T \left(\frac{\partial a}{\partial \theta}\right)(\theta - \theta^{(k)}) = \left(\frac{\partial a}{\partial \theta}\right)^T (t - a(x, \theta^{(k)}))$$

This is the same solution, as in the Gauss-Newton method:

$$\theta - \theta^{(k)} = -G^{-1}(\theta^{(k)})g(\theta^{(k)}), \quad G \geq 0.$$

Instead of G we can make use of $G + \lambda P$:

$$G + \lambda P > 0, \quad \lambda > 0, P > 0. \tag{3.30}$$

It is possible to put $P = I$, I being a unit matrix (*Levenberg's option*).

Denoting the $N \times L$ Jacobian matrix of $e(\theta)$ as $J(\theta)$, the search direction on the k*th* iteration as $d^{(k)}$, ($d^{(k)} = \theta - \theta^{(k)}$) and taking into account modification 3.30 one obtains the linear set of equations [30, 31]:

$$\left(J(\theta^{(k)})^T J(\theta^{(k)}) + \lambda^{(k)} I\right) d^{(k)} = -J(\theta^{(k)})e(\theta^{(k)}), \tag{3.31}$$

The above is called the *Levenberg-Marquardt Method.* The scalar $\lambda^{(k)}$ in 3.31 controls both the magnitude and the direction of $d^{(k)}$. When $\lambda^{(k)}$ is zero, the direction $d^{(k)}$ is identical to that of the Gauss-Newton method. As $\lambda^{(k)}$ tends to infinity, $d^{(k)}$ tends towards a vector of zeros and a steepest descent direction (see 3.22).

The complete algorithm is as follows:

1. Create an initial parameter vector $\theta^{(0)}$ and an initial value $\lambda^{(0)}$ (e.g. $\lambda^{(0)} = 0.01$).
2. Determine the search direction $d^{(k)}$ from 3.31.
3. If $f(\theta^{(k+1)}) < f(\theta^{(k)})$ then $\lambda^{(k+1)}$ is reduced (e.g. $\lambda^{(k+1)} = \lambda^{(k)}/10$) otherwise it is increased. Here $f(\theta)$ is a functional 3.25.

4. Check the stop criterion. If it is satisfied, then $\theta^* = \theta^{(k)}$ and stop, else go to 2. Stop criterion: error goal is met, λ becomes too large (in this case $\lambda^{-1}J^Te$ approaches zero and no learning takes place, (see 3.31), or the maximum number of iterations (epochs) has been reached.

The back-propagation algorithm applies a correction Δw_{ji} to the synaptic weight w_{ji} connecting the output of neuron i to the input of neuron j. When applied to multi-element network, the back-propagation technique adjusts the weights in the direction opposite to the instantaneous gradient $\partial e_k^2/\partial w_{ij}$ of the sum square error in weight space [27], where e_k^2 is the *instantaneous sum of squared errors* of the multi-output network given as:

$$e_k^2 = \frac{1}{2}\sum_{j\in C} e_{jk}^2 \tag{3.32}$$

where index k corresponds to the kth pattern (input-output pair) of the training set, index j corresponds to the jth output neuron and the set C includes all the neurons in the output layer of the network.

The derivatives of a network's sum squared error with respect to a layer's net input are called *delta*. Let us notice however that the Jacobian in 3.31 represents a matrix of partial derivatives of e (not e^2 as in 3.32) with respect to network weights $w_{\alpha\beta}$. Therefore in this case *delta* has a different meaning:

$$\frac{\partial e_{jk}}{\partial w_{ji}} = \frac{\partial e_{jk}}{\partial v_j}\frac{\partial v_j}{\partial w_{ji}} = \delta_{jk}\frac{\partial v_j}{\partial w_{ji}} \tag{3.33}$$

where

$$\delta_{jk} = \frac{\partial e_{jk}}{\partial v_j}$$

v_j is the activation function associated with neuron j:

$$v_j = \sum_{i\in I} w_{ji}y_i \tag{3.34}$$

where I is a set of layer's inputs and y_i is the output of neuron i (see fig.3.17).

Taking into account 3.34 one obtains from 3.33:

$$\frac{\partial e_{jk}}{\partial w_{ji}} = \delta_{jk} y_i \tag{3.35}$$

The delta vector of an output layer can be derived from the network error vector (see fig.3.17) according to the chain rule :

$$\delta_{jk} = \frac{\partial e_{jk}}{\partial y_j} \frac{\partial y_j}{\partial v_j} \tag{3.36}$$

$$e_{jk} = t_{jk} - y_j \tag{3.37}$$

t_{jk} represents desirable NN output (target) and y_j is the output of neuron j.

Taking into account 3.37 one obtains from 3.36:

$$\delta_{jk} = -\varphi_j'(v_j)$$

The delta vector for each hidden layer can be calculated from the next layer's delta vector according to the δ-rule [27]:

$$\delta_{jk} = \varphi_j'(v_j) \sum_{l \in \mathcal{O}} \delta_{lk} w_{lj}$$

where $\mathcal{O}$ is a set of layer's output.

Finally the elements of the Jacobian corresponding to the $m\,th$ layer of the network and the $k\,th$ pattern (input-output pair) are as given by 3.35:

$$J_{k,l(j,m)} = \delta_{jk}^{(m)} y_{jk}^{(m)}$$

where $y_{jk}^{(m)}$ is the $m\,th$ layer's input vector of the network.

Neural Network Design Models

The network design was perfomed by using MATLAB M-scripts and special NN toolboxes [32, 33]. All the programs were run on Sun SPARCstation 10 under UNIX operating system.

Half of the available data was chosen for training while another half was reserved for the validation of the models.

The first model was for a NN approximator of the reflection coefficient of a dielectric ring resonator antenna as a function of frequency and dielectric constant. Figure 3.18 depicts 3 layer NN which consists of two input neurons, one hidden layer of 10 neurons with hyperbolic tangent activation function, and one output linear neuron. Positive weights are represented by a solid line while a dashed line represents a negative weight. A bias is represented by a vertical line through the neuron.

Free NN parameters to determine during the training process are: a 10×3 weight matrix of hidden layer and a 1×11 weight matrix of output layer. Input data was scaled before training to zero mean and variance 1. Initial values of weights were randomized between 0 and 1.

Training process with Levenberg-Marquardt algorithm took approximately 180 seconds of CPU time. Then the model was validated on the data different from the training set (fig.3.19). Table (3.1) compares NN modeling and classical numerical analysis (finite element method).

The second model was a NN approximator of the reflection coefficient of a dielectric ring resonator antenna as a function of ring radius and dielectric constant. A 3D plot of numerical analysis results is presented in figure 3.20. The attempts to design a NN model based on the use of only one hidden layer architecture did not bring any stable appropriate results. According to [27, 25] neurons in a single hidden layer network tend to interact with each other globally. In complex situations this interaction makes it difficult to improve the approximation at one point without worsening it at some other point. On the other hand, with two hidden layers the approximation process becomes more manageable. In particular [25]:

- *Local features* are extracted in the first hidden layer. Specifically, some neurons in the first hidden layer are used to partition the input space into regions, and other neurons in that layer learn the local features characterizing those regions.
- *Global features* are extracted in the second hidden layer. Specifically, a neuron in the second hidden layer combines the outputs of neurons in the first hidden layer operating on a particular region of the input space, and thereby learns the global features for that region and outputs zero elsewhere.

Therefore the two hidden layer network model was implemented. Each hidden layer consists of 5 neurons with hyperbolic tangent activation function, and the output is a linear neuron. Weight matrices to determine are: w_1 of size 5×3, w_2 of size 5×6 and w_3 of size 1×6. As in the first model, initial data was scaled before training and weigts were randomized between 0 and 1.

Training process with Levenberg-Marquardt algorithm took approximately 55 seconds of CPU time or 200 iterations (see fig.3.21). Testing of the model on the data different from the training set showed sufficient performance of the network (see fig.3.22). Figure 3.23 showes a 3D plot of the simulated surface. It took about 0.5 seconds of CPU time to get values for 5000 points of the surface.

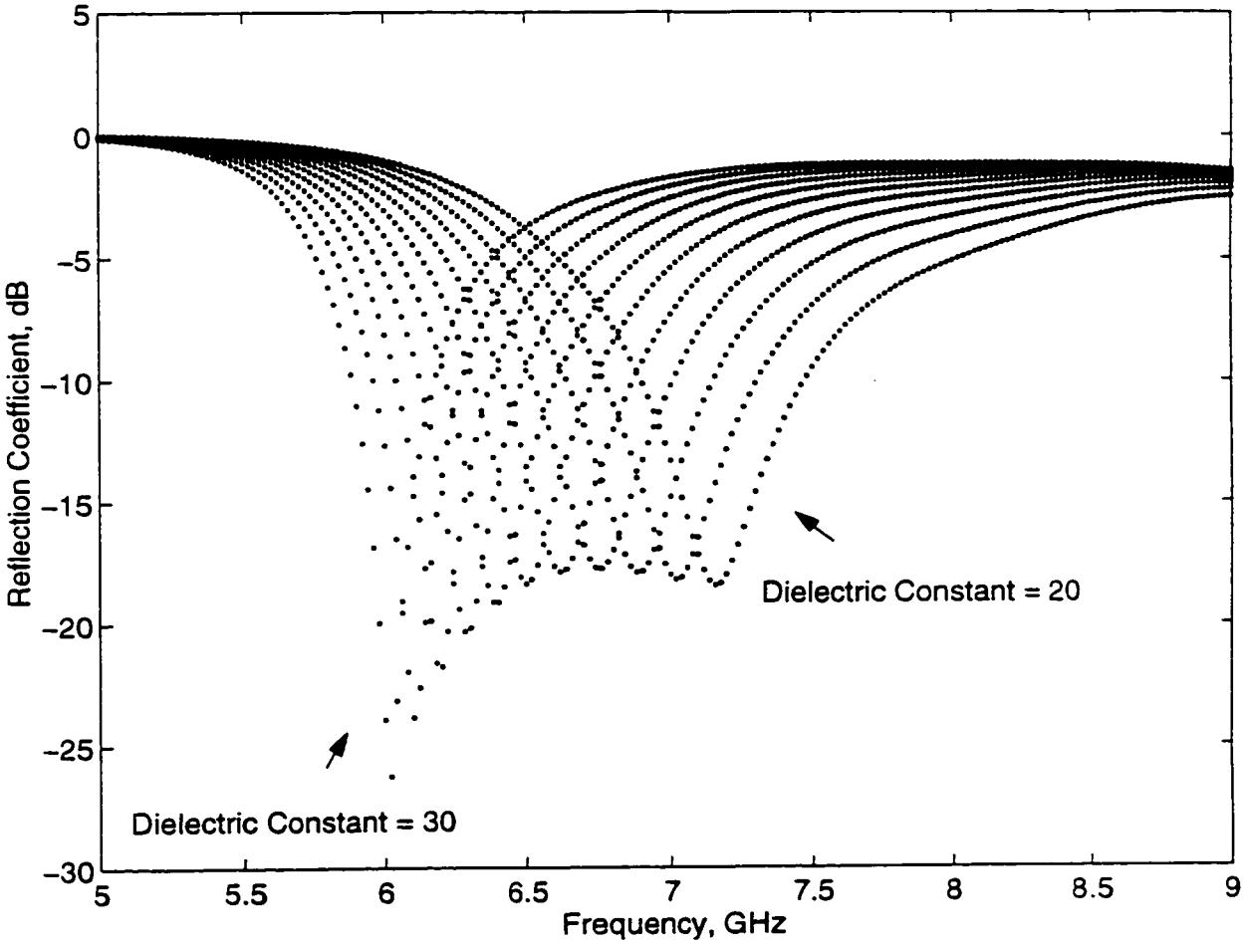

Figure 3.16: Input reflection coefficient of a dielectric-ring resonator antenna as a function of frequency and dielectric constant; $a = d$ =5.14 mm

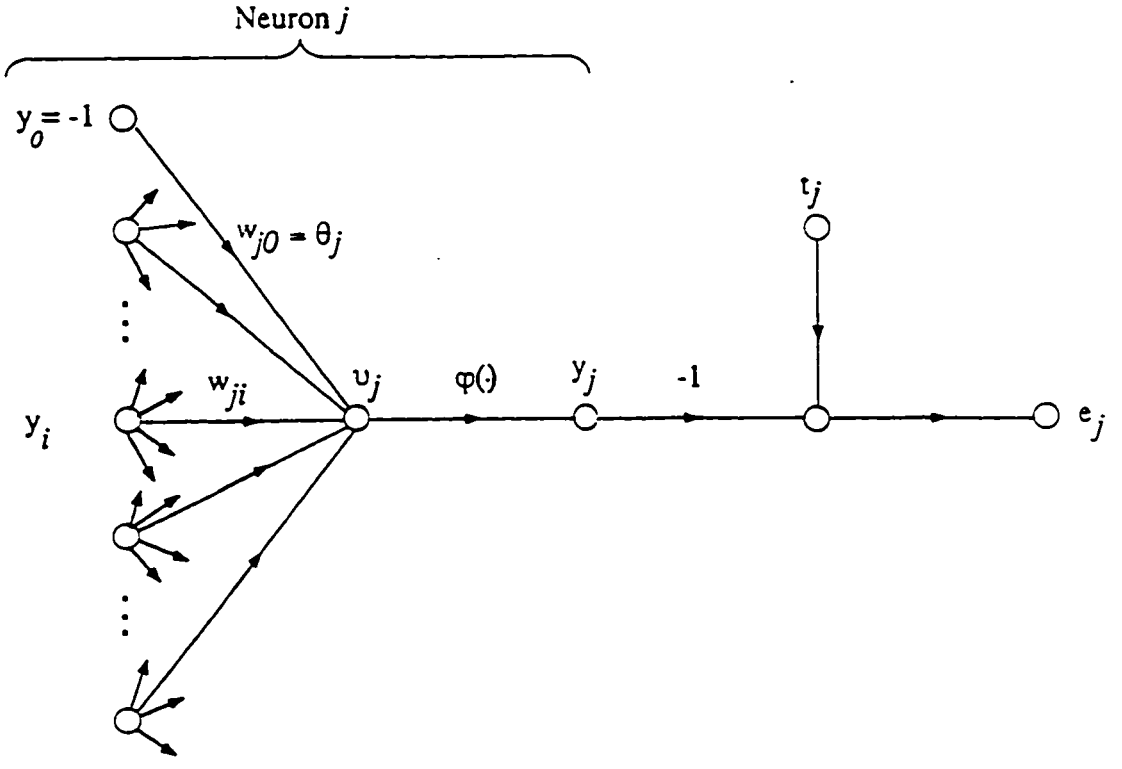

Figure 3.17: Output layer of the network

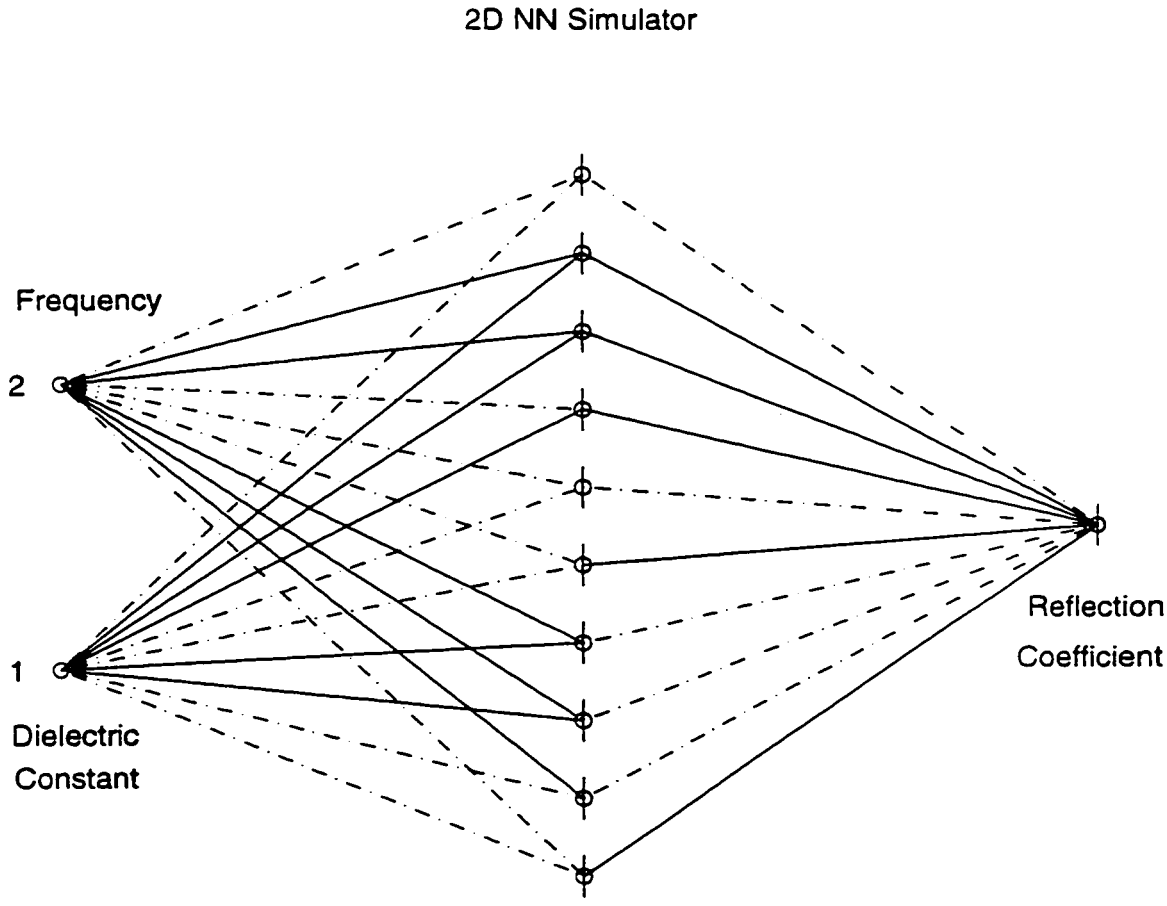

Figure 3.18: Model architecture: two input neurons, one hidden layer of 10 neurons. one output neuron.

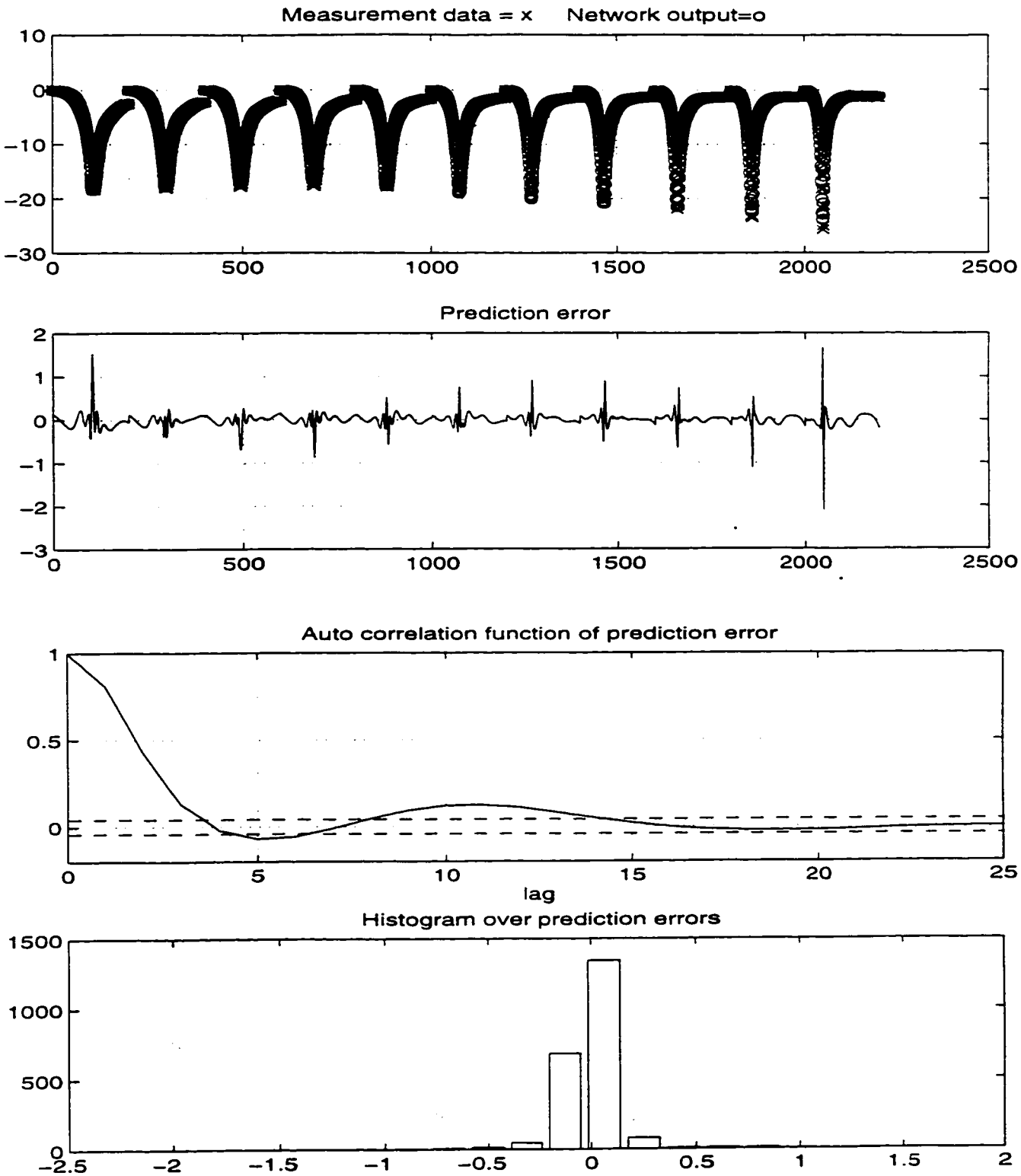

Figure 3.19: Validation of the neural network model: two input neurons, one hidden layer of 10 neurons, one output neuron.

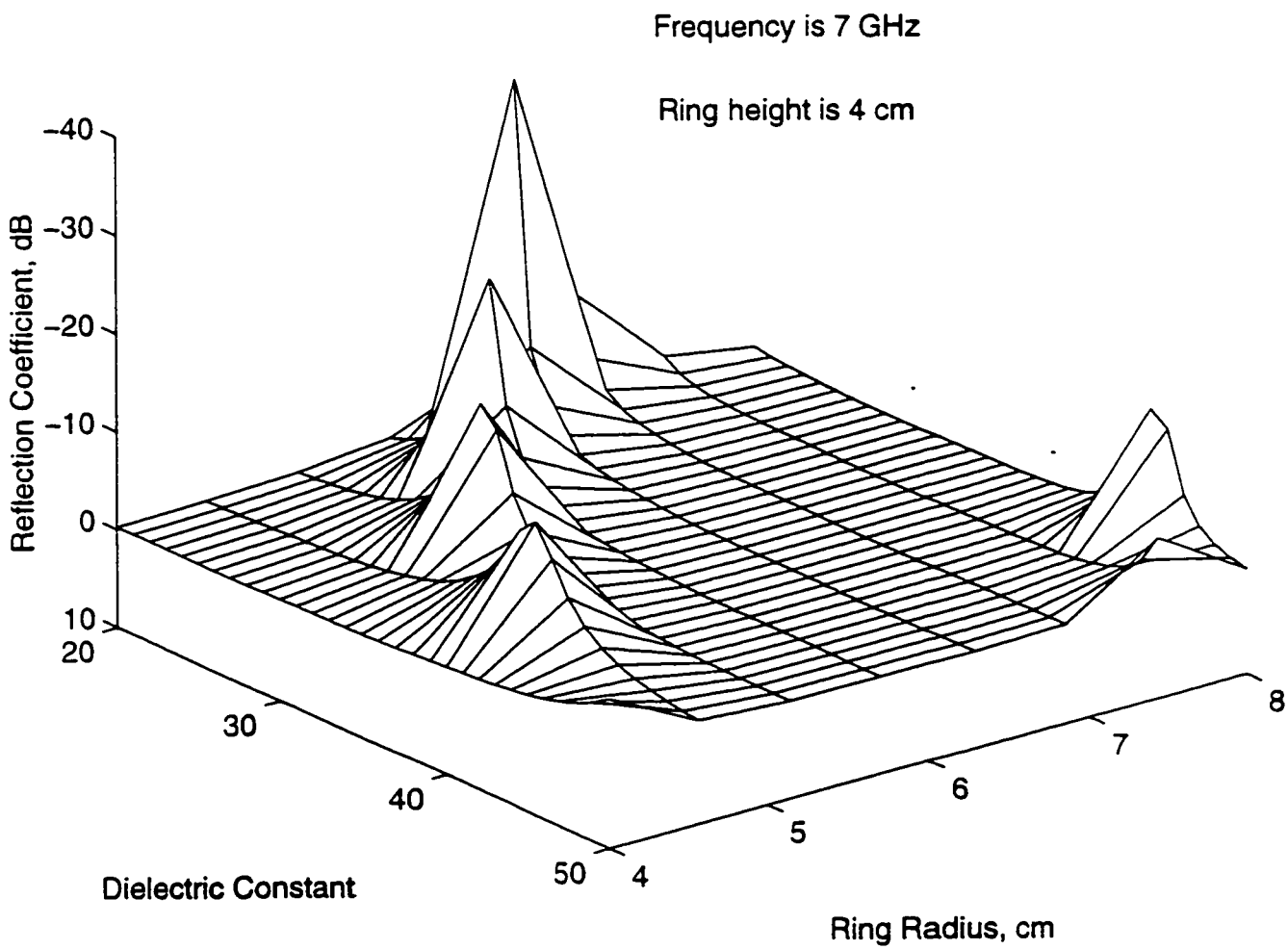

Figure 3.20: The output surface of numerical simulation: reflection coefficient of a dielectric ring resonator antenna as a function of ring radius and dielectric constant.

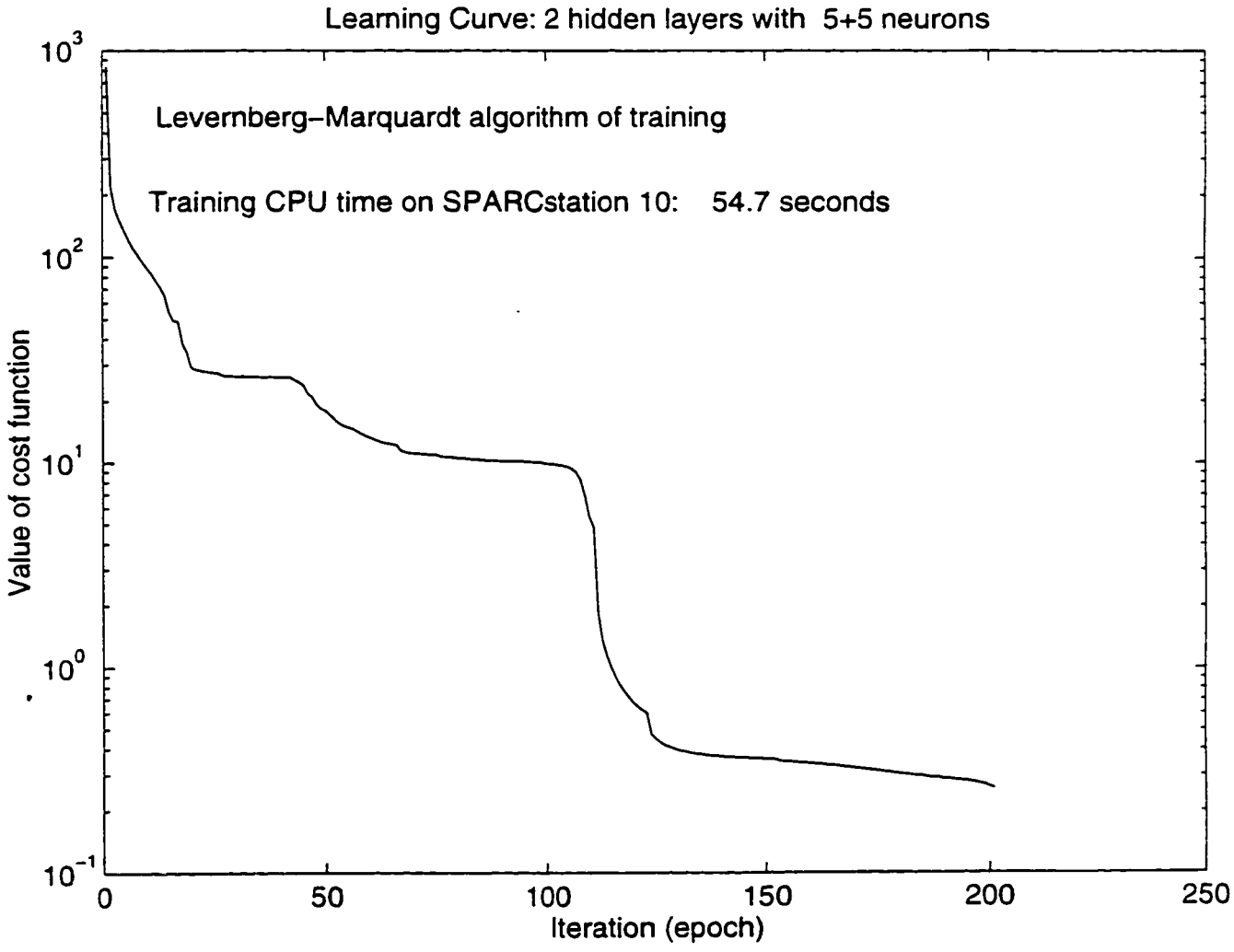

Figure 3.21: Neural network training process: two input neurons, two hidden layers (5 neurons each), one output neuron.

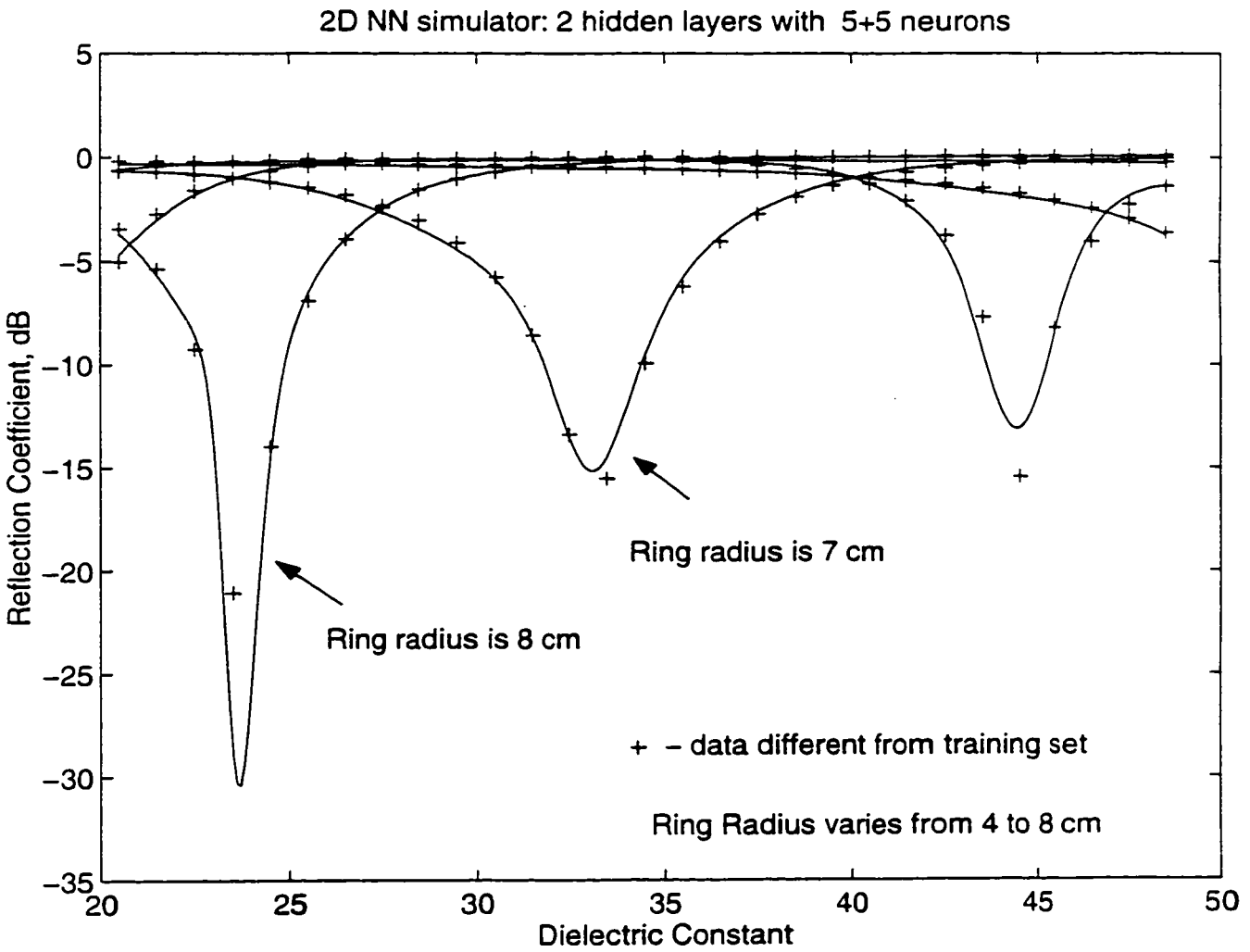

Figure 3.22: Validation of the neural network model: two input neurons, two hidden layers (5 neurons each), one output neuron.

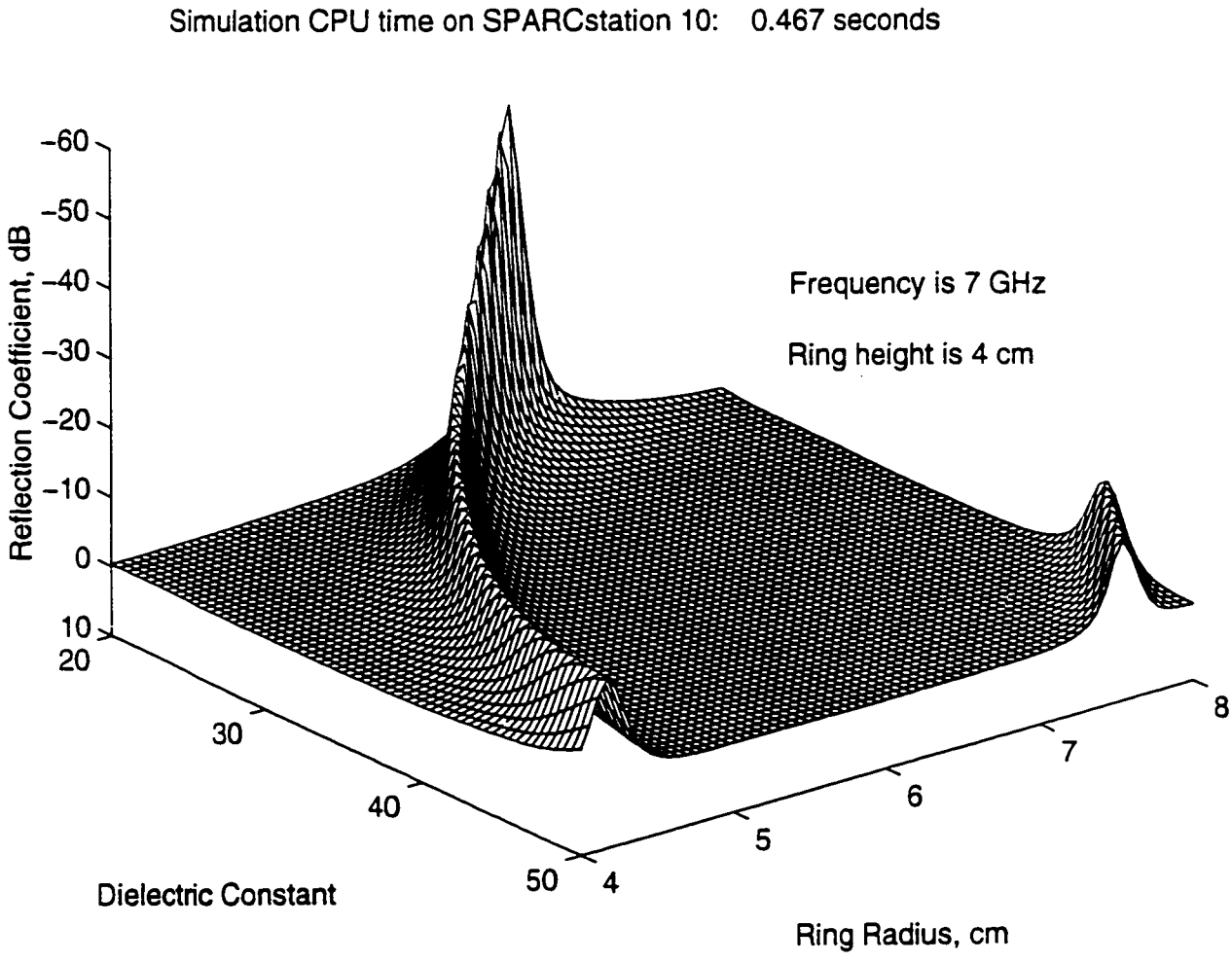

Figure 3.23: Simulation results of a multilayer network: two input neurons, two hidden layers (5 neurons each), one output neuron.

3.5 Conclusion

An accurate method of analysis for coaxially-driven, axisymmetric microwave structures has been presented. The method accurately models both the coaxial feeds and open boundaries, hence fixing the shortcomings of those available methods that only treat well one, but not both, of the above boundaries. The method has been shown to work very well with various coaxially-driven axisymmetric structures. It can indeed be used to model monopole antennas of various shapes, dielectric resonators, cavities, filters, coaxial connectors, and virtually all geometries that exhibit axisymmetry.

The method introduced implements a simple absorbing boundary condition for open boundaries, which works very well especially in lossy media where the field decays very fast with distance. One may wish to use better absorbing boundary conditions to have the boundary much closer to the discontinuities thereby reducing the mesh size and hence increasing the efficiency of the method.

Neural network techniques have been implemented along side the finite element method and found to be very well suited in saving computer memory as well as improving interactibility with other CAD tools used by providing high computational speed.

	Simulation CPU Time (seconds)	Training CPU Time (seconds)	Storage requirement (bytes)	Data representation
Classical Numerical Analysis (FEA)	1.3×10^{5}	N/A	1,032,657	Discrete
Neural Network	2.0×10^{-1}	1.8×10^{2}	378	Continuous

Table 3.1: Performance estimate of a 2D NN simulator: two input neurons, one hidden layer of 10 neurons, one output neuron.

Chapter 4

Three-Dimensional Field Computation Using Vector Finite Element Method

The traditional node-based FEM has been widely and very successfully used in the literature. Its main drawback, however, is its incapability to model sharp corners, as well as its tendency to give spurious, non-physical solutions. This has been considered to be a result of its failure to model properly the continuity of the fields between finite elements and the lack of proper enforcement of the divergence condition.

Not long ago [34], what is known as the vector finite element method, VFEM, has been used to overcome the problems inherent in the node-based FEM. In [34] VFEM is used to solve eddy current problems. VFEM makes it easy to impose edge and material-interface boundary conditions and does not suffer from spurious solutions. Moreover, VFEM treats well conducting and dielectric edges and corners whose field singularities are a major problem encountered in node-based FEM. In VFEM the degrees of freedom are assigned to the edges rather than the nodes of the elements. For this reason, vector finite elements are also known as edge elements. The two names will be used arbitrarily.

In the foregoing sections a detailed description of the way VFEM is used in modelling general electromagnetic wave propagation problems, will be provided. Two formulations will be discussed: one based on the magnetic, H, field and the other

that involves direct computation of the electric, E, field. Both two formulations are based on the material provided in [6]. Before presenting the formulations, the general review of vector finite elements is provided below.

4.1 Vector Finite Elements

The concept behind vector elements, owe its origin from the so called Whitney elements described by Whitney [35] as early as 1957. Following the Nedelec's paper in 1980 [36] that described the construction of edge elements in tetrahedra and rectangular bricks, it did not take long before their use in electromagnetics.

Researchers in the field of magnetics were among the first to use them in the solution of three-dimensional eddy current problems [34],[37]. Independently, and about the same time, Hano [38] used edge elements to analyse dielectric-loaded waveguides. In late 1985, Mur [39] tackled a problem of general nature to demonstrate the application of edge elements for the computation of three-dimensional electromagnetic fields in a highly inhomogeneous media. Barton and Cendes recently were successful in using tetrahedral edge elements for three-dimensional magnetic field computations [40]. More recently, Crowley [41] developed a more sophisticated element type, what he called covariant projection elements, which permits elements with curved edges.

Several works have been carried out in the analysis of electromagnetic problems using edge elements as well as an extensive discussion of their importance and apparent problems encountered in using them. Most of them ventured to solve closed boundary-value problems and little has been done in demonstrating the suitability of the method in solving electromagnetic scattering problems and those involving open boundaries as in radiation problems. It is the main purpose of this work to fill up that gap. But first, the scratch details of the theory behind the three-dimensional tetrahedral edge elements (used in this work) is provided below.

4.1.1 Three-Dimensional Tetrahedral Edge Elements

Tetrahedral edge elements are quite suitable in modelling three-dimensional geometries especially those with irregular shapes since they can easily made to fit in virtually any arbitrary shape. Tetrahedral element is as illustrated in Figure 4.1. There are

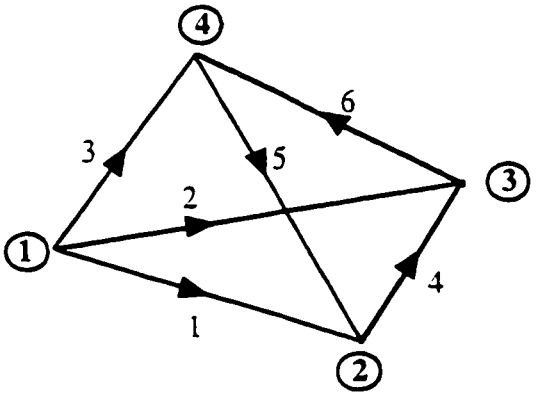

Figure 4.1: The tetrahedral element showing the node and edge numbering.

Edje j	Node j1	Node j2
1	1	2
2	1	3
3	1	4
4	2	3
5	4	2
6	3	4

Table 4.1: Edge numbering order on a tetrahedral element

varying ways of defining edge numbering and directions. The only thing important is consistency. That is, for one problem all the elements should have to adopt same mode of edge definition. The edge definition used in this work is as shown in Table 4.1.

4.2 Magnetic Field Formulation

4.2.1 The Method

Electromagnetic wave propagation phenomenon is generally expressed by the famous Maxwell's equations 3.1 and 3.2

Eliminating $\vec{E}$ from equations 3.1 and 3.2, yields the vector (curl-curl) wave equation. In a region V, making up the problem domain, the wave equation expressed in terms of the magnetic, $\vec{H}$, field vector is.

$$\nabla \times \nabla \times \vec{H} - k^2 \vec{H} = 0 \tag{4.1}$$

where $k = \omega\sqrt{\mu\epsilon}$, $\omega = 2\pi f$, and f is the frequency.

In the VFEM implementation, the problem domain, V, is subdivided into tetrahedral subdomains (elements), V^e. The three-dimensional edge-based, vector basis functions, $\vec{W}_j^e$, are defined in the tetrahedrons as,

$$\vec{W}_j^e = \ell_j^e (L_{j1}^e \nabla L_{j2}^e - L_{j2}^e \nabla L_{j1}^e) \tag{4.2}$$

where L_j are three-dimensional, linear, nodal finite element interpolatory functions discussed in the previous Chapter 3. ℓ_j is the length of a tetrahedron edge. The edge and node numbering used for this analysis is shown in the Figure 4.1 and Table 4.1.

Over each tetrahedron, the H-field is expressed in terms of the linear vector basis functions as,

$$\vec{H} = \sum_{j=1}^{6} H_j^e \vec{W}_j^e \tag{4.3}$$

where H_j represents the edge values of the H-field.

Applying the Galerkin's, weighted residual method on equation 4.1 using the expansion given in equation 4.3, converts equation 4.1 into the weak form. This weak form, using the first vector Green's theorem and other appropriate vector identities can be written as a 6×6 matrix equation for a single element as,

$$\left\{ [PM^e] - k^2 [FM^e] \right\} [H^e] = [R^e] \tag{4.4}$$

where the respective matrix elements are:

$$PM_{ij}^e = \int_{V^e} (\nabla \times \vec{W}_i^e) \cdot (\nabla \times \vec{W}_j^e)\, dV \tag{4.5}$$

$$FM_{ij}^e = \int_{V^e} \vec{W}_i^e \cdot \vec{W}_j^e\, dV \tag{4.6}$$

$$R_i^e = \oint_{S^e} \vec{W}_i^e \cdot (\hat{n} \times \nabla \times \vec{H})\, dS \tag{4.7}$$

where V^e is the elemental volume, S^e is the elemental surface, and $\hat{n}$ is the outer vector normal to S^e. $[H^e]$ is the coefficient vector of the six edge basis functions which represents the tangential H fields on the element edges in the local directions given in Figure 4.1. Indices i and j vary from 1 to 6 for tetrahedral elements corresponding to the tetrahedron edges.

The elemental matrices are evaluated and assembled in a way that will maintain tha global direction of the edge fields. The evaluation of the integrals in equations 4.5 - 4.7 and the implementation of various boundary conditions is not so simple. That will be discussed in the following sub-section.

4.2.2 Evaluation of the Integrals

Evaluation of the PM_{ij}^e Integral

The matrix contributions, PM_{ij}^e, are given in equation 4.5. Using the expression for $\vec{W}$ as given in equation 4.2, we know that the linear, finite element, nodal interpolatory functions (using simplex coordinates) for a tetrahedral element are given as.

$$L_i^e(x,y,z) = \frac{1}{6V^e}(a_i^e + b_i^e x + c_i^e y + d_i^e z) \tag{4.8}$$

where the coeffients a_i^e, b_i^e, c_i^e and d_i^e can be generally expressed as:

$$\begin{aligned}
a_i^e &= (-i)^{i+1}\left[x_{i+1}(y_{i+2}z_{i+3}) - z_{i+2}y_{i+3}) + x_{i+2}(y_{i+3}z_{i+1}) - z_{i+3}y_{i+1}\right) \\
&\quad + x_{i+3}(y_{i+1}z_{i+2}) - z_{i+1}y_{i+2})] \qquad (4.9)\\
b_i^e &= (-i)^i(y_{i+1}z_{i+2} - z_{i+1}y_{i+2} + y_{i+2}z_{i+3} - z_{i+2}y_{i+3} \\
&\quad + y_{i+3}z_{i+1} - z_{i+3}y_{i+1}) \qquad (4.10)\\
c_i^e &= (-i)^{i+1}(x_{i+1}z_{i+2} - z_{i+1}x_{i+2} + x_{i+2}z_{i+3} - z_{i+2}x_{i+3} \\
&\quad + x_{i+3}z_{i+1} - z_{i+3}x_{i+1}) \qquad (4.11)\\
d_i^e &= (-i)^i(x_{i+1}y_{i+2} - y_{i+1}x_{i+2} + x_{i+2}y_{i+3} - y_{i+2}x_{i+3} \\
&\quad + x_{i+3}y_{i+1} - y_{i+3}x_{i+1}) \qquad (4.12)
\end{aligned}$$

where i proceeds modulo 4 and represents tetrahedron node numbers.

Using equations 4.2 and 4.8, it can be shown that,

$$\begin{aligned}
\nabla \times \vec{W}_i^e &= 2\ell_i^e(\nabla L_{i1}^e \times \nabla L_{i2}^e) \\
&= \frac{2\ell_i^e}{(6V^e)^2}\left[(c_{i1}^e d_{i2}^e - d_{i1}^e c_{i2}^e)\hat{x} + (d_{i1}^e b_{i2}^e - b_{i1}^e d_{i2}^e)\hat{y}\right. \qquad (4.13)\\
&\quad \left. + (b_{i1}^e c_{i2}^e - c_{i1}^e b_{i2}^e)\hat{z}\right]
\end{aligned}$$

Substituting equation 4.13 in equation 4.5 and integrating, gives:

$$\begin{aligned} PMij^e &= \frac{4\ell_i^e \ell_j^e V^e}{(6V^e)^4}\Big[(c_{i1}^e d_{i2}^e - d_{i1}^e c_{i2}^e)(c_{j1}^e d_{j2}^e - d_{j1}^e c_{j2}^e) \\ &+ (d_{i1}^e b_{i2}^e - b_{i1}^e d_{i2}^e)(d_{j1}^e b_{j2}^e - b_{j1}^e d_{j2}^e) \\ &+ (b_{i1}^e c_{i2}^e - c_{i1}^e b_{i2}^e)(b_{j1}^e c_{j2}^e - c_{j1}^e b_{j2}^e)\Big] \end{aligned} \tag{4.14}$$

Evaluation of the FM_{ij}^e Integral

The elemental contribution, FM_{ij}^e, is as shown in equation 4.6. Again, using equation 4.2, it can be shown that,

$$\begin{aligned} \vec{W}_i^e \cdot \vec{W}_j^e &= \frac{\ell_i^e \ell_j^e}{(6V^e)^2}\Big(L_{i1}^e L_{j1}^e f_{i2j2} - L_{i1}^e L_{j2}^e f_{i2j1} \\ &- L_{i2}^e L_{j1}^e f_{i1j2} + L_{i2}^e L_{j2}^e f_{i1j1}\Big) \end{aligned} \tag{4.15}$$

where

$$f_{pq} = b_p^e b_q^e + c_p^e c_q^e + d_p^e d_q^e \tag{4.16}$$

Since f_{pq} is constant, the expressions for the integral FM_{ij}^e can be easily found using the formula,

$$\int_{V^e} L_p L_q \, dV = \frac{V^e}{20}(1 + \delta_{pq}) \tag{4.17}$$

where p, q are tetrahedron node numbers, $\delta_{pq} = 1$ for $p = q$ and $\delta_{pq} = 0$ otherwise.

Therefore,

$$\begin{aligned} FM_{ij}^e &= \frac{\ell_i^e \ell_j^e}{720V^e}[f_{i2j2}(1 + \delta_{i1j1}) - f_{i2j1}(1 + \delta_{i1j2}) \\ &- f_{i1j2}(1 + \delta_{i2j1}) + f_{i1j1}(1 + \delta_{i2j2})] \end{aligned} \tag{4.18}$$

Evaluation of the R_i^e Integral

This integral is only evaluated on the boundary, S, of the problem domain. On a perfectly conducting surface the integral vanishes since,

$$\hat{n} \times \nabla \times \vec{H} = (\sigma + j\omega\epsilon)(\hat{n} \times \vec{E}) = (\sigma + j\omega\epsilon)\vec{E}_t \tag{4.19}$$

and a tangential E-field, $E_t = 0$ on a perfectly conducting boundary surface.

On a surface where the tangential electric field, defined as $\vec{E}_t = \hat{n} \times \vec{E}$, (where $\vec{E}$ is the boundary electric field), is constant and non-zero, R_i^e, using equation 4.7 and

4.19. can be expressed as.

$$R_i^e = \oint_{S^e} (\sigma + j\omega\epsilon)\vec{E}_t^e \cdot \vec{W}_i^e \, dS \tag{4.20}$$

Now if the tangential, boundary electric field is given as.

$$\vec{E}_t^e = E_{tx}^e \hat{x} + E_{ty}^e \hat{y} + E_{tz}^e \hat{z} \tag{4.21}$$

Using equations 4.2, 4.20 and 4.21, it can be easily shown that,

$$R_i^e = (\sigma + j\omega\epsilon)\frac{\ell_i^e \Delta^S}{18V^e}\left[E_{tx}^e(b_{i2} - b_{i1}) + E_{ty}^e(c_{i2} - c_{i1}) + E_{tz}^e(d_{i2} - d_{i1})\right] \tag{4.22}$$

where Δ^S is the area of the element lying on the boundary.

On an absorbing boundary placed far from the inhomogeneities to terminate the problem domain, first order absorbing boundary condition (ABC) for scattered H-field is,

$$\hat{n} \times \nabla \times \vec{H}^{sc} = -jk(\hat{n} \times \hat{n} \times \vec{H}^{sc}) \tag{4.23}$$

For antenna problems, the scattered field at the external boundary is the same as the total field and equation 4.23 can be written as,

$$\hat{n} \times \nabla \times \vec{H} = -jk(\hat{n} \times \hat{n} \times \vec{H}) \tag{4.24}$$

Substituting equation 4.24 in equation 4.7 gives,

$$R_i^e = -jk \oint_{S^e} \vec{W}_i^e \cdot (\hat{n} \times \hat{n} \times \vec{H}) \, dS \tag{4.25}$$

This can be expanded using equations 4.2 and 4.3 to yield,

$$R_{ij}^e = -\kappa \sum_{j=1}^{6} H_j^e \oint_{S^e} \vec{W}_i^e \cdot (\hat{n} \times \hat{n} \times \vec{W}_j^e) \, dS \tag{4.26}$$

where $\kappa = jk$, ($j = \sqrt{-1}$, k is the propagation constant), has deliberately been introduced here to avoid the confusion between the j used in this case and the one used as a tetrahedron edge index.

Evaluation of equation 4.26 is a bit involved. It can be deduced that,

$$\begin{aligned} \vec{W}_i^e \cdot (\hat{n} \times \hat{n} \times \vec{W}_j^e) \;=\; & \frac{\ell_i^e \ell_j^e}{(6V^e)^2}\left[T_{i1j1}L_{i1}L_{j1}\right. \\ & \left. - T_{i1j2}L_{i1}L_{j2} - T_{i2j1}L_{i2}L_{j1} + T_{i2j2}L_{i2}L_{j2}\right] \end{aligned} \tag{4.27}$$

where,

$$\begin{aligned} T_{pq} &= n_x n_y (b_{p'} c_{q'} + c_{p'} b_{q'}) + n_x n_z (b_{p'} d_{q'} + d_{p'} b_{q'}) + n_y n_z (c_{p'} d_{q'} - d_{p'} c_{q'}) \\ &\quad - (n_y^2 + n_z^2) b_{p'} b_{q'} - (n_z^2 + n_x^2) c_{p'} c_{q'} - (n_x^2 - n_y^2) d_{p'} d_{q'} \end{aligned} \tag{4.28}$$

and when $p = \imath 1$, $p' = \imath 2$ and vice versa; and when $q = \jmath 1$, $q' = \jmath 2$ and vice versa. n_x, n_y, and n_z are the components of the unit normal vector, $\hat{n}$.

R_{ij}^e can now be evaluated on the absorbing boundary surface and sent to the left-hand side (LHS) of equation 4.4 with the help of equations 4.26 and 4.28 along with the integral,

$$\int_S L_p L_q \, dS = \frac{\Delta^S}{12}(1 + \delta_{pq}) \tag{4.29}$$

p, q are for node numbers.

For a plane wave excitation, equation 4.23 can be written in terms of the incident and the total magnetic field as,

$$\hat{n} \times (\nabla \times \vec{H}) = -jk\hat{n} \times (\hat{n} \times \vec{H}) + \hat{n} \times (\nabla \times \vec{H}^{inc}) + jk\hat{n} \times (\hat{n} \times \vec{H}^{inc}) \tag{4.30}$$

and when the above is substituted into equation 4.7 and expanding as usual, yields,

$$\begin{aligned} R_{ij}^e &= -\kappa \sum_{j=1}^{6} H_j^e \oint_{S^e} (\hat{n} \times \hat{n} \times \vec{W}_i^e) \, dS \\ &\quad - \oint_{S^e} \left[\hat{n} \times (\nabla \times \vec{H}^{inc}) + jk\hat{n} \times (\hat{n} \times \vec{H}^{inc}) \right] \cdot \vec{W}_i^e \, dS \end{aligned} \tag{4.31}$$

The first integral in equation 4.31 has been worked out already above and contributes to the LHS of the elemental matrix equation. To evaluate the second integral, we let the plane wave excitation be expressed as,

$$\vec{H}^{inc} = \hat{y} \, e^{\jmath kx} \tag{4.32}$$

assuming the wave is propagating along the negative x-axis with the H-field having a y component only. It can then be easily shown that,

$$\hat{n} \times (\nabla \times \vec{H}^{inc}) = jk \, e^{\jmath kx} \left[n_y \hat{x} - n_x \hat{y} \right] \tag{4.33}$$

and

$$\hat{n} \times (\hat{n} \times \vec{H}^{inc}) = e^{\jmath kx} \left[n_x n_y \hat{x} - (n_x^2 + n_z^2) \hat{y} + n_y n_z \hat{z} \right] \tag{4.34}$$

Equations 4.33 and 4.34 when substituted into the the second integral of equation 4.31 yield the right-hand side (RHS) of the elemental matix equation as.

$$\begin{aligned} RHS_i^e &= -jk\frac{\ell_i^e}{6V^e}\oint_{S^e}\Big\{e^{jkx}\Big[(n_y+n_xn_y)(L_{i1}b_{i2}-L_{i2}b_{i1}) \\ &\quad -(n_x+n_x^2+n_z^2)(L_{i1}c_{i2}-L_{i2}c_{i1}) \\ &\quad +n_yn_z(L_{i1}d_{i2}-L_{i2}d_{i1})\Big]\Big\}\,dS \end{aligned} \tag{4.35}$$

If e^{jkx} is assumed to have a constant value over a triangular surface of a boundary element, given by its value at the centroid of the triangle, it can be taken out of the integral in equation 4.35. While this is just an approximation, it works fine for small triangular surfaces and reduces the analytical complexity of the integral in question. Using the generic integral,

$$\int_S L_p\,dS = \frac{\Delta^S}{3} \tag{4.36}$$

the RHS. for a given plane wave case, can now be written as,

$$\begin{aligned} RHS_i^e &= -jk\frac{\ell_i^e\Delta^S e^{jkx_c}}{18V^e}[(n_y+n_xn_y)(b_{i2}-b_{i1}) \\ &\quad -(n_x+n_x^2+n_z^2)(c_{i2}-c_{i1})+n_yn_z(d_{i2}-d_{i1})] \end{aligned} \tag{4.37}$$

where the centroid x-coordinate, $x_c = \frac{1}{3}\sum_{i=1}^{3} x_i$, and i represents a triangular surface node number.

Elemental matrix equations as given by equation 4.4 whose components are computed as discussed above, are assembled in a manner that respects the global directions of the edge fields to give rise to a large complex sparse matrix equations for the whole computation domain. One of the many ways of fixing the global edge directions and edge numbers is to go through all the elements, one after another and fix edge numbers while noting the global node numbers that define the edge. If an already assigned edge is encountered in an element it is first checked the way it is regarded positive locally: if it is in the same sense as the previously assigned edge then the contributions of that edge to the global system of matrix will be possitive, otherwise the contributions should be multiplied by -1.

Solution to the system of equations is efficiently solved using sparse matrix routines. For reduced memory storage requirements, iterative solvers [42] are strongly recommended. A diagonally pre-conditioned biconjugate gradient method was used

to solve the system of equations in this work. Discussion of the technique is discussed in Appendix A. Iterative solvers are suitable when one is having limited computer storage capacities, however they may prove to be slow for some problems. The convergence of the iterative relies very much on the nature of the problem and the initial assummed solution.

Solution to the system of equations directly gives the edge H-fields. H-field at any point in a given element can be computed through the edge fields using equation 4.3.

From the Maxwell's curl equation 3.1, it can be easily shown that the electric field, $\vec{E}$, is related to the magnetic field as,

$$\vec{E} = \frac{1}{(\sigma + j\omega\epsilon)}(\nabla \times \vec{H}) \tag{4.38}$$

Substituting equation 4.3 in equation 4.38 yields,

$$\vec{E} = \frac{1}{(\sigma + j\omega\epsilon)} \sum_{i=1}^{6} H_i^e (\nabla \times \vec{W}_i^e) \tag{4.39}$$

Now using equation 4.13, equation 4.39 can be written as,

$$\begin{aligned} \vec{E} \;=\; & \frac{1}{(\sigma + j\omega\epsilon)} \frac{2}{(6V^e)^2} \sum_{i=1}^{6} \ell_i^e H_i^e \left[(c_{i1}^e d_{i2}^e - d_{i1}^e c_{i2}^e)\hat{x} \right. \\ & \left. + (d_{i1}^e b_{i2}^e - b_{i1}^e d_{i2}^e)\hat{y} + (b_{i1}^e c_{i2}^e - c_{i1}^e b_{i2}^e)\hat{z} \right] \end{aligned} \tag{4.40}$$

Note that, owing to the linear vector basis functions used to approximate the edge H-field, the E-field is constant over each tetrahedron.

The power density or the Poynting vector is computed as,

$$\text{Power Density} = \frac{1}{2} \left| \text{Re} \left(\vec{E} \times \vec{H}^* \right) \right| \tag{4.41}$$

The current distribution over a perfectly conducting surface is computed as,

$$\vec{J}_S = \hat{n} \times \vec{H} \tag{4.42}$$

where $\hat{n}$ is the outer vector normal to the surface.

4.3 Electric Field Formulation

4.3.1 The Method

The electric field formulation is quite similar to the magnetic field formulation discussed in the previous section, but for the sake of completeness, its details will be

provided below.

The vector wave equation in this case is obtained by eliminating $\vec{H}$ from the Maxwell's curl equations 3.1 and 3.2, to yield.

$$\nabla \times \nabla \times \vec{E} - k^2 \vec{E} = 0 \tag{4.43}$$

where $k = \omega\sqrt{\mu\epsilon}$, $\omega = 2\pi f$, and f is the frequency.

Over each tetrahedral element of the problem domain, V, the E-field is expressed in terms of the linear basis functions as,

$$\vec{E} = \sum_{j=1}^{6} E_j^e \vec{W}_j^e \tag{4.44}$$

where E_j represents the edge values of the E-field.

The Galerkin's method implemented on equation 4.43 using equation 4.44 gives rise to the following complex matrix equation,

$$\left\{[PM^e] - k^2[FM^e]\right\}[E^e] = [R^e] \tag{4.45}$$

where

$$PM_{ij}^e = \int_{V^e} (\nabla \times \vec{W}_i^e) \cdot (\nabla \times \vec{W}_j^e)\, dV \tag{4.46}$$

$$FM_{ij}^e = \int_{V^e} \vec{W}_i^e \cdot \vec{W}_j^e\, dV \tag{4.47}$$

$$R_i^e = \oint_{S^e} \vec{W}_i^e \cdot (\hat{n} \times \nabla \times \vec{E})\, dS \tag{4.48}$$

where V^e is the elemental volume, S^e is the elemental surface, and $\hat{n}$ is the outer vector normal to S^e. $[E^e]$ is the coefficient vector of the six edge basis functions which represents the tangential E fields on the element edges in the local directions given in Figure 4.1 and Table 4.1.

4.3.2 Evaluation of the Integrals

The evaluation of the integrals given in equations 4.46 and 4.47 has already been discussed in the previous section. The only integral whose evaluation is discussed below is the one given in equation 4.48, that is, the R_i^e integral.

The R_i^e integral is only evaluated on the boundary surface, S, of the problem domain. On a perfect conducting surface the tangential (edge) E-field is known to

vanish. ($E_t = 0$), hence tetrahedron edges on perfect conducting boundaries do not contribute at all to the system of equations. In other words, they can be safely eliminated.

On a surface where the tangential E-field is constant and non-zero, the usual FEM treatment of inhomogeneous Dirichlet boundary conditions can be used where those edges only modify the RHS of the system of equations. To be precise, the matrix contributions corresponding to the inhomogeneous Dirichlet boundary edges are pre-multiplied with the non-zero E-field values and subtracted from the RHS of the corresponding edge matrix rows.

On a surface where the magnetic field is constant and non-zero, using equation 4.48 and the fact that

$$\hat{n} \times \nabla \times \vec{E} = -j\omega\mu(\hat{n} \times \vec{H}) = -j\omega\mu\vec{H}_t = -j\omega\mu\vec{J}_s \tag{4.49}$$

where $\vec{H}_t$ is the tangential magnetic field on the boundary and $\vec{J}_s$ is the induced surface current density if the boundary is a perfect conductor. R_i^e can then be expressed, using 4.49, as

$$R_i^e = -jw\mu \oint_{S_e} \vec{H}_t \cdot \vec{W}_i \, dS = -jw\mu \oint_{S_e} \vec{J}_s \cdot \vec{W}_i \, dS \tag{4.50}$$

If the boundary is a perfect conductor, it is essential to adopt the following expansions for $\vec{H}_t$ or $\vec{J}_s$:

$$\vec{H}_t = \sum_{j=1}^{6} H_{tj}^e \vec{W}_i^e \tag{4.51}$$

$$\vec{J}_s = \sum_{j=1}^{6} J_{tj}^e \vec{W}_i^e \tag{4.52}$$

Since the expansions involve all the six edges of the boundary tetrahedral elements, the effect of the boundary condition will remain in the system of equations even if the rows corresponding to boundary edges (known to have zero tangential electric field) are eliminated. Substituting 4.51 in 4.50 yields

$$R_{ij}^e = -j\omega\mu \sum_{j=1}^{6} H_{tj}^e \oint_{S^e} \vec{W}_i^e \cdot \vec{W}_j^e \, dS \tag{4.53}$$

which can be shown to simplify as

$$R^e_{ij} = -j\omega\mu\sum_{j=1}^{6} H^e_{tj}\frac{\ell^e_i\ell^e_j\Delta^S}{432(V^e)^2}[f_{i2j2}(1+\delta_{i1j1}) - f_{i2j1}(1+\delta_{i1j2}) - f_{i1j2}(1+\delta_{i2j1}) + f_{i1j1}(1+\delta_{i2j2})] \quad (4.54)$$

where f_{pq} are as defined in 4.16.

The obtain the corresponding expression where $\vec{J}_s$ is specified just substitute $\vec{J}_{sj}$ in place of $\vec{H}_{tj}$ in the above equation 4.54. If the absolute element boundary current, $\vec{I}$ is specified and if it is assumed to flow in one particular direction across the element surface, the corresponding, $\vec{J}_s$, in that direction can be easily computed as $\vec{J}_s = \vec{I}/\Delta^S$. where Δ^S is the element surface area.

Note that the induced surface current density, J_s discussed above is not the same as an impressed surface current density, J^{imp}. The former is just the effect of the presence of electromagnetic field while the latter excites electromagnetic field. To include into the formulation the impressed current, one has to start with the generalised vector wave equation of the form:

$$\nabla \times \nabla \times \vec{E} - k^2\vec{E} + j\omega\mu J^{imp} = 0 \quad (4.55)$$

which when discretized as before using the Galerkin's method, yields a matrix equation of the form:

$$\left\{[PM^e] - k^2[FM^e]\right\}[E^e] + j\omega\mu[FM^e][J^{imp}] = [R^e] \quad (4.56)$$

where the previous used notation applies and $[J^{imp}]$ is a vector of the components of the impressed current density along the element edges. Since these are known, they will directly contribute to the RHS of the equation to effectively implement injected (impressed) current boundary conditions that are important in implementing VFEM along with other circuit analysis tools.

On an absorbing boundary placed far from the inhomogeneities to terminate the problem domain, first order absorbing boundary condition for scattered E-field is.

$$\hat{n} \times \nabla \times \vec{E}^{sc} = -jk(\hat{n} \times \hat{n} \times \vec{E}^{sc}) \quad (4.57)$$

But as in the case of H-field, for antenna problems, the scattered field at the external boundary is the same as the total field and equation 4.57 can be written as.

$$\hat{n} \times \nabla \times \vec{E} = -jk(\hat{n} \times \hat{n} \times \vec{E}) \quad (4.58)$$

Substituting equation 4.58 in equation 4.48 gives.

$$R_i^e = -jk \oint_{S^e} \vec{W}_i^e \cdot (\hat{n} \times \hat{n} \times \vec{E})\, dS \tag{4.59}$$

This can be expanded using equations 4.2 and 4.44 to yield.

$$R_{ij}^e = -\kappa \sum_{j=1}^{6} E_j^e \oint_{S^e} \vec{W}_i^e \cdot (\hat{n} \times \hat{n} \times \vec{W}_j^e)\, dS \tag{4.60}$$

again here $\kappa = jk$ has been introduced to avoid the confusion with the edge index j. R_{ij}^e can be evaluated fully on the absorbing boundary surface and sent to the left-hand side (LHS) of equation 4.45 with the help of equations 4.60, 4.28 and 4.29.

For a plane wave case, the same procedure applies as in the H-field formulation and would thus be skipped here for brevity. In short, the right-hand side contributions in the E-field formulation is given by.

$$\begin{aligned} R_{ij}^e \;=\; & -\kappa \sum_{j=1}^{6} E_j^e \oint_{S^e} (\hat{n} \times \hat{n} \times \vec{W}_i^e)\, dS \\ & - \oint_{S^e} \left[\hat{n} \times (\nabla \times \vec{H}^{inc}) + jk\hat{n} \times (\hat{n} \times \vec{H}^{inc})\right] \cdot \vec{W}_i^e\, dS \end{aligned} \tag{4.61}$$

The first integral of equation 4.61 contributes to the LHS of the system of equations and the remaining integrals give rise to the RHS contribution same as the one given in equation 4.37 if the incident E-field is assumed as, $\vec{E}^{inc} = \hat{y}\, e^{jkx}$, and the field is assumed constant over a triangular surface.

Solution to the assembled system of complex equations directly gives the edge E-field. E-field at any point in a given element can be computed through the edge fields using equation 4.44.

Computation of the magnetic field is carried out using the following relation obtained from the two Maxwell's curl equation:

$$\vec{H} = \frac{j}{\omega\mu}(\nabla \times \vec{E}) \tag{4.62}$$

Substituting equation 4.44 in equation 4.62 yields,

$$\vec{H} = \frac{j}{\omega\mu} \sum_{i=1}^{6} E_i^e (\nabla \times \vec{W}_i^e) \tag{4.63}$$

Now using equation 4.13, equation 4.63 can be written as,

$$\begin{aligned} \vec{H} \;=\; & \frac{j}{\omega\mu} \frac{2}{(6V^e)^2} \sum_{i=1}^{6} \ell_i^e E_i^e \left[(c_{i1}^e d_{i2}^e - d_{i1}^e c_{i2}^e)\hat{x}\right. \\ & \left. + (d_{i1}^e b_{i2}^e - b_{i1}^e d_{i2}^e)\hat{y} + (b_{i1}^e c_{i2}^e - c_{i1}^e b_{i2}^e)\hat{z}\right] \end{aligned} \tag{4.64}$$

Note that, owing to the linear vector basis functions used to approximate the edge E-field, the H-field is constant over each tetrahedron.

4.4 Computational Results

4.4.1 A Parallel-Plate Waveguide

To test the formulation discussed in the preceding sections, we first solve the problem shown in Figure 4.2 that consists of a parallel-plate waveguide short-circuited on one end. The problem essentially consists of six square faces or boundaries, whose sides are quarter of wavelength, $(\lambda/4)$, long. Let the boundary conditions be fixed as follows: On the face $ABCD$, the tangential electric field, $E_t = E_0\hat{y}$; on faces $AFED$ and $BCHG$, the tangential electric field is given as, $E_t = E_0 \cos\frac{2\pi}{\lambda}x\hat{y}$; faces $ABGF$, $EFGH$, and $CDEH$ are perfect conductors on which the tangential electric field, $E_t = 0$. The value of E_0 is taken as 1 volt/meter and the solution is made at 1GHz.

It is desired in this problem to find the electric field distribution along a line in the middle of the waveguide and parallel to the x-axis. Theoretically the field distribution must follow the cosine function. The comparison of the threoretical and numerical results are shown in Figure 4.3.

4.4.2 A Cylindrical Monopole Antenna above a Perfect Ground Plane

As a further test to the formulation, a cylindrical monopole antenna above a perfectly conducting ground plane was modelled. The antenna dimensions were chosen arbitrarily as: height = 250 mm, diameter = 50.8 mm. An air gap of width = 5 mm was placed between the base of the monopole and the ground plane thus making the conducting length of the antenna as 245 mm.

The complete domain of computation was taken to be an imaginary cylinder of height above ground = 500 mm and diameter = 500 mm as shown in Figure 4.4. The problem domain was discretized into 7188 tetrahedral elements made up of 1466 nodes.

For simplicity an approximate delta-gap excitation was used by letting the E-field

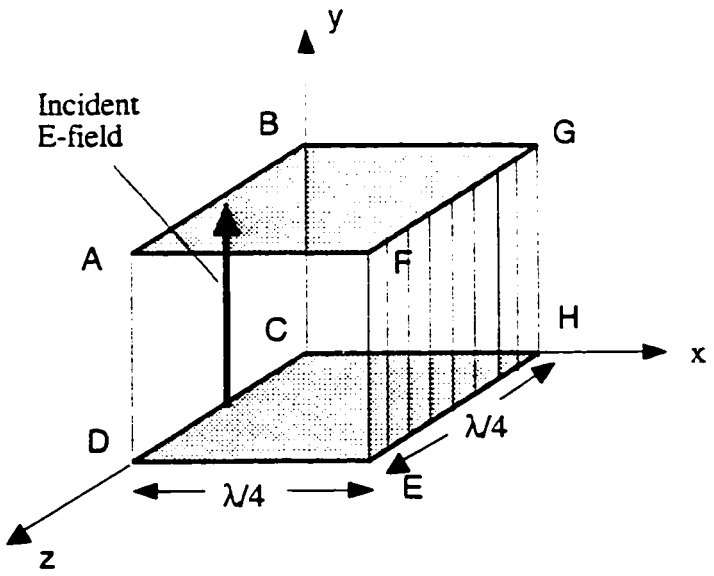

Figure 4.2: A short-circuited parallel-plate waveguide.

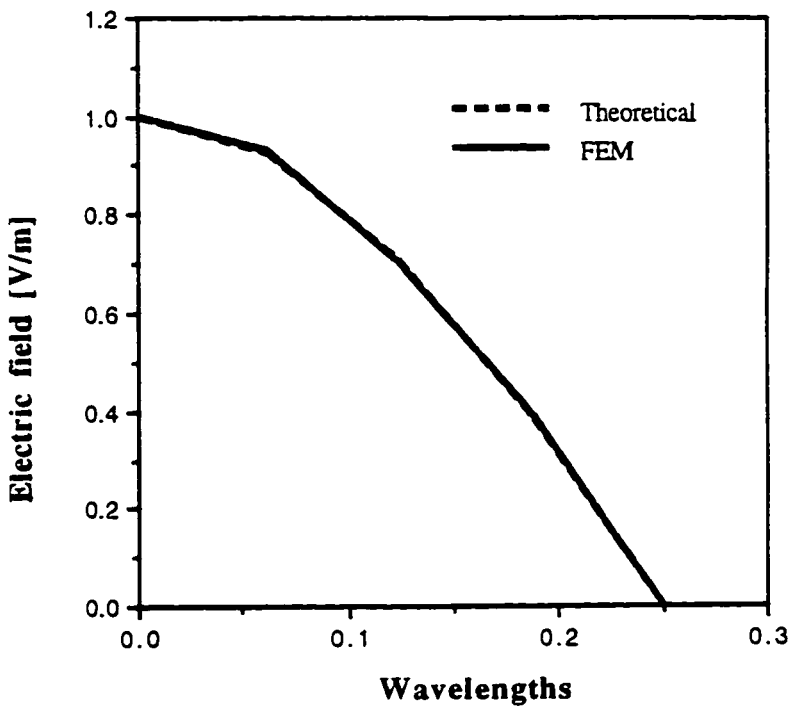

Figure 4.3: Electric field distribution along x-axis in the middle of a terminated parallel-plate waveguide

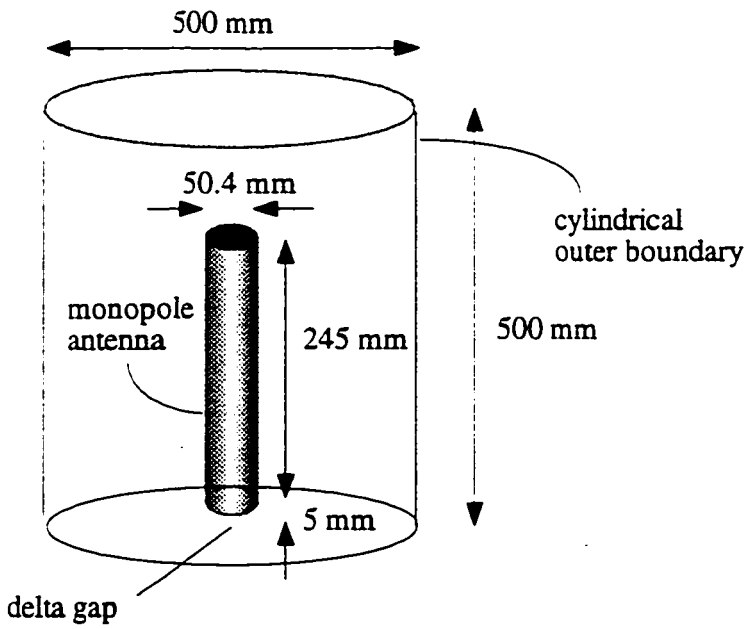

Figure 4.4: Problem geometry for the modelling of a cylindrical monopole antenna above a perfect ground plane

in the air gap just below the antenna to assume a constant value of 1 V/m and directed towards the positive y-axis i.e from the ground to the base of the monopole antenna. First order absorbing boundary condition (ABC) is implemented on the outer boundary of the problem domain. The computation was made at 300 MHz frequency.

The results for a cylindrical monopole antenna above a perfectly conducting ground plane are given in Figure 4.5 for the E-field distribution around the antenna.

4.4.3 Conclusion

A method of analysis of three-dimensional electromagnetic wave propagation problems has been discussed. The method implements the vector finite element method to model closed as well as open boundary problems. Thorough discussion of the electric

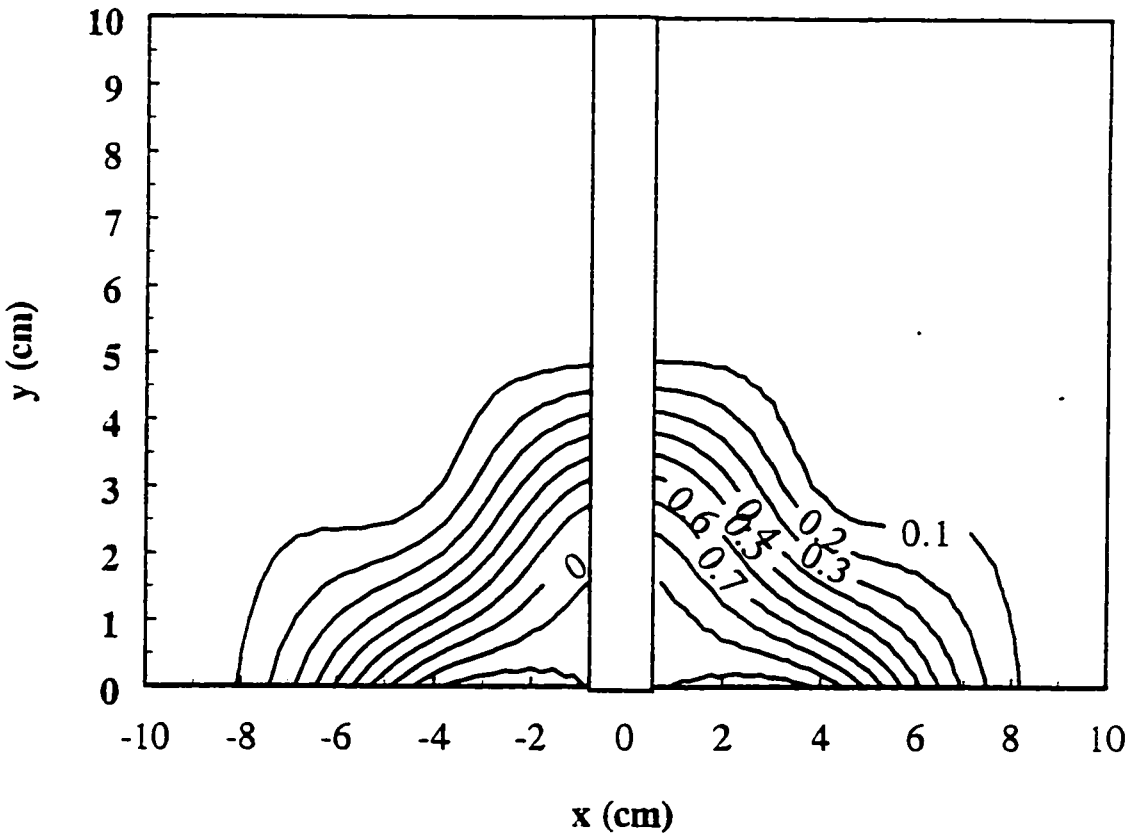

Figure 4.5: Electric field (V/m) distribution around a monopole antenna above a perfectly conducting ground plane in the $z = 0$ plane.

field as well as magnetic field formulations for various situations of interest has been provided along with the closed-form expressions for all the integrals involved. The method has been implemented to a parallel-plate waveguide and a monopole antenna. in both cases yielding excellent results. It is thus evident that the method can be applied to model radiation, scatterring as well as closed problems of interest in the field of electromagnetics.

Chapter 5

Conclusion

5.1 Summary of the Thesis Research

This work set out to achieve two main things. The first thing was to realize a tool for accurate frequency domain modelling of microwave structures that are driven through coaxial lines. Nodal finite element method was found handy for such a task. A major class of microwave structures targetted for that tool are those exhibiting axisymmetry in geometry and excitation. The tool realized has been found to work well in modelling such structures as dielectric ring resonator antennas, complex coaxial junctions and simple monopole antennas. A novel technique to model the coaxial feed using the finite element method is introduced in this work.

The second thing was to come up with a tool that could model fully, in the frequency domain, three-dimensional microwave structures especially in radiation and scattering problems. The method employed, uses vector finite element method for both electric field and magnetic field formulations. Vector finite element not only provides an easy way of implementing material and interface boundary conditions, but also does not suffer from the problems encountered in nodal finite element method such as spurious solutions, and singularities on sharp edges and tips.

A great deal of work has been done in deriving closed-form expressions for all the integrals involved for different cases of interest. That is by itself a very important contribution provided by this work, that will be of great benefit to future researchers in that area. The tool realized has been shown to work well in radiation and scattering

problems. Results for parallel-plate waveguide and a cylindrical monopole antenna above a perfect ground plane have been presented and both agree well with the theory.

5.2 Future Work

At this time when electronic and microwave engineers are designing high speed devices and systems, transient modelling of the structures involved is necessary. That calls for the need to extend this work to be able to perfom time domain modelling of both axisymmetrical as well as three dimensional structures using both, the nodal and vector finite element methods.

Since only a few cases have been modelled in this work, it is desirable to apply it to other problems of interest, such as in the design of shields against EMI and their effectiveness, optimization of various kinds of dielectric resonator antennas and other types of antennas, modelling of cross-talk in printed circuit boards, optimization of heatsinks used in PCBs, determination of electrical properties of different materials, and field computation in a region surrounding high power (e.g broadcasting) antennas in close proximity to large conducting structures.

The vector finite element, electric field formulation presented in this work can very easily be integrated with circuit analysis CAD software to make them handle well high frequency situations. For example, the method presented in this work can successfully be implemented in finding characteristics of very high speed interconnects in printed circuit boards through a full-wave analysis of those interconnects.

Since in all the cases dealt in this work, only the nearfield is computed in the problem domain, a way could be found to integrate this work to other near-to-far field transformation algorithms already in the literature so as to make the tools more versatile. That would also go along creating better and easier graphical user interfaces to the tools.

Appendix A

Preconditioned Biconjugate Gradient Method

To solve a system of linear complex equations of the type $\mathbf{Ax} = \mathbf{b}$ using iterative methods saves a lot of computer memory and CPU time. This way, makes it possible to solve very large problems that would be impossible to solve with direct matrix solution methods even those that tend to reduce the matrix fill-ins during LU decompositions. A diagonally preconditioned biconjugate gradient method [42] was found to be quite appropriate and was used in this work.

The complex matrix equation to be solved is,

$$[\mathbf{A}][\mathbf{x}] = [\mathbf{b}] \tag{A.1}$$

where [**A**] is $n \times n$ complex coefficient matrix.

[**b**] is $n \times 1$ complex vector which is known.

[**x**] is $n \times 1$ complex vector to be determined.

To solve the equation the following steps are followed:

Assign an initial guess for the solution vector **x**. In the absence of any intelligent guess it suffices to start with $\mathbf{x} = \underline{0}$ guess.

Compute:

$$\begin{aligned} [\mathbf{r}] &= [\mathbf{b}] - [\mathbf{A}]\,[\mathbf{x}] \\ [\mathbf{p}] &= [\mathbf{r}] \end{aligned}$$

$$anum = \langle \mathbf{r}, \mathbf{r} \rangle$$

where

$$\langle \mathbf{r}, \mathbf{r} \rangle = [\mathbf{r}]^T [\mathbf{r}] = \sum_{i=1}^{n} r(i) r(i)$$

Repeat until: either *error* < *tolerance*

or *number of iterations* = *maximum number fixed*

Do *iter* = 1,*niter*

$$\begin{aligned} [\mathbf{q}] &= [\mathbf{A}]\,[\mathbf{b}] \\ \alpha &= anum \,/\, \langle \mathbf{q}, \mathbf{p} \rangle \\ [\mathbf{x}] &= [\mathbf{x}] - \alpha[\mathbf{p}] \\ [\mathbf{r}] &= [\mathbf{r}] - \alpha[\mathbf{q}] \\ [\mathbf{C}]_{n \times n} &= \mathrm{diag}[\mathbf{A}] \qquad \text{preconditioning matrix} \\ [\mathbf{q}] &= [\mathbf{C}]^{-1} [\mathbf{r}] \end{aligned}$$

Compute error:

$$\begin{aligned} [\mathbf{e}] &= [\mathbf{A}]\,[\mathbf{x}] - [\mathbf{b}] \\ error &= \sqrt{\frac{\|e\|^2}{\|b\|^2}} \cdot 100\%; \text{ where } \|e\|^2 = \sum_{i=1}^{n} |e(i)|^2 \end{aligned}$$

if *error* < *tolerance* then STOP

else continue:

$$\begin{aligned} \beta &= \langle \mathbf{q}, \mathbf{p} \rangle \,/\, anum \\ [\mathbf{p}] &= [\mathbf{q}] + \beta[\mathbf{p}] \end{aligned}$$

Bibliography

[1] R. L. Ferrari and R. L. Naidu, "Finite-element modelling of high-frequency electromagnetic problems with material discontinuities," *IEE Proc. A*, vol. 137, pp. 313-320, Nov. 1990.

[2] J. Meixner, "The behaviour of electromagnetic fields at edges," *IEEE Trans. Antennas Propagat.*, vol. AP-20, pp. 442-446, July 1972.

[3] J. B. Andersen and V. V. Solodukhov, "Field behaviour near a dielectric wedge," *IEEE Trans. Antennas Propagat.*, vol. AP-26, pp. 598-602, July 1978.

[4] J. Van Bladel, "Field singularities at metal-dielectric wedges," *IEEE Trans. Antennas Propagat.*, vol. AP-33, pp. 450-455, Apr. 1985.

[5] R. De Smedt, "Field singularities at the tip of a metallic cone of arbitrary cross section," *IEEE Trans. Antennas Propagat.*, vol. AP-34, pp. 865-870, 1986.

[6] Jianming Jin, "The finite element method in electromagnetics," New York: John Wiley & Sons, 1993.

[7] S. N. Karp, "A convergent far-field expansion for two-dimensional radiation functions," *Commun. Pure Appl. Math.*, vol. 14, pp. 427-434, 1961.

[8] C. H. Wilcox, "An expansion theorem for electromagnetic fields," *Commun. Pure Appl. Math.*, vol. 9, pp. 115-132, 1956.

[9] J. P. Webb and V. N. Kanellopoulos, "Absorbing boundary conditions for the finite element solution of the vector wave equation," *Microwave Opt. Tech. Lett.*, vol. 2, pp. 370-372, Oct. 1989.

[10] O. C. Zienkiewicz and R. L. Taylor, "The finite element method (4th. edition). Vol. 1: Basic Formulation and Linear Problems," New York: McGraw-Hill, 1989.

[11] S. G. Mikhlin, "Variational Methods in Mathematical Physics," New York: Macmillan, 1964.

[12] W. R. Scott, Jr., "Accurate modelling of axisymmetric two-port junctions in coaxial lines using the finite element method," *IEEE Trans. Microwave Theory Tech.*, vol. 40, pp. 1712-1716, Aug. 1992.

[13] H. O. Ali and G. Costache "Finite-element time-domain analysis of axisymmetrical radiators," *IEEE Trans. Antennas Propagat.*, vol. AP-42, pp. 272-275, Feb. 1994.

[14] G. M. Wilkins, J.-F. Lee, and R. Mittra, "Numerical modelling of axisymmetric coaxial waveguide discontinuities," *IEEE Trans. Microwave Theory Tech.*, vol. 39, pp. 1323-1328, Aug. 1991.

[15] E. Marouby, M. Aubourg, and P. Guillon, "Application of the finite element method to the design of transitions between coaxial lines," *Proc. IEE*, pt. H. vol. 137, no. 4, pp. 219-225, Aug. 1990.

[16] E. Sumbar, F. E. Vermeulen, and F. S. Chute, "Implementation of radiation boundary conditions in the finite element analysis of electromagnetic wave propagation," *IEEE Trans. Microwave Theory Tech.*, vol. 39, pp. 267-273, Feb. 1991.

[17] H. O. Ali and G. I. Costache, "Accurate frequency domain modelling of coaxially driven axisymmetric microwave structures," *IEEE Microwave Guided Wave Lett.*, vol. 4, no. 12, pp. 390-392, Dec. 1994.

[18] J. G. Maloney, G. S. Smith and W. R. Scott, "Accurate computation of the radiation from simple antennas using the finite-difference time-domain method," *IEEE Trans. Antennas Propagat.*, vol. AP-38, pp. 1059-1068, July 1990.

[19] W. L. Stutzman and G. A. Thiele, "Antenna theory and design," New York: John Wiley & Sons, 1981.

[20] J. H. Lee, H. J. Eom, and K. H. Jun, "Reflection of a coaxial line radiating into a parallel plate," *IEEE Microwave Guided Wave Lett.*, vol. 6, no. 3, pp. 135-137, March 1996.

[21] R. K. Mongia, A. Ittipiboon, and M. Cuhaci, "Electric-monopole antenna using a dielectric ring resonator," *Electron. Lett.*, vol. 29, no. 17, pp. 1530-1531, Aug. 1993.

[22] R. B. Keam and A. G. Williamson, "Radial-line to coaxial-line junction with a dielectrically sheathed post," *IEEE Microwave Guided Wave Lett.*, vol. 2, no. 3, pp. 102-104, March 1992.

[23] I. Ratner, H. Ali, E. Petriu, and G. Eatherly, "Nural network modelling of electromagnetic field problems," *Proc. NICROSP'96 Int. Workshop on Neural Networks for Identification, Control, Robotics, and Signal/Image Processing*, pp. 387-391, IEEE Computer Society Press, Venice, Italy, Aug. 21-23, 1996.

[24] G. Cybenko, "Approximation by superpositions of a sigmoidal function," *Mathematics of Control, Signals, and Systems*, vol. 2, pp. 303-314, 1989.

[25] K. Funahashi, "On the approximate realization of continuous mapping by neaural networks," *Neural Networks*, vol. 2, pp. 183-192, 1989.

[26] K. Hornic, M. Stinchcombe, and H. White, "Multilayer feedforward networks are universal estimators," *Neural Networks* , vol. 2, pp. 359-366, 1989.

[27] S. Haykin, "Neural Networks: A comprehensive Foundation," Macmillan College Publishing Company, 1994.

[28] P. E. Gill, W. Murray, and M. H. Wright, "Practical Optimization," Academic Press, 1981.

[29] R. Fletcher, "Practical Methods of Optimization, Volume 1," John Wiley and Sons, 1980.

[30] K. Levenberg, "A Method for the Solution of Certain Problems in Least Squares," *Quart. Appl. Math.*, vol. 2, pp. 164-168, 1944.

[31] D. Marquardt, "An Algorithm for Least-squares Estimation of Nonlinear Parameters," *SIAM J. Appl. Math.* vol. 11, pp. 431-441, 1963.

[32] M. Norgaard, "Neural network based system identification toolbox," Institute of Automation, Technical University of Denmark, Tech. Report 95-E-773", 1995.

[33] H. Demuth and M. Beale, "Neural Network Toolbox User's Guide," The Mathworks Inc., 1994.

[34] A. Bossavit and J. C. Verite, "A mixed FEM-BIEM method to solve 3-D eddy current problems," *IEEE Trans. Magnetics*, vol. MAG-18, pp. 431-435, Mar. 1982.

[35] H. Whitney, "Geometric Integration Theory," Princeton, NJ: Princeton University Press, 1957.

[36] "Mixed finite elements in R^3, *Numer. Meth.*, vol. 35, pp. 315-341, 1980.

[37] J. S. van Welij, "Calculation of eddy current in terms of H on hexahedra," *IEEE Trans. Magnetics*, vol. MAG-21, pp. 2239-2241, Nov. 1985.

[38] M. Hano, "Finite-element analysis of dielectric-loaded waveguides," *IEEE Trans. Microwave Theory Tech.*, vol. 32, pp. 1275-1279, Oct. 1984.

[39] G. Mur and A. T. de Hoop, "A finite-element method for computing three-dimensional electromagnetic fields in inhomogeneous media," *IEEE Trans. Magnetics*, vol. MAG-21, pp. 2188-2191, Nov. 1984.

[40] M. L. Barton and Z. J. Cendes, "New vector finite elements for three-dimensional magnetic field computation," *J. Appl. Phys.*, vol. 61, no. 8, pp. 3919-3921, Apr. 1987.

[41] C. W. Crowley, "Mixed order covariant projection finite elements for vector fields," Ph.D. dissertation, McGill University, Montreal, 1988.

[42] A. Chatterjee, J. L. Volakis and D. Windheiser, "Parallel computation of 3D electromagnetic scattering using finite elements," *International Journal of Numerical Modelling: Electronic networks, devices and fields*, vol. 7, pp. 329-342, July 1994.

IMAGE EVALUATION
TEST TARGET (QA-3)

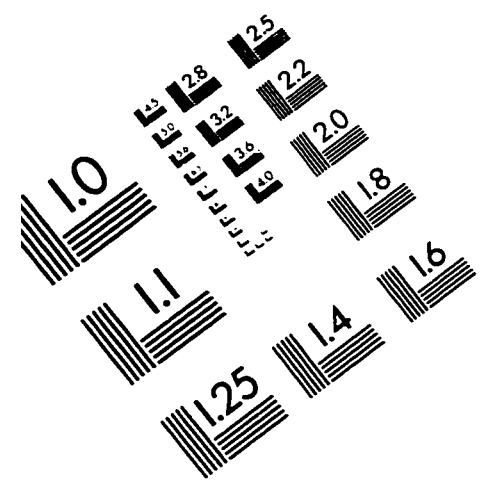

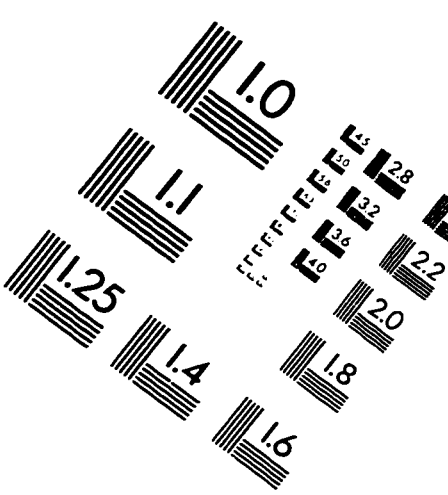

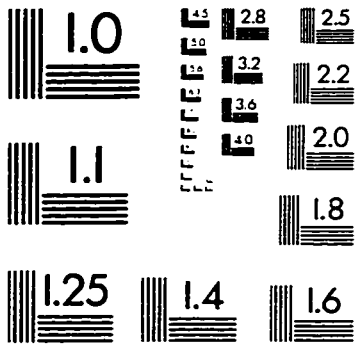

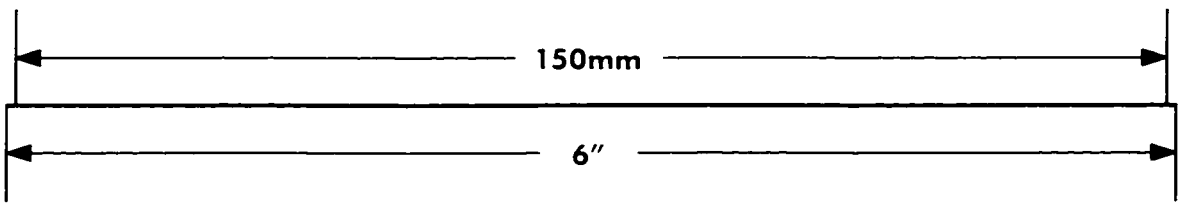

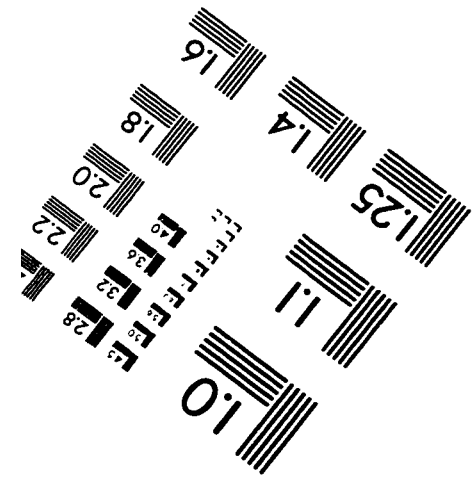

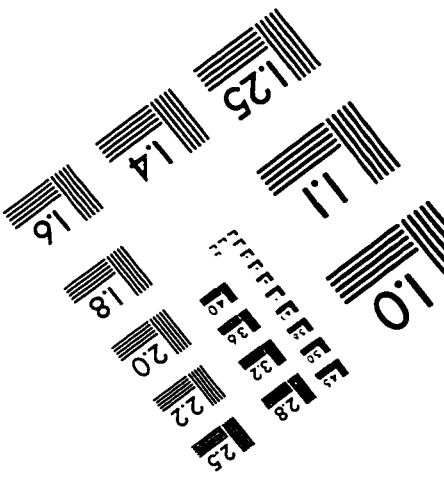

APPLIED IMAGE, Inc
1653 East Main Street
Rochester, NY 14609 USA
Phone: 716/482-0300
Fax: 716/288-5989